Modeling and Control of Voltage Source Converters Connected to the Grid

Michael Lindgren

Technical Report No. 351

1998

Modeling and Control of Voltage Source Converters Connected to the Grid

by

Michael Lindgren

Technical Report No. 351

Submitted to the School of Electrical and Computer Engineering
Chalmers University of Technology
in partial fulfilment of the requirements
for the degree of
Doctor of Philosophy

Department of Electric Power Engineering
Chalmers University of Technology
Göteborg, Sweden
November 1998

CHALMERS UNIVERSITY OF TECHNOLOGY
Department of Electric Power Engineering
S-412 96 Göteborg
ISBN: 91-7197-710-4
ISSN: 0346 - 718X
Chalmers Bibliotek, Reproservice
Göteborg, 1998

Abstract

This thesis deals with the modeling and control of pulse width modulated (PWM) voltage source converters connected to the grid. When voltage source converters are connected to the grid, the power quality and the dynamic performance are affected by the line filter connected between the converter and the grid, and by nonlinearities caused by the switching converter. In the thesis, the dynamic performance and power quality of converters connected to the grid by first-order L-filters and third-order LCL-filters are focused on. For each line filter, predictive vector control principles that allow the independent control of the active and the reactive powers are developed and verified by measurements. It is shown that a similar dynamic performance can be obtained with both line filters. To obtain a high power quality, it is advantageous to use LCL-filters. The thesis also deals with different nonlinearities and their influence on dynamic performance. Measured small-signal frequency responses are compared with Bode diagrams obtained from linear analytical models. The analytical models are created by using a technique based on state space equations that is developed in the thesis. In the thesis, switching frequencies and sampling frequencies from 5 to 7 kHz are used. At such switching and sampling frequencies, nonlinearities and cross coupling caused by the uniform PWM method and the coordinate transformation in the control system do not have any significant effect on the small-signal frequency responses for frequencies below 1 kHz. It is, however, shown that a more ideal performance of the vector control system can be obtained by compensating for errors due to the non-ideal commutation caused by the blanking time and on-state voltage drops across the non-ideal IGBT valves of the converter. Moreover, measurements have shown that non-modeled losses in the line filter inductors have an impact on the small-signal frequency responses. When voltage source converters are used as active filters, the performance of the active filters are affected by phase shifts in the current control system, and also by the cross coupling between the control of the active and the reactive currents. Different principles for compensating for the phase shifts have been evaluated. Measurements show that it is possible to compensate for the phase shifts and thereby obtain efficient active filters also at moderate switching frequencies such as 5 to 7 kHz.

Keywords: Power electronics, Voltage source converter, IGBT valve, Line filter, L-filter, LCL-filter, Pulse width modulation, switching frequency, sampling frequency, small-signal, frequency response, transfer function, active filtering.

Preface

This thesis is an important part of the result of my time at the Department of Electric Power Engineering at Chalmers University of Technology. It has been a privilege for me to work in an area related to the proper utilization of energy resources. Hopefully, the results will contribute to an improved base for design of power converters, or, at least, to future relevant research projects.....

First of all, I would like to thank Sydkraft ABs Research Foundation for fully financing the project. I also had the support from the reference group constituted by Bengt Ahlman and Peter Bäckström at AB Sydkraft and Professor Mats Alaküla at the department of Industrial Electrical Engineering and Automation, Lund Institute of Technology. I would also like to thank Professor Alaküla and Anders Carlsson at the same department for making it possible to utilize the DSP system developed at their department. I would also like to thank my industrial adviser, Tommy Lejonberg, previously with ABB and now Technical Director of Elmo Industries for useful comments on the research.

At our department at Chalmers, first of all, I would like to thank Dr. Jan Svensson for all cooperation during the preparation of the experimental system and the measurements in the laboratory, as well as several of the publications in the thesis. Furthermore, I would like to thank Professor Jorma Luomi for his support throughout the project and for his excellent comments, proof reading, and general advice during the preparation of the thesis. I also want to thank my supervisors during the first part of the project; Dr. Tore Svensson and Professor Kjeld Thorborg.

I also want to express my sincere gratitude to my dear parents Aina and Bengt for their encouragement and support.

Finally, thank you Karin for your love and never ending support.

List of Appended Publications

A M. Lindgren, J. Svensson, "Connecting Fast Switching Voltage Source Converters to the Grid — Harmonic Distortion and its Reduction," *IEEE Stockholm Power Tech Conference*, Stockholm, Sweden, June 18-22, 1995, Proceedings of Power Electronics, p. 191-195.

B M. Lindgren, "Analysis and Simulation of Digitally Controlled Grid-connected PWM-converters using the Space-vector Average Approximation, " *IEEE 5th Workshop on Computers in Power Electronics*, Portland, USA, August 11-14, 1996, p. 157-162.

C J. Svensson, M. Lindgren. "Influence of Non-linearities on the Frequency Response of a Grid-Connected Vector-Controlled VSC," to appear in *IEEE Transactions on Industrial Electronics.*

D J. Svensson, M. Lindgren, "Vector Current Controlled Grid Connected Voltage Source Converter — Influence of Non-linearities on the Performance," *IEEE Power Electronics Specialists Conference (PESC 98*), Fukuoka, Japan, May 17-22, 1998, Vol. 1, p. 531-537.

E M. Lindgren, J. Svensson, "A Method to Compensate for Errors Caused by the Blanking Time in PWM Systems with High Ripple Currents," *1998 IEEE Nordic Workshop on Power and Industrial Electronics* (*NORPIE/98*), Espoo, Finland, August 26-27, 1998, p. 147-152.

F M. Lindgren, "Feed forward — Time Efficient Control of a Voltage Source Converter Connected to the Grid by Lowpass Filters," *IEEE Power Electronics Specialists Conference (PESC 95)*, Atlanta, USA, June 18-22, 1995, Vol. 2, p. 1028-1032.

G M. Lindgren, J. Svensson, "Control of a Voltage-source Converter Connected to the Grid through a LCL-filter — Application to Active Filtering," *IEEE Power Electronics Specialists Conference (PESC 98*), Fukuoka, Japan, May 17-22, 1998, Vol. 1, p. 229-235.

List of Symbols

Symbol	Description	Unit
$\mathbf{A}$	system matrix of continuous state space model	
$\mathbf{B}$	input matrix of continuous state space model	
$\mathbf{C}$	output matrix	
C_f	capacitance of filter capacitor	[F]
C_{dc}	capacitance of dc link capacitor	[F]
$\mathbf{D}$	initial state matrix of state space model	
$\mathbf{F}$	system matrix of discrete state space model	
f_{res}	resonance frequency	[Hz]
f_s	sampling frequency	[Hz]
f_{sw}	switching frequency of a semiconductor valve	[Hz]
f_{mod}	frequency of carrier-wave	[Hz]
$\mathbf{G}$	input matrix of discrete discrete state space model	
i_{load}	current of dc load	[A]
$\underline{i}$	line current vector	
$\underline{i}_1$	converter current vector	
$\underline{i}_2$	line current vector when the LCL-filter is used	
I_{base}	base current	[A]
κ_p	proportional gain	
κ_{p1}	proportional gain in inner loop	
κ_{p2}	proportional gain in outer loop	
κ_{pd}	gain to obtain dead beat control of inductor current	
κ_{pd2}	gain to obtain dead beat control of capacitor voltage	
L_1	inductance of filter inductor connected to the converter	[H]
L_2	inductance of filter inductor connected to the grid	[H]
L_{grid}	inductance of grid	[H]
M	ratio between output voltage and maximum output voltage	
P	ratio between switching frequency and line frequency	
R	resistance	[Ω]
R_1	resistance of filter inductor connected to converter	[Ω]
R_2	resistance of filter inductor connected to the grid	[Ω]
R_{onD}	resistance of diode of IGBT	[Ω]
R_{onT}	resistance of transistor of IGBT	[Ω]
$\underline{Sw}$	switching vector of converter output voltage	
s	Laplace operator	
T_{blank}	blanking time	[s]
T_s	sampling time	[s]
t_k	time at sample k	[s]
$\underline{u}_1$	converter output voltage vector	
$\underline{u}_2$	grid voltage vector	
$\underline{u}_c$	capacitor voltage vector	
$\mathbf{u}$	input vector of state space model	
U_{base}	base voltage	[V]
u_{dc}	dc link voltage	[V]
U_{D0}	forward voltage across diode of IGBT at zero current	[V]
U_{T0}	forward voltage across transistor of IGBT at zero current	[V]
$\mathbf{x}$	state vector of state space model	
X_C	reactance of filter capacitor	[p.u.]
X_L	reactance	[p.u.]
X_{L1}	reactance of filter inductor connected to converter	[p.u.]
X_{L2}	reactance of filter inductor connected to grid	[p.u.]

$\mathbf{y}$	output vector of state space model	
Z	impedance	[p.u.]
Z_{base}	base impedance	[Ω]
Z_{cable}	wave impedance of cable	[Ω]
Z_{conv}	wave impedance of converter	[Ω]
Z_{load}	wave impedance of load	[Ω]
Z_1	impedance of filter inductor connected to converter	[Ω]
Z_2	impedance of filter inductor connected to grid	[Ω]
z	z operator	
Δu_{blank}	error in average phase voltage due to blanking time	
Δu	compensation voltage for delay time	[V]
θ	angle of grid-flux vector	[rad]
θ_1	average angle of grid-flux vector of sampling interval k+1, k+2	[rad]
ω_{g}	angular frequency of grid voltage vector	[rad/s]
ω_{s}	angular frequency of grid voltage vector	[rad/s]
$\underline{r}_{conv}$	converter reflexion coefficient of converter	
$\underline{r}_{load}$	reflexion coefficient of load	

Superscripts

*	reference
$\alpha\beta$	vector in $\alpha\beta$-reference frame
dq	vector in dq-reference frame

Subscripts

a	phase a
b	phase b
c	phase c
dc	dc link
d	vector component in d-direction
q	vector component in q-direction
$d0$	vector component in d-direction in steady state
$q0$	vector component in q-direction in steady state
α	vector component in α–direction
β	vector component in β–direction
L	L-filter
LCL	LCL-filter

Table of Contents

Part II. Appended Publications

Chapter 1

Introduction

1.1. Power Converters and Power Quality

In this thesis, switching power converters for industrial applications are investigated. As a result of tremendous developments in the semiconductor industry, switching pulse width modulation (PWM) converters are becoming cheaper and available at increased power levels. Today, PWM converters are widely used in industrial applications, such as adjustable-speed drives (ASDs) and uninterruptible power supplies (UPSs). This is advantageous since the use of power electronics results in equipment with higher performance and lower energy consumption. The development is, however, not only positive since almost all power electronic circuits behave as nonlinear loads. Therefore, harmonic currents are injected into the grid.

The nonlinear loading of the grid increases continuously since the standards for the emission of harmonic currents still allow a high total harmonic distortion. As a consequence, the power quality is reduced in several ways. Usually a poor power quality refers to the presence of disturbances and harmonic distortion in the grid voltage. Harmonic distortion and disturbances may cause malfunction of equipment, such as computers and ASDs. Harmonic currents can also cause fires due to overheating of neutral conductors. The problem of harmonics can be solved either by reducing the harmonic distortion, or by increasing immunity to harmonic distortion and designing the system to provide efficient and safe operation even with a large amount of harmonics present.

In industry, the major part of electricity is used to supply electrical machines. Due to the increased prices for electricity and reduced cost of power converters, more and more machines are being replaced with ASDs. In these drives, a converter from ac to dc voltage (i.e., a rectifier) is connected to the grid. Today, line commutated rectifiers using diodes or thyristors are used. Such a rectifier is a nonlinear load that generates harmonic currents.

As a result of the development of new semiconductors and control computers, it would be possible to use PWM rectifiers and, thereby, obtain sinusoidal line currents. Today, PWM converters are mainly used as converters from dc voltage to ac voltage (i.e., inverters) in ASDs and in UPSs. Compared with line-commutated rectifiers, significantly higher power quality and increased dynamic performance can be obtained with PWM rectifiers. These rectifiers are not usually used today since existing harmonic standards can be fulfilled by using cheap line-commutated rectifiers. This situation may, however, change as soon as customers start to request grid friendly rectifiers. Such a development can take place due to new standards that reduce the permitted emission of harmonic currents, or due to a reduced cost for grid friendly rectifiers.

1.2. Line Interference and Control

To obtain a high efficiency and a high power rating from a PWM converter, the current and the voltage across the semiconductor valves should not be high simultaneously. This is solved by using PWM. At each switching of a valve, however, a high instantaneous power dissipation occurs in the valve. Therefore, the switching times must be short to obtain high efficiency and rated power. As a consequence of very low switching times of below 1 μs, high voltage derivatives occur at each switching of a valve. These voltage derivatives give rise to disturbances at high frequencies. Both radiated and conducted emission may occur. The disturbances caused by switching are, consequently, affected by the switching frequency. If the switching frequency is reduced, the power dissipation in the valves at each switching may be increased and the switching speed can, thus, be reduced compared to operation at a higher switching frequency. Therefore, it is advantageous to operate at moderate switching frequencies. In high-power applications, the switching frequency has to be below a few kHz with the valves available today.

Due to the PWM principle, harmonics occur even when PWM converters are used. To obtain a converter system with sinusoidal line currents and a low emission of disturbances due to the switching, a line filter is connected between the converter and the grid. The selection of the line filter is important since it affects both the power quality and the dynamic performance. To obtain both low cost and high dynamic performance, a line filter consisting of a series inductor in each phase can be used. This filter is called an L-filter. To obtain sinusoidal line current with an L-filter, the switching frequency of the converter, or the inductance of the line filter, has to be high. An alternative solution for obtaining sinusoidal line currents, is to use low-pass filters, such as LC- or LCL-filters. Such filters can be designed to have a very high attenuation of harmonics due to the PWM even at moderate switching frequencies.

In most applications for grid connected PWM converters, a control system that can control the active and the reactive current independently is appropriate. At low switching frequencies, controllers based on stationary models of the line filter, such as power angle controllers are often used. At high switching frequencies, however, the ability to obtain a high bandwidth by using vector control should by utilized. In a vector control system, the active and reactive current and, consequently, the active and the reactive power, are controlled by separate controllers. As a result, a high bandwidth and a low cross coupling between the control of the active and the reactive currents can be obtained. The final performance of the control system depends on the line filter, on the switching frequency, and on the control principle. In some applications, such as the active filtering of current harmonics, the phase-shifts and the cross coupling between the control of the active and the reactive currents should be predicted in order to obtain the desired performance.

In the design of control systems for PWM converters, analytical models are important for the prediction of dynamic performance with different control laws and system parameters. Using linear time-invariant (LTI) models is most attractive since it is much more complex to design control systems for nonlinear and time-variant systems.

1.3. The Present Thesis

In applications for grid-connected voltage source converters, obtaining a high power quality and dynamic performance is important. In addition, independent control of the active and the reactive powers should be obtained.

An important goal of the thesis is to compare the power quality and dynamic performance of vector controlled PWM converters connected to the grid by an L-filter and an LCL-filter. The dynamic performance and power quality are affected by nonlinearities in the converter system. The thesis investigates different nonlinearities and their influence on dynamic performance and power quality. To reduce the complexity of the system design, linear analytical models should be used. Methods of analytical modeling and the accuracy of linear analytical models are studied by comparing frequency responses obtained from analytical models and measured small-signal frequency responses. In the active filtering of harmonic currents, phase shifts between the reference currents and the active and reactive currents, and cross coupling between the control of the active and the reactive currents reduce the performance. Methods to predict and compensate for phase-shifts are dealt with and the influence of cross coupling are displayed.

The thesis consists of two parts. In Chapters 2 and 3 of Part I, different phenomena that influence the controllability and power quality are described, and references to previous publications in the area of research are given. Furthermore, the objectives and some of the results of the publications appended in Part II are described. Chapter 2 gives an introduction to vector control of PWM converters and describes different nonlinearities. Chapter 3 deals with analytical modeling. In Chapter 4, the objectives and results of the publications in Part II of the thesis are summarized and Chapter 5 concludes the thesis work. Part II of the thesis consists of the appended publications.

Chapter 2

Control System Design and Influence of Nonlinearities

In this chapter, an introduction to vector control of grid-connected PWM converters is presented. The operating principle of a vector controlled PWM converter connected to a three-phase grid is described, as well as different parts of the converter system that introduce nonlinearities and consequently affect the performance of the converter system.

In the literature, control principles usually applied for linear systems, such as PI control [1][2], state feedback control [3][4], as well as control principles intended for nonlinear systems are proposed. Another most frequently proposed control structure is to use comparators that control the phase currents, or the active and reactive currents of a vector control system, within specified tolerance bands [5]-[7]. Such a controller, along with phase current estimators, can be used to obtain sensorless current control [7].

Among the control principles intended for nonlinear systems, neural network controllers and fuzzy logic controllers [8]-[10], are becoming popular. The control principle of neural networks is based on the learning of the control system based on the consequences of different operations. When a fuzzy logic controller is used, the operation of the converter is determined by predetermined rules. By using such a controller, the operation of the converter can be programmed to obtain high performance by using a physical knowledge of the system. As an example, it is possible to implement a vector control system without measuring the line voltages by using fuzzy logic control [9]. In some publications, other control principles for nonlinear systems, such as sliding mode control [11] and Lyaponov based control [12], are proposed.

When hysteresis controllers such as tolerance band and fuzzy controllers are used, neither parameter variation in the line filter nor errors caused by the PWM converter or by non-symmetrical or distorted grid voltages have a significant impact on the performance of the converter system. However, when hysteresis controllers are used, it is usually difficult to predict the harmonic spectra of the line currents since the switching frequency of the converter varies with the operating conditions and the amplitude of the phase voltages of the grid.

In the thesis, the objective is to investigate the performance of linear control systems that can be modeled by linear analytical models. Nonlinear controllers such as hysteresis controllers are, consequently, not studied. In the thesis, predictive vector controllers are used. Using such a controller is appropriate for obtaining both high dynamic performance and phase currents with a specified harmonic distortion. For a predictive vector controller, the dynamic performance depends on the linearity of the PWM converter, on the line filter, and on the control principle used.

2.1. The Operating Principle of a Vector Controlled PWM Converter

A principal scheme of a PWM converter with a predictive vector control system is displayed in Fig. 2.1. The control system is based on an inner loop and an outer loop. The inner loop controls the power between the dc link and the grid, while the reference current of the inner loop is provided by the outer loop and depends on the application. In Fig. 2.1, the outer loop is designed to control the dc voltage of the load. To obtain sinusoidal line currents, a line filter is connected between the converter and the grid. The line filter attenuates the voltage harmonics caused by the PWM converter and is also necessary in the control of the power between the dc link and the grid.

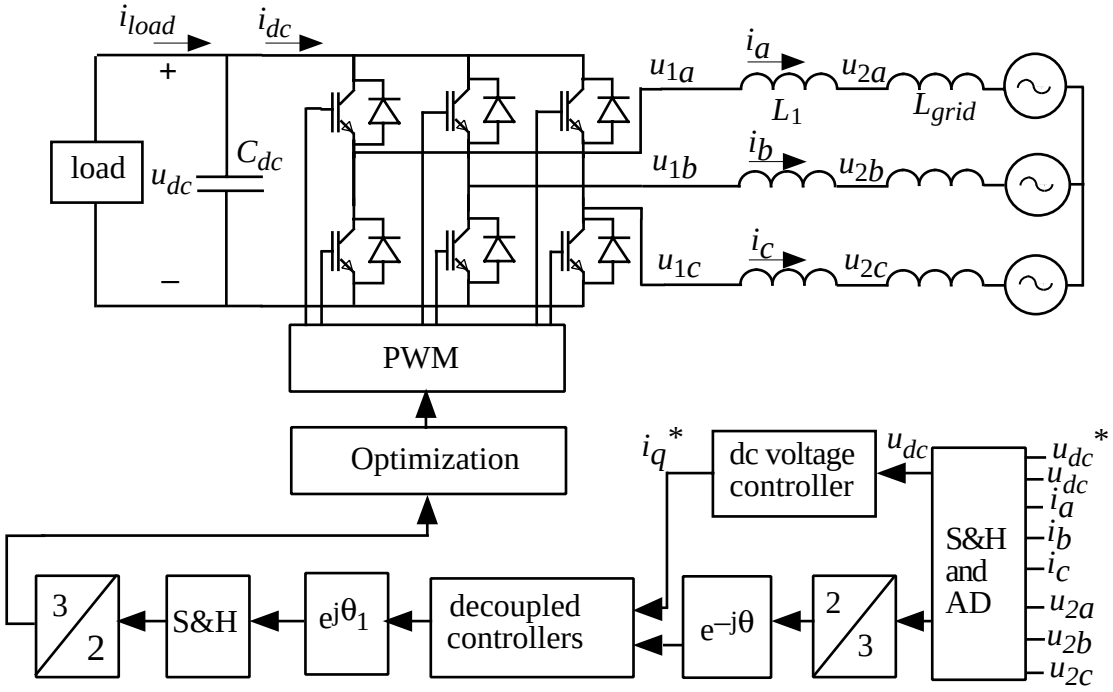

Fig. 2.1. System layout vector controlled PWM converter connected to a three-phase grid.

In PWM converters for ac applications, vector control systems can be utilized to obtain independent control of the active and the reactive powers. One of the most advantageous characteristic of a vector control system is that vectors of ac currents and voltages occur as constant vectors in steady state. Therefore, static errors in the control system can be avoided by using PI controllers. The theory for modeling three-phase systems by using vector theory was originally developed to analyze transient phenomena in ac machines [13][14]. Later on, vector theory was applied to the analysis and control of grid-connected converters [15]. Today, vector theory is widely used in the control of three-phase PWM converters.

In a vector control system, three-phase currents and voltages are described as vectors in a complex reference frame, usually called the $\alpha\beta$-frame. In addition, for a grid-connected converter, a rotating reference frame that is synchronized to the grid-flux vector is introduced; this frame is usually called the *dq*-frame. Since the *dq*-frame is synchronized to the positive-sequence fundamental part of the grid-flux vector, positive-sequence voltages and currents of the fundamental frequency occur as constant vectors in the *dq*-frame in steady state. In

systems with a significant voltage harmonic distortion and non-symmetrical grid voltages, the control system should separate the positive-sequence voltages from the negative-sequence voltages [16], and take into account the influence of the voltage harmonics of the grid voltages [17].

In the literature, no standard definition seems to be used and the *d*-axis is used to represent the direction of the grid-voltage vector, as well as the grid-flux vector. In this thesis, the grid-voltage vector occurs in the *q*-direction, and the grid-flux vector in the *d*-direction. The angle between the α-axis of the $\alpha\beta$-frame and the *d*-axis of the *dq*-frame is used in the transformations between the $\alpha\beta$- and the *dq*-frame. In Fig. 2.1, the angle between the α-axis of the $\alpha\beta$-frame and the *d*-axis of the *dq*-frame is denoted by θ and by θ_1. θ is the angle at the time instant of the sample k, t_k. The value of the angle θ is obtained by using a synchronization method [18].

As described in Fig. 2.1, the currents and voltages used in the control system are sampled and AD converted in the block S&H and AD. In the measurements in the thesis, all currents and voltages are sampled synchronously at the same instants of time. Sampling the phase-currents synchronously is important, since a significant current ripple occurs in the phase-currents. The AD converted currents and voltages are transformed into *d*- and *q*-components in the *dq*-frame, where individual controllers for the active and the reactive powers are used.

When high sampling frequencies are used, a time delay of one sampling interval occurs in the control loop due to the AD conversion and the calculation time in the digital control system. At low switching frequencies, such as 1 kHz, it is possible to avoid the delay of one sampling interval since each sampling interval starts with the output of the same voltage vector for a long time. Normally, high sampling frequencies are used, and a time delay of one sampling interval occurs in the feedback loop. The voltage vector required by the control system during the sampling interval from sample k+1 to sample k+2 is, consequently, based on the sampled currents and voltages at the sample k. The reference voltages for the phase voltages of the VSC are obtained by transforming the reference voltage in the *dq*-frame back into the three-phase system. To obtain the *d*- and *q*-voltages required by the controllers on average during the sampling interval from k+1 to k+2, the angle θ_1 in the transformation from the *dq*-frame to the $\alpha\beta$-frame, is the average angle of the grid-flux vector during the sampling interval from k+1 to k+2.

A three-phase voltage is transformed into a vector in the $\alpha\beta$-frame by the transformation

$$\underline{u}_1{}^{\alpha\beta}(u_a, u_b, u_c) = \sqrt{\frac{2}{3}}\left(u_a + u_b e^{j\frac{2\pi}{3}} + u_c e^{-j\frac{2\pi}{3}} \right) \tag{2.1}$$

In the transformation, the factor $\sqrt{2/3}$ is introduced to obtain a power invariant transformation. Thus, the same power in the two-axis system and in the three-phase system. In the thesis, power invariant transformations are used exclusively. In the literature, amplitude invariant transformations are also commonly used. When amplitude invariant transformations are used, the phase currents and voltages can be directly obtained as the

projections of current vectors and voltage vectors on the reference axes of the three phases, at the angles 0, $2\pi/3$ rad and $-2\pi/3$ rad.

The phase voltages of the VSC are defined by

$$u_{1a} = v_{1a} - v_0 \tag{2.2}$$

$$u_{1b} = v_{1b} - v_0 \tag{2.3}$$

$$u_{1c} = v_{1c} - v_0 \tag{2.4}$$

where v_0 is the potential in the neutral point, and v_{1a}, v_{1b} and v_{1c} are the phase potentials of phase *a*, phase *b*, and phase *c*, respectively. Thus, the voltage vector of the VSC can be written as

$$\underline{u}_1^{\alpha\beta}(u_a, u_b, u_c) = \sqrt{\frac{2}{3}}\left[v_{1a} + v_{1b}e^{j\frac{2\pi}{3}} + v_{1c}e^{-j\frac{2\pi}{3}} - v_0\left(1 + e^{j\frac{2\pi}{3}} + e^{-j\frac{2\pi}{3}}\right)\right] \tag{2.5}$$

Since PWM is used, each phase of the converter is connected to the positive or the negative side of the dc link. In analytical models, the converter can be conveniently modeled by introducing switching states. In these models, the voltage drops across the valves are usually not taken into account. Furthermore, the models assume that the converter switches instantaneously. By using the switching states s_{wa}, s_{wb}, and s_{wc} that can be equal to 1 or –1, the phase potentials of the VSC can be written

$$v_{1a} = s_{wa}\frac{u_{dc}}{2} \tag{2.6}$$

$$v_{1b} = s_{wb}\frac{u_{dc}}{2} \tag{2.7}$$

$$v_{1c} = s_{wc}\frac{u_{dc}}{2} \tag{2.8}$$

Now, the voltage vector of the VSC can be written as

$$\underline{u}_1^{\alpha\beta}(s_{wa}, s_{wb}, s_{wc}) = \sqrt{\frac{2}{3}}\frac{u_{dc}}{2}\left(s_{wa} + s_{wb}e^{j\frac{2\pi}{3}} + s_{wc}e^{-j\frac{2\pi}{3}}\right) \tag{2.9}$$

By introducing a switching vector, this can be simplified to

$$\underline{u}_1^{\alpha\beta} = u_{dc}\underline{sw}^{\alpha\beta} \tag{2.10}$$

where the switching vector is defined by

$$\underline{sw}^{\alpha\beta} = \sqrt{\frac{1}{6}}\left(s_{wa} + s_{wb}e^{j\frac{2\pi}{3}} + s_{wc}e^{-j\frac{2\pi}{3}}\right) \tag{2.11}$$

The three switches of the converter can be combined in eight ways; the resulting voltage vectors for these combinations are displayed in Fig. 2.2. A vector $\underline{u}(s_{wa}, s_{wb}, s_{wc})$ with switching states $s_{wa} = 1, s_{wb} = -1$, and $s_{wc} = -1$ is denoted by $\underline{u}(100)$.

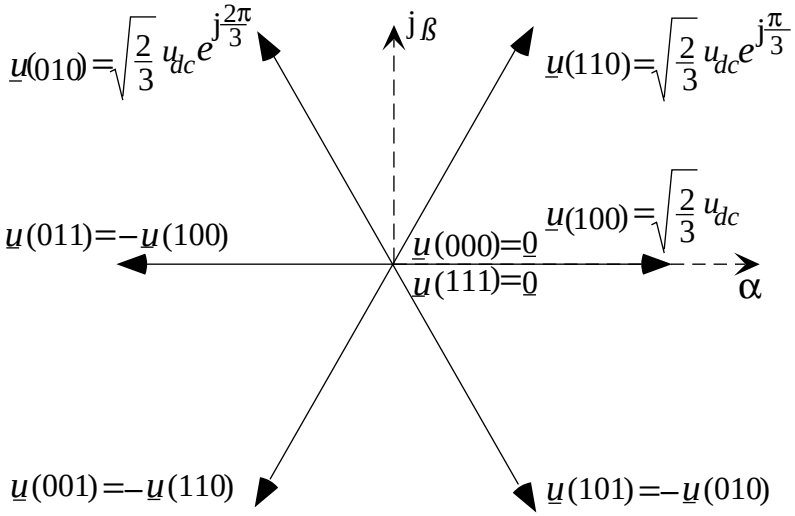

Fig. 2.2. The voltage vectors of the ideal VSC .

2.2. Influence of PWM Method and Switching Frequency

In the design of a PWM converter system with a predictive current controller, the selection of the modulation principle and the switching frequency are important for obtaining the desired performance. The switching frequency has an impact on the current harmonic distortion, the losses in the line filter and the converter valves, as well as the accuracy and the dynamic performance of the current control system. It is important that the output voltages of the converter are linear functions of the reference voltages. To obtain linear operation, the ratio between the switching frequency and the frequency of the modulated signal, called the frequency ratio, should be sufficiently high [19][20]. Moreover, due to the PWM, harmonic voltages at the converter output occur at frequencies close to multiples of the switching frequency.

If a high switching frequency is used, the harmonics caused by the PWM can be attenuated by the use of a small line filter. Furthermore, a high switching frequency makes it possible to use a high sampling frequency in the digital control system since the maximum feasible sampling frequency is twice the switching frequency.

The main drawback of a high switching frequency is that the losses in the valves become high. To avoid high losses, the semiconductor valves can be switched rapidly. However, rapid switching increases the high frequency distortion introduced by the converter into the grid and also gives rise to high voltage derivatives that may damage the insulation of the line filter connected between the converter and the grid.

An alternative solution for reducing the losses of the semiconductor valves is to use soft switching. In such a converter, usually called a resonant or quasi-resonant converter, the

commutation of the valves takes place at zero current or zero voltage [21]. Such solutions are often proposed for dc-dc converters and also for ac-dc converters [10], [22]–[24].
Another important advantage of resonant converters is that the reduced voltage derivatives of the converter output voltages reduces the high frequency distortion and also allow the use of long cables between the converter and the line filter or the machine [23].

By using a randomized PWM method, a more continuous spectrum than with a regular PWM method using a constant sampling frequency is obtained [25]. Such methods are often utilized to reduce the audible noise in ASDs. One drawback of randomized methods is that the design of the current control system becomes more complex [26]. Randomized methods are mainly proposed for inverters in ASDs.

In digitally controlled PWM converters with predictive controllers, space vector modulation (SVM) or carrier-wave based PWM is used. For SVM, the time instants at which each switching is to be performed are evaluated analytically. In a carrier-wave based method, reference voltages are compared with a triangular or sawtooth wave, and the commutations occur at the intersection of the references and the wave. When three-phase voltages are compared with a single carrier wave, a sub-oscillating carrier-wave PWM method is obtained [27]. Thus, a sub-oscillating method denotes a PWM method for three-phase systems. When a sub-oscillating method is used, an optimized PWM method should be implemented to fully utilize the dc voltage [27][28]. An important advantage of SVM is that the number of switchings during each sampling interval can be reduced in comparison with a carrier-wave based method [29].

The modulation method has an impact on the size of the line filter. The influence of different modulation methods on the line filter can be studied by using a frequency analysis of the modulation methods [30]. For each PWM method, it is important to synchronize the sampling of the phase currents to the time instants corresponding to the average values of the phase currents. When this is performed accurately, the current harmonic distortion introduced by the PWM converter is not present in the sampled phase currents and consequently not in the *d*- and *q*-currents either. Sampling at the accurate time instants is most important in systems with high ripple currents due to high current derivatives [31]. For a sub-oscillating PWM method with a triangular carrier-wave, the time instants corresponding to the average phase currents occur at the maximum and the minimum of the triangular carrier wave.

When a sub-oscillating method is used, a reference value for each phase voltage is compared with a common carrier wave, as illustrated in Fig. 2.3. In the figure, the sampling frequency is equal to the switching frequency. The voltage vectors $\underline{u}(000)$and $\underline{u}(111)$ result in the same output voltage and consequently, three different voltage vectors are active during one sampling interval.

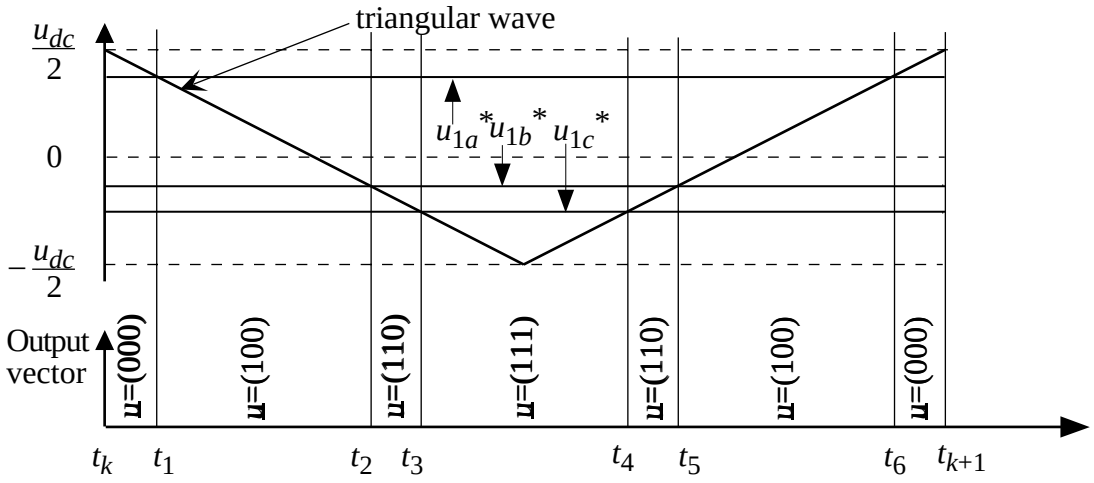

Fig. 2.3. Triangular carrier-wave based PWM and the output voltage vectors of the VSC during one sampling interval. The switching frequency is equal to the sampling frequency.

To obtain the voltage vector that is required by the vector controller, the reference vector in the *dq*-frame is transformed into a vector in the $\alpha\beta$-frame. Due to the uniform sampling, the reference voltage vector is constant during the sampling interval. The reference voltage vector in the $\alpha\beta$-frame is determined by

$$\underline{u}_1^{\alpha\beta *} = \underline{u}_1^{dq*} e^{j\left(\theta + \frac{3}{2}\omega_g T_s\right)} \tag{2.12}$$

where ω_g is the angular frequency of the grid and T_S is the sampling time. The transformation angle in the exponent, θ_1, is equal to the average angle during the succeeding sampling interval. In this transformation, it is also possible to compensate for small time delays of a few μs due to the gate circuits and the capacitive gates of the valves.

The reference vector required by the control system is obtained on average during the sampling interval, assuming that the *d*- and *q*-components of the voltage vectors of the VSC are constant throughout the sampling interval. Furthermore, the converter should switch according to the PWM pattern determined by the PWM circuit. However, the *d*- and *q*-components of the different voltage vectors are projections of the voltage vectors of the VSC onto the *dq*-frame and are, therefore, functions of the angle of the *dq*-frame. Consequently, due to the rotation of the *d*- and *q*-axes during the sampling intervals, time varying errors occur in the average voltage vector during the sampling intervals. The errors correspond to a nonlinearity and a coupling between the *d*- and *q*-directions in the control system.

The average *d*- and *q*-components obtained as a function of the angle of the reference voltage vector are displayed in Figs. 2.4 and 2.5 for a sampling frequency equal to the switching frequency, and for a sampling frequency at twice the switching frequency, respectively. A reference voltage vector of 0 V in the *d*-direction and of 400 V in the *q*-direction has been applied. The results have been obtained by integrating the projection of each voltage vector used during a sampling interval onto the *d*- and *q*-axes and dividing the result by the angle of one sampling interval.

According to Fig. 2.4, only minor errors occur when the sampling frequency is equal to the switching frequency. As shown in Fig. 2.5, significant errors that change signs between two sampling intervals occur if the sampling frequency is twice the switching frequency. This is unfortunate since it is important to use as high sampling frequency as possible at low switching frequencies, in order to reduce the time delay in the digital control system. However, as shown in Figs 2.4 and 2.5, the errors are functions of the angle of the reference voltage vector, and the sampling frequency, and it should, thus, be possible to compensate for the errors.

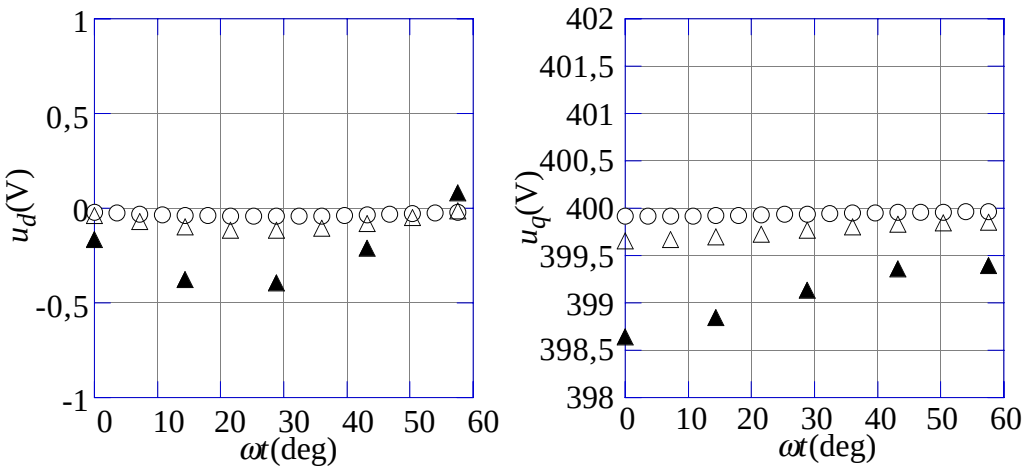

Fig. 2.4. The average d- *and* q-*components of the converter output voltage vector during the sampling intervals when the reference voltage vector rotates from 0 to 60 degrees in the* αβ-*frame. The sampling frequency is equal to the switching frequency. The sampling frequency is 1.25 kHz (solid triangles), 2.5 kHz (triangles), and 5 kHz (circles).*

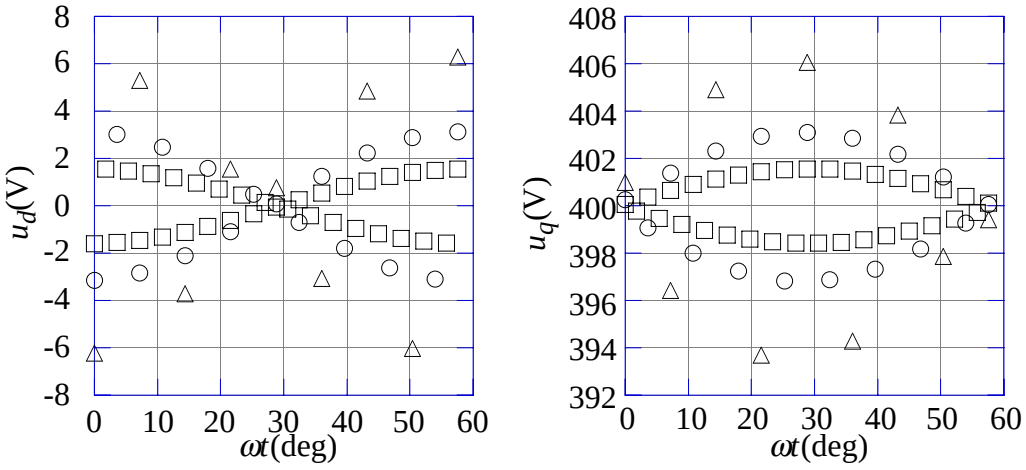

Fig. 2.5. The average d- *and* q-*components of the converter output voltage vector during the sampling intervals when the reference voltage vector rotates from 0 to 60 degrees in the* αβ-*frame. The sampling frequency is twice the switching frequency. The sampling frequency is 2.5 kHz (triangles), 5 kHz (circles) and 10 kHz (squares).*

The influence of the PWM method on the small-signal performance of PWM converters has been investigated by a few authors. An analog control system using continuous natural sampling PWM has been investigated in [17]. Natural sampling PWM denotes that the reference voltages of the PWM change during the sampling intervals; this is the case in an analog control system. In a digital control system, a uniform sampling PWM is normally used and the reference voltages are constant during the sampling intervals. In [17], the transfer functions from a reference voltage vector to an output voltage vector of an ideally switched PWM converter were investigated. Constant gain was obtained except for the frequencies where harmonics due to the PWM occur.

Analytical expressions of the spectral output for sinusoidal inputs with carrier-wave based PWM can be obtained by using the technique described in [19]; both natural sampling and uniform sampling have been considered. According to this reference, natural sampling is linear and the phase-shift is zero. With uniform sampling, the amplitude of the fundamental output is a function of the frequency ratio and, furthermore, a phase-shift is introduced. Publication [19] presents theoretical results, and consequently describes the operation of an ideally switching converter with ideal valves that switch according to the PWM pattern obtained from the modulator. Thus, only the influence of the PWM method is studied.

In [32], the linearity of a uniform space-vector PWM method was studied in the *dq*-frame. Measured and theoretical transfer functions from reference voltages in the *d*- and *q*-directions to average voltages in the *d*- and *q*-directions were displayed. These transfer functions are nonlinear and in addition time variant with the angle of the reference voltage vector. The nonlinearity varies with the ratio between the PWM frequency and the frequency of the reference voltage, and also with the amplitude of the components of the reference voltage vector. In addition to the nonlinear gain, a cross coupling between the *d*- and *q*-directions was displayed. According to the publication, uniform PWM methods are nonlinear. The measured results are, however, influenced not only by the uniform PWM method, but also by the *dq*-transformations and the errors caused by the non-ideal valves of the converter.

In the thesis, the small-signal transfer functions from current references in the *d*- and the *q*-directions to currents obtained in the *d*- and *q*-directions are presented in **Publications C**, **D** and **G**. An important objective of these publications has been to study the influence of nonlinearities and to verify whether any nonlinearity or cross coupling is introduced in comparison with the ideal performance of the vector control system. In **Publication C** and **D**, the L-type line-filter is used. In **Publication G**, transfer functions are also presented for the LCL-filter. In all publications, high performance predictive vector controllers are developed and utilized.

In **Publication C**, small-signal transfer functions for different current controllers of the P- and PI-type are presented. The transfer functions are compared with Bode-diagrams obtained from linear analytical models. No significant coupling is introduced by the PWM method and the coordinate transformations between the $\alpha\beta$- and the *dq*-frame. In the publications in the thesis, the switching frequency has been from 6 to 7.2 kHz, and the sampling frequency has been equal to the switching frequency. As displayed in Fig. 2.4, the influence of the coordinate transformations has been of minor significance.

As described in **Publicaton C**, the transfer functions are affected by losses in the line filter and by the errors introduced by the non-ideal converter.

In **Publications D**, the influence of the losses is described further by comparing operations with two different inductors. Transfer functions are presented for line filter inductors with oriented and non-oriented cores of 0.3 and 0.5 mm laminations, respectively. The publication also describes the influence of the operating point based on measured small-signal frequency responses both in inverter and rectifier operations. In **Publication G**, small-signal frequency responses are used to verify the dynamic performance of a control principle for the LCL-filter.

2.3. Nonlinearities due to the Non-ideal Converter

In the converter, nonlinearities occur due to two different phenomena: blanking time and forward voltage across valves.

The nonlinearity due to the blanking time occurs as a result of the non-instantaneous commutation of a valve. Each commutation between two valves in a phase leg is divided into two steps. First, the valve that is conducting is turned off. Since a semiconductor valve needs time to recover before it can block voltages, a blanking time is introduced between the turn-off of one valve and the turn-on of the other valve in the phase leg. If the transistor is conducting in the valve that is turned off, the diode in the valve that is to be turned on starts to conduct as soon as the transistor is turned off. Thus, the switching time instant is not influenced by the blanking time. At a commutation from a diode to a transistor, the commutation is delayed by the blanking time since the diode in the conducting valve is not affected by the gate of the valve. The delay of the commutation introduces an error

$$\Delta u_{blank} = u_{dc} \frac{T_{blank}}{T_s} \tag{2.13}$$

between the average phase voltage during a sampling interval and the phase voltage required by the PWM modulator. T_{blank} is the blanking time and T_s is the sampling time.

Thus, a commutation from the lower valve to the upper valve is delayed by the blanking time if the phase current is positive, according to the reference direction in Fig. 2.1. A commutation from the upper valve to the lower valve is delayed by the blanking time if the current is negative. Consequently, the average voltage during a sampling interval is reduced by Δu_{blank} if the current is positive at the commutation from the lower valve to the upper valve and is increased by Δu_{blank}, if the current is negative at the commutation from the upper valve to the lower valve.

If the sampling frequency is equal to the switching frequency, two commutations occur in each phase during a sampling interval. In this case, the average phase voltage is increased by Δu_{blank} if the current is negative at both commutations, and reduced by Δu_{blank} if the current is positive at both commutations. If the current is positive at the first commutation and negative at the second commutation, errors of different signs occur and the total error due to the blanking time is zero. Similarly, if the current is negative at the first commutation and positive at the second commutation, no errors are introduced by the blanking time.

Consequently, no error occurs if the phase-current has different signs at the two commutations during a sampling interval. For a converter with IGBT valves, blanking times of a few μs are used; this is sufficient to introduce significant errors at switching frequencies above a few kHz.

In addition to the errors introduced by the blanking time, the forward voltage across the valves gives rise to an error between the reference phase voltages and the average phase voltages. The forward voltage across the transistor, u_{onT}, and the diode, u_{onD}, of the valves can be determined from the equations

$$u_{onD} = U_{D0} + R_{onD} i \tag{2.14}$$

$$u_{onT} = U_{D0} + R_{onT} i \tag{2.15}$$

where U_{D0} and U_{T0} are the no-load voltages for the diode and the transistor, respectively, and R_{onD} and R_{onT} are the resistances for the diode and the transistor, respectively.

The forward voltage across the valves varies with the rated current of the valves. In the publications in Part II of the thesis, IGBT valves with a rated current of 400 A have been used. According to the data sheets, the typical voltage across the transistor is 3 V at the rated current 400 A. The the forward voltage across the valves have been identified from measurements of the voltage across the valves for phase currents between 0 and 50 A. The resulting parameters are listed in Table I.

TABLE I

MEASURED PARAMETERS OF THE IGBT VALVES USED IN THE THESIS

U_{D0} = 1.05 V	U_{T0} = 1.08 V	R_{onD} = 10 mΩ	R_{onT} = 12 mΩ

As reported in [33], the harmonic distortion of the phase currents for electrical machines supplied by PWM inverters can be reduced by compensating for the nonlinearities caused by the blanking time and non-ideal valves. In ASDs with IGBT valves, the current ripple caused by the PWM is usually low due to high switching frequencies and due to the leakage inductance of the machine. At low ripple currents, it is sufficient to use the sign of the phase current at the samples in the compensation for errors. When converters are connected to the grid, however, the current ripple caused by the PWM may be high, especially in systems with a high transient capability and when the LCL-filter is used. In systems with a high current ripple, the sign of the phase currents at the commutations may be the opposite of the sign at the sample. In such a system, a method for predicting the sign of the phase currents at the commutations during each sampling interval should be used to compensate for the error caused by the blanking time accurately.

In the thesis, methods for compensating errors caused by the non-ideal valves and by the blanking time for grid-connected PWM converters are dealt with. The goal has been to investigate the influence of the valves and study if small-signal performance can be improved by including feedforward compensation for the errors.

In **Publication C**, it is verified that the dynamic performance can be increased and that the coupling between the *d*- and *q*-directions can be reduced by compensating for the errors caused by the blanking time and non-ideal valves. In the publication, the compensation

function is not used at low currents to avoid erroneous compensation due to the current ripple caused by the PWM.

Publication D shows the influence of the compensation function at different operating points.

In **Publication E**, a compensation method based on prediction is introduced to make it possible to compensate for errors due to the blanking time even at low currents, and in systems with a high current ripple. The phase currents and the currents in the *dq*-frame are shown in the time domain with and without the compensation method based on prediction. The operation of the compensation principle is verified at different operating points, and also at low currents, where the phase currents change signs between the commutations during a large part of the line period.

2.4. Influence of Line Filter

In applications of voltage source converters, two types of line filters are mainly used: the L-filter and the LCL-filter. The L-filter is a first-order filter that is obtained by using a series inductor in each phase. With the L-filter, the switching frequency of the converter has to be high to obtain sufficient attenuation of the harmonics caused by the PWM converter at a reasonable size of the line filter. An LCL-filter is obtained by connecting capacitors in delta- or wye-connection on the line side of the L-filter. Furthermore, inductors are connected on the line side of the capacitors to stop current harmonics from parallel loads from overloading the capacitors of the line filter. The inductors on the line side of the capacitors are also used to tune the resonance frequency of the line filter. Since capacitors are used in the LCL-filter, reactive power is produced. This makes the filter most suitable for applications where the converter system is used to generate reactive power.

The LCL-filter has two main advantages compared to the L-filter. When the LCL-filter is used, the attenuation of the harmonics that are caused by the PWM converter increases at a rate of 60 dB per decade above the resonance frequency in comparison with the increase of 20 dB per decade for the L-filter. This is most advantageous since it makes it possible to obtain sinusoidal line currents even at low and moderate PWM frequencies.

The possibility of using a low inductance in the line filter is the second main advantage of the LCL-filter; if high switching frequencies are used, the total inductance of the line filter can be reduced as compared with the L-filter. In such a system, the transient performance of the converter system can be very high since the dc voltage required for performing current steps is proportional to the inductance of the line filter. When the L-filter is used, the transient response is limited by the inductance required to obtain sufficient attenuation of the harmonics caused by the PWM. The transient response at overmodulation can be optimized to obtain the fastest possible response or to avoid coupling between the *d*- and *q*-directions [34][34]. Moreover, integrator wind-up should be avoided when overmodulation occurs.

Selecting the parameters of an LCL-filter is a complicated task. The resonance frequency should be set to obtain sufficient attenuation of the harmonics caused by the PWM converter. In applications above approximately 500 kVA, the switching frequency should be below approximately 1-2 kHz with the semiconductor valves available today. Therefore, to obtain

sinusoidal line currents, the resonance frequency of the filter should be set to approximately 0.5 to 1 kHz. At more moderate power levels, higher switching frequencies, such as 5 to 10 kHz can be used. In this case, a resonance frequency of a few kHz is appropriate.

The losses in the line-filter inductors, especially in the inductor connected to the converter, are affected by the switching frequency of the PWM converter. If inductors with a low inductance are connected on the converter side of the capacitors, a significant current ripple occurs, and to avoid saturation of the magnetic core, the physical size of the inductors may need to be almost as large as the size of the inductors with a higher inductance.

In addition to the static characteristics, the dynamic performance of the control system is affected by the resonance frequency since it is difficult to obtain a bandwidth above the resonance frequency. Furthermore, harmonic distortion of the grid voltages or current harmonics injected by parallel loads may initiate oscillations between the capacitors of the line filter and the inductance of the line. To avoid oscillations, the resonance frequency of the line filter should be set to a frequency with a low harmonic distortion.

When the L-filter is used, predictive dead-beat vector controllers or hysteresis controllers are usually used. To obtain dead-beat performance, compensation for the time delay of one sampling interval should be incorporated into the controllers. If no compensation is used, an oscillatory behavior is obtained at high gains such as dead-beat gain. In general, prediction methods can be used for the compensation [36][37]. Another solution is to utilize two intervals of PWM during each sampling interval. This facilitates supplying the desired voltage vector within one sampling interval [38]. However, when such a method is used, setting the sampling frequency to twice the switching frequency is not possible.

Control principles for the LCL-filter have been described in a few publications. In [2], different PWM methods and controllers for a VSC connected to the grid by LCL-filters are described. It is concluded that a modulation method with a fixed switching frequency should be used to obtain a stable system, since harmonics at frequencies close to the resonance frequency of the line filter give rise to a nonstable system otherwise.

In [10], the static characteristics of a control principle utilizing space vector modulation, as well as a fuzzy logic controller are compared. It is verified that the fuzzy controller increases the performance compared to the SVM controller. At low loads, a significant current harmonic distortion occur at frequencies of a few hundred Hz when a controller utilizing SVM is applied . These harmonics at low frequencies are significantly reduced by the use of the fuzzy controller. Another advantage of the fuzzy controller is that the calculation time in the digital control system is reduced by 30 % compared to the SVM controller. Moreover, a soft switching VSC is successfully implemented and connected to the grid by an LCL-filter in [10].

A high-performance predictive vector control principle has been presented in [28]. In [28], the controller is used as a tracking controller in the active filtering of current harmonics. Furthermore, a control principle without current sensors has been described in [39].

In this thesis, dynamic performances of converters connected to the grid by the L-filter as well as the LCL-filter are dealt with. An important goal has been to investigate the potential of obtaining a high dynamic performance also for the LCL-filter.

In **Publication C**, the dynamic performance obtained when using an L-filter and a predictive dead-beat current control system is investigated. In the publication, measure small-signal frequency responses for different current controllers of the P- and PI-type are presented.

In **Publication F**, a control principle for the LCL-filter designed to reduce the number of measurements is presented. In this control principle, the inner current loop is used to attenuate oscillations in the capacitor voltage. When this control principle is used, only the currents in the inner current loop and the line voltages are measured. Thus, the number of measurements is the same as for the L-filter. Still, rather a high dynamic performance is obtained, as shown in simulations. Moreover, a method for compensating for the time delay of one sampling interval is introduced. The method uses the prediction of the *d*- and *q*-currents to compensate for the time delay and is based on a dead-beat current response. The method for compensating for the time delay has been used in the measurements in each publication in Part II of the thesis.

In **Publication G**, the capacitor voltages are measured and used to improve the performance as compared with the principle in **Publication F**. Measured small-signal frequency responses are presented for the LCL-filter, as well as for the L-filter with a dead-beat control system. A similar dynamic performance is obtained with the LCL-filter and the L-filter. In the publication, the dynamic performance of the current control systems are also verified by the active filtering of the current harmonics generated by a parallel thyristor rectifier. Furthermore, different principles of active filtering are compared. As shown by measurements, the performance of an active filter is reduced due to phase shifts between the reference current components in the *d*- and *q*-directions and the currents in the *d*-and *q*-directions in the vector control system. The result is also affected by coupling between the *d*- and *q*-directions. As verified by the measurements, by compensating for the phase shifts in the current control system of the VSC, it is possible to implement efficient active filters even when high phase shifts occur in the vector current control system of the VSC.

Chapter 3

Analytical Modeling

In the design of control systems for PWM converters, analytical models are important tools for predicting dynamic performance and stability limits of different control laws and system parameters. This chapter deals with techniques to model vector controlled grid connected VSCs.

3.1. State Space Modeling of VSCs Connected to the Grid

The system to be modeled is described in Fig. 3.1. In the thesis, the inductance L_{grid} is assumed to be zero and the *q*-axis of the *dq*-frame is synchronized to the vector set up by the voltages u_{2a}, u_{2b}, and u_{2c}. If a significant inductance is present, the angle of the *dq*-frame changes rapidly at steps in the line currents, and the inductance L_{grid} should be included in the analytical models.

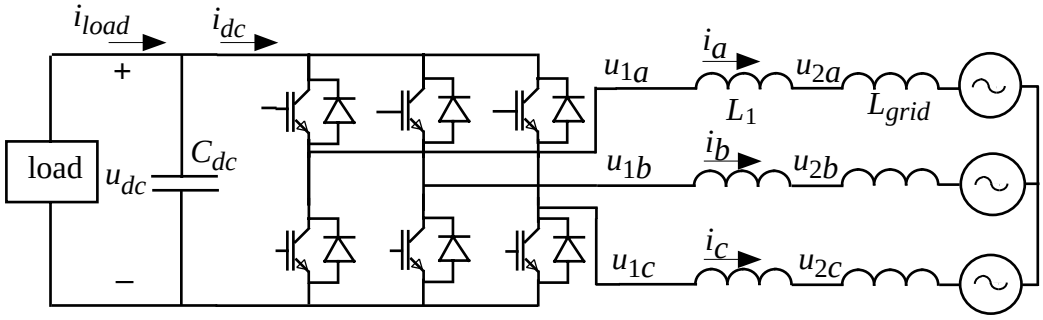

Fig. 3.1. Main circuit of the VSC connected to a three-phase grid.

The ac side of the converter system is modeled by differential equations for each phase. Assuming that the inductors are not saturated and that iron losses and copper losses due to the skin effect can be neglected, the equations for the L-filter are

$$L_1 \frac{di_a}{dt} + R_1 i_a = u_{1a} - u_{2a} \tag{3.1}$$

$$L_1 \frac{di_b}{dt} + R_1 i_b = u_{1b} - u_{2b} \tag{3.2}$$

$$L_1 \frac{di_c}{dt} + R_1 i_c = u_{1c} - u_{2c} \tag{3.3}$$

By using vector notation, these equations can be written in the $\alpha\beta$-frame

$$L_1 \frac{d\underline{i}^{\alpha\beta}}{dt} + R_1 \underline{i}^{\alpha\beta} = \underline{u}_1{}^{\alpha\beta} - \underline{u}_2{}^{\alpha\beta} \tag{3.4}$$

and in the rotating *dq*-frame as

$$L_1 \frac{d\underline{i}^{dq}}{dt} + \left(R_1 + j\omega_g L_1\right)\underline{i}^{dq} = \underline{u}_1{}^{dq} - \underline{u}_2{}^{dq} \tag{3.5}$$

The decoupled equation can be written in the state space form as

$$\frac{d\mathbf{x}_L}{dt} = \mathbf{A}_L \mathbf{x}_L + \mathbf{B}_L \mathbf{u}_L \tag{3.6}$$

where the state vector and the input vector are defined by

$$\mathbf{x}_L = \begin{bmatrix} i_d & i_q \end{bmatrix}^T \tag{3.7}$$

and

$$\mathbf{u}_L = \begin{bmatrix} u_{1d} & u_{1q} & u_{2d} & u_{2q} \end{bmatrix}^T \tag{3.8}$$

respectively. The system matrix and the input matrix are given by

$$\mathbf{A}_L = \begin{bmatrix} -\frac{R_1}{L_1} & \omega_g \\ -\omega_g & -\frac{R_1}{L_1} \end{bmatrix} \tag{3.9}$$

and

$$\mathbf{B}_L = \begin{bmatrix} \frac{1}{L_1} & 0 & -\frac{1}{L_1} & 0 \\ 0 & \frac{1}{L_1} & 0 & -\frac{1}{L_1} \end{bmatrix} \tag{3.10}$$

The state space equation for the ac side of the system is linear for the L-filter. The same applies for the LCL-filter as shown in **Publication G.**

The dc side of the system is modeled by the equation

$$C_{dc} \frac{du_{dc}}{dt} = i_{load} - i_{dc} \tag{3.11}$$

The current in the dc link can be found from the power of the ac side since the power on the dc side must be equal to the power on the ac side of the converter. Here, the losses in the valves are neglected. The instantaneous power on the ac side and the dc side of the converter can be obtained from

$$p_{ac} = \mathrm{Re}\left\{ \underline{u}_1^{\alpha\beta} \underline{i}_1^{\alpha\beta *} \right\} \tag{3.12}$$

and

$$p_{dc} = u_{dc} i_{dc} \tag{3.13}$$

respectively. As shown in Chapter 2, the voltage vector of the converter can be described by a switching function. By inserting (2.10) into (3.12), and setting (3.12) equal to (3.13), the dc current is obtained as

$$i_{dc} = \mathrm{Re}\left\{ \underline{sw}^{\alpha\beta} \underline{i}_1^{\alpha\beta *} \right\} \tag{3.14}$$

which is equal to

$$i_{dc} = sw_\alpha i_\alpha + sw_\beta i_\beta \tag{3.15}$$

where sw_α and sw_β are the α- *and* β-components of the switching vector $\underline{sw}^{\alpha\beta}$. The dc current can also be written in *dq*-coordinates as

$$i_{dc} = sw_d i_d + sw_q i_q \tag{3.16}$$

As a result, a complete state space equation in the *dq*-coordinates for the VSC connected to the grid by the L-filter, can be formed by adding the first order equation

$$C_{dc} \frac{du_{dc}}{dt} = i_{load} - sw_d i_d - sw_q i_q \tag{3.17}$$

to the state space equation (3.6). Thus, the system order is increased by one when the dc side is included in the model. The system is both nonlinear and time variant since switching functions that are functions of the states occur in the system matrix. This is a main drawback since it is much more complex to evaluate the stability and dynamic performance of nonlinear systems [40]. However, a linearized small-signal model can be used to obtain the transfer-function matrix of the linearized system [17]. In the linearized model, the PWM converter is assumed to be linear and the switching behavior of the converter is omitted. As a result, the output vector of the converter is assumed to have a constant amplitude and rotate at a constant angular frequency in steady state. In this case, the components of the switching vector, sw_d and sw_q, are constants and the system can, thus, be linearized in the operating point sw_{d0} and sw_{q0} of the switching vector.

In [17], transfer functions for VSCs are derived for linearized models of the VSC connected to the grid. Transfer function matrices are derived both in the $\alpha\beta$-frame and in the *dq*-frame. The poles of the transfer functions of the linearized model are significantly affected by the operating point. Therefore, the Bode diagrams or the eigenvalues of the linearized system model should be studied at no load and at full load rectifier as well as inverter operations.

The modeling of the closed loop system is a complicated task due to the multiple-input multiple-output (MIMO) structure of the system. In [17], the control system for the dc voltage of a VSC is designed by the use of the transfer function matrices of the linearized system. In this publication, an analog control system is modeled. Therefore, the time delay occurring in a predictive digital control system is not present. Still, the transfer functions become complicated. The gains in the control system were tuned to obtain sufficient amplitude and gain margins in the operating point with the lowest gain and

amplitude margins. The stability of nonlinear control systems should, however, be studied by the use of methods for nonlinear systems in order to guarantee stability not only for small-signal pertubations in the vicinity of the operating point, usually denoted by global stability [40]. Such a technique is utilized in [12].

In the thesis, the dynamic performance of different current control systems are studied by using state space equations. An important objective is to study if the dynamic performance of the current control system can be predicted by using Bode-diagrams of linear analytical models. In each publication in Part II of the thesis, the dc voltage is assumed to be constant or slowly varying, and the equation for the dc voltage is not included in the state space models of the converter system. In the measurements, variations in the dc voltage are compensated in the reference voltages of the PWM. As a result, small variations in the dc voltage do not affect the performance of the current control system.

In **Publication B**, the modeling of the closed-loop converter system by means of a discrete state space equation is described. In the publication, the time-delay of one sampling interval is conveniently taken into account by modeling the converter voltage vector and the time delay of one sampling interval by using state variables. The reference voltage vector from the control system is assumed to be obtained on average during each sampling interval, with a time delay of one sampling interval. Consequently, the errors introduced by the blanking time and the non-ideal valves, as well as the errors introduced by the coordinate transformations are neglected. The state vector of the line filters is expanded with two states, one state for each component of the voltage vector. As a result, the transfer functions for the closed-loop system conveniently can be obtained by the z-transformation of the discrete state space equation, or directly by using the Matlab TM function DBODE, intended for state space models.

In **Publications C**, **D** and **G,** measured small-signal frequency responses are compared with Bode diagrams obtained from an analytical model created by the technique described in **Publication B**. The small-signal frequency responses are affected by the blanking time and the non-ideal valves, and also by the losses in the line filter, still, the measured frequency responses at different operating points are very similar to the Bode diagrams obtained from the linear analytical models. The linearity of the system, however, relies on the linearity of the PWM and that the errors due to coordinate transformations are small. Therefore, the results may be different at lower sampling frequencies.

Chapter 4

Summary of Appended Publications

The publications appended in Part II of the thesis can be divided into three sections. Section one deals with the line interference of PWM converters. In section two, analytical modeling and the influence of nonlinearities on the dynamic performance is on focus. Section three deals with control techniques. In the following, the objectives and the results of the appended publications are summarized.

4.1. Line Interference of PWM Voltage Source Converters

The objective of the publication "Connecting Fast Switching Voltage Source Converters to the Grid — Harmonic Distortion and its Reduction" (**Publication A**) are to describe the consequences of high switching speeds, and to compare the attenuation of the harmonics caused by the PWM converter when the L-filter or the LCL-filter is used. Fast-switching voltage source converters may give rise to significant over voltages at the load connected to the converter. This is verified by measurements of transients at an asynchronous machine connected to the converter by cables of different lengths. Such transients can be avoided by a reduction of the switching speed. As described in the publication, a third-order line filter can be used to obtain a high power quality even at low to moderate switching frequencies.

4.2. Analytical Modeling

In the publication "Analysis and Simulation of Digitally Controlled Grid-connected PWM Converters using the Space-vector Average Approximation" (**Publication B**), a modeling technique based on discrete state-space modeling is presented. The technique is most useful in modeling of the closed loop converter system with a time-delay of one sampling interval due to the sampled control system. By modeling the converter system in the rotating *dq*-frame, a linear time-invariant analytical model is obtained. In the model, the converter is modeled by using the space-vector average approximation. The publication shows the influence of the space-vector approximation by using simulations.

The objectives of the publication "Influence of Non-linearities on the Frequency Response of a Grid-connected Vector-controlled VSC" (**Publication C**) are to study the influence of nonlinearities on the performance of the control system and the accuracy of linear analytical models. It is most difficult to verify the dynamic performance of PWM converter systems in the time domain. Therefore, a small-signal analysis is used for this purpose. Small-signal transfer functions of gain and coupling for the vector current control system are displayed. In the evaluation of the dynamic performance of the current control system, frequencies up to 1 kHz are considered. The accuracy of the analytical models are described by comparing measured small-signal frequency responses with Bode diagrams from analytical models. One conclusion from the transfer functions is that space-vector averaging can be used in modeling the investigated closed-loop converter system.

In the literature, losses in the line filter and their effect on dynamic performance are usually not described. In **Publication C**, it is also shown that dynamic performance is affected by the losses in the line-filter inductors. Furthermore, it is verified that an improved dynamic performance and reduced coupling between the control of the *d*- and *q*-components of the current vector can be obtained by compensating for nonlinearities caused by the blanking time and non-ideal semiconductor valves.

The influence of the losses in the line-filter is further described in the publication "Vector Current Controlled Grid Connected Voltage Source Converter — Influence of Nonlinearities on the Performance" (**Publication D**). Measured small-signal frequency responses are presented for two different line-filter inductors. As shown, a more ideal response is obtained by using inductors with low iron losses. To verify that the LTI analytical model is valid for different operating points, small-signal frequency responses are presented at four different operating points representing rectifier, as well as inverter, operation. At each operating point, experimental results are presented with and without the compensation for the nonlinearities caused by the blanking time and non-ideal semiconductor valves. As reported, the compensation function improves the performance at each operating point. The small-signal responses are similar at the different operating points. An important result of this is that the performance of current control systems can be predicted by the analytical model both in inverter as well as in rectifier operation.

4.3. Control Techniques

As shown in **Publications C** and **D**, the dynamic performance of PWM converters can be improved by compensating for the nonlinearity caused by the blanking time and non-ideal valves. Such a compensation is based on the sign of the phase currents. When the phase currents are close to zero, the sign of the current at the commutations may be different from the sign at the samples, and an accurate compensation principle has to apply a prediction method to compensate for the error caused by the blanking time.

In the publication "A Method to Compensate for Errors Caused by the Blanking Time in PWM Systems with High Ripple Currents" (**Publication E**), a method for predicting the signs of the phase currents at the commutations is introduced. Experimental results are presented with and without the compensation method. The focus is on the line-current distortion and static errors introduced in the vector control system. As shown in the publication, the static errors caused by the blanking time and non-ideal valves can be avoided by using the compensation method. The principle makes it possible to apply compensation even at low phase currents, and when small line filters or low switching frequencies resulting in high current ripples are used.

In power electronic systems, the number of measurements contributes to the cost of the system. With the principle proposed in the publication "Feed Forward — Time Efficient Control of a Voltage Source Converter Connected to the Grid by Lowpass Filters" (**Publication F**), only one third of the states are measured. Still, rather a high bandwidth can be obtained. The principle is an alternative to the reduction of measurements by using estimation. When the principle is used, the number of measurements in the control system become the same as for the L-filter. The publication

also presents a method for compensating for the delay time of one sampling interval introduced by the sampled control system.

In the publication "Control of a Voltage-source Converter Connected to the Grid through an LCL-filter — Application to Active Filtering" (**Publication G**), a control principle for the LCL-filter is introduced. The dynamic performance of a converter connected to the grid through two different line filters is compared. As shown in measured frequency responses, the dynamic performance obtained when the LCL-filter is used is similar to that of the L-filter. The current harmonic distortion in the line currents, due to the PWM, is significantly lower for the LCL-filter.

Publication G also describes the influence of the active filtering principle on the control system. When a direct method is used, the active filter tries to compensate for all harmonics based on the instantaneous active and reactive currents. When such a method is used, high derivatives occur in the control system for the active filter. As shown in measurements, these derivatives saturate the controller in the *q*-direction.

By using a Fourier method, the saturation can be avoided solely by only including the low-frequency components in the references for the active filter. In addition, a flexible compensator is obtained since individual harmonics can be compensated separately. Furthermore, when the Fourier method is used, the compensation for phase shifts in the current control system is done in the frequency domain. Another advantage obtained by the use of the Fouriermethod is that dead-beat control does not have to be applied, which is the case if the phase shifts in the current control system are compensated in the time domain. The compensation can also be based on measured frequency responses, which makes it feasible to apply individual compensation in the *d*- and *q*-directions.

By compensating for phase shifts, it is possible to operate even at low switching and sampling frequencies, which is a major advantage at high power levels and for the LCL-filter.

Chapter 5

Conclusions

As shown in this thesis, PWM converters can be used to obtain a high power quality and dynamic performance of ac to dc converters. Compared with line-commutated converters, the harmonic distortion of the line currents is very low and it is fair to say that sinusoidal line currents can be obtained. Another important advantage of PWM converters as compared with line-commutated converters is that the active and reactive powers can be independently controlled, thus a unity power factor can be obtained. Moreover, by using high performance vector control systems, PWM converters can be used in new applications, such as active filtering, where the controllability of the PWM converter is utilized to compensate for harmonic currents that are injected into the grid by nonlinear loads.

The power quality of a PWM converter depends on the switching frequency and on the line filter that is connected between the converter and the grid. As shown in the thesis, it is advantageous to use LCL-filters since sinusoidal line currents can be obtained even at low and moderate switching frequencies, such as 5 to 7 kHz. It is also verified that a high dynamic performance can be obtained with the LCL-filter. A control principle for the LCL-filter resulting in a high dynamic performance is developed. Experiments have shown that the small-signal dynamic performance is rather close to the small-signal dynamic performance when using a dead-beat controller for the L-filter. One drawback of the LCL-filter as compared with the L-filter is that the control system becomes more expensive if each current and voltage are used in the control. To avoid an increased cost, a method resulting in the same number of measurements as with the L-filter has been developed.

The dynamic performance of a vector control system is affected by nonlinearities that may occur due to the PWM method, due to coordinate transformations in the control system, and due to the non-ideal converter. These nonlinearities depend on the switching and sampling frequency. In the thesis, switching frequencies from 5 to 7 kHz are used. At such switching and sampling frequencies, nonlinearities and cross couplings caused by the uniform PWM method and by coordinate transformations, do not have a significant effect of the small-signal frequency responses for frequencies below 1.2 kHz.

The nonlinearities due to the blanking time between the switch-off of one valve in a phase leg, and the turn-on of the other valve in a phase leg, introduce an error that affects the small-signal dynamic performance. In the thesis, a method for compensating for the blanking time and non-ideal vales is developed. As shown in experimental results, a more ideal small-signal frequency response is obtained by using the compensation method.

Moreover, in the measured frequency responses, small errors are introduced by losses in the line filter. Experimental results show that the nonlinearity due to the losses in the line filter is reduced when inductors with lower iron losses are used.

A method to model switching PWM converters by using discrete state space models is described and utilized in the design of control principles for the L-filter as well as the LCL-filter. As shown in Bode diagrams and measured small-signal frequency responses, the small-signal dynamic performance can be predicted rather accurately from the Bode diagrams obtained from analytical models.

In a vector control system used for the active filtering of harmonic currents, the performance of the active filter is affected by the phase shifts in the current control system, and by the cross coupling between the control of the active and the reactive currents. If a direct method is used, it is possible to compensate for the phase shifts if a dead-beat performance is obtained in the current control system of the PWM converter. By using a Fourier method, it is possible to compensate for the phase shifts even when a dead-beat performance is not obtained. This is most advantageous since it makes active filtering possible even when the LCL-filter is used. Furthermore, the compensation can be based on measured small-signal frequency responses. By compensating for phase shifts, it is possible to obtain high-performance active filtering even at moderate switching frequencies.

References

[1] H. Mao, D. Boroyevich, and F. C. Lee, "Novel Reduced Order Small-Signal Model of a Three-Phase PWM Rectifier and Its Application in Control Design and System Analysis," *IEEE Transactions on Power Electronics,* Vol. 13, No. 3, May 1998, p. 511-521.

[2] A. M. Hava, T. A. Lipo, and W. L. Erdman, "Utility Interface Issues for Line Connected PWM Voltage Source Converters: A Comparative Study," *IEEE Applied Power Electronics Conference (APEC'95),* Dallas, USA, March 5-9, 1995, Vol. 1, p. 125-132.

[3] D -C. Lee, G -M. Lee, D -H. Kim, "Multivariable State Feedback Control for Three-Phase Power Conversion Systems," *7th European conference on power Electronics and Applications (EPE'97),* Trondheim, Norway, September 8-10, 1997, Vol. 1. p. 1348-1353.

[4] S. Fukuda, "LQ Control of Sinusoidal Current PWM Rectifiers," *IEE Proc. Power Appl.,* Vol. 144, N0. 2, March 1997.

[5] A. W. Green and J. T. Boys, "Hysteresis Current-forced Three-phase Voltage-source Reversible Rectifier," *IEE PROCEEDINGS,* Vol. 136, Pt. B, No. 3, May 1989.

[6] P. Doulai and G. Ledwich, "Co-ordinated Three-phase Hysteretic-control Scheme for Active Power Filtering," *IEE PROCEEDINGS-B,* Vol. 139, No. 5, September 1992.

[7] S. Bhowmik, A. van Zyl, R. Spée, and J. R. Enslin, "Sensorless Current Control for Active Rectifiers," *IEEE Transactions on Industry Applications,* Vol. 33, No. 3, May/June 1997, p. 765-772.

[8] B -R. Lin, "Power Converter Control Based on Neural and Fuzzy Methods," Journal on Electric Power Systems Research, Vol. 35, 3, December 1995.

[9] T. Noguchi, H. Tomiki, S. Kondo, and I. Takahashi, "Direct Power Control of PWM Converters Without Power-Source Voltage Sensors," *IEEE Transactions on Industry Applications,* Vol. 34, No. 3, May/June 1998, p. 473-479.

[10] S. Saetieo, *Current Control Techniques for Three Phase Power Converters,* Rensselaer Polytechnic Institute, Troy, New York, 1997.

[11] S. Guffon, A. Toledo, S. Bacha, G. Bornard, "Indirect Sliding Mode Control of a Three-Phase Active Power Filter," *IEEE Power Electronics Specialists Conference, (PESC-98*), Fukuoka, Japan, May 17-22, 1998, Vol. 2. p. 1408-1414.

[12] H. Kömürcügil and O. Kükrer, "Lyaponov-Based Control for Three-Phase PWM AC/DC Voltage-Source Converters," *IEEE Transactions on Power Electronics,* Vol. 13, No. 5, September 1998, p. 801-813.

[13] W. V. Lyon, *Transient Analysis of Alternating-Current Machinery,* M.I.T. Press and John Wiley, N.Y. 1954.

[14] R. P. Kovacs, J. Racz, *Transiente Vorgänge in Wechselstrommaschinen*, Ung. Akad. d. Wissenschaften, Budapest 1959.

[15] H. Akagi, Y. Kanazawa, A. Nabae, "Instantaneous Reactive Power Compensators Comprising Switch Devices without Energy Storage Components," *IEEE Transactions on Industry Applications*, Vol. IA-20, No. 3, May/June 1984, p. 625–630.

[16] P. Hsu and M. Behnke, "A Three-Phase Synchronous Frame Controller for Unbalanced Load," *IEEE Power Electronics Specialists Conference, (PESC-98*), Fukuoka, Japan, May 17-22, 1998, Vol. 2. p. 1369-1374.

[17] J. Ollila, *Analysis of PWM-converters Using Space vector theory: application to a voltage source rectifier*, Jaakko Ollila- Tampere University of Technology, Tampere, 1993.

[18] J. Svensson, "Synchronization Methods for Grid Connected Voltage Source Converters," to appear in *IEE Proceedings of Electric Power Applications*.

[19] S. R. Bowes, "New Sinusoidal Pulsewidth-modulator Inverter," *Proc. IEE*, Vol. 122, No. 11, November, 1975, p. 1279-1285.

[20] H. S. Black, *Modulation theory* , Van Nostrand, Princeton, N.Y, 1953.

[21] N. Mohan, T. Undeland, W. Roberts, *Power Electronics: Converters, Applications, and Design*., John Wiley & Sons, 1989.

[22] S. Salama, Y. Tadros, "Quasi Resonant 3-phase IGBT Inverter," *IEEE Power Electronics Specialists Conference (PESC'95)*, Atlanta, USA, June 18-22, 1995, Vol. 1, p. 28-33.

[23] S. M. Nielsen, F. Blaabjerg, and J. K. Pedersen, "A new robust and simple three-phase resonant converter," 1997 *IEEE Industry Applications Conference*, Vol. 2 p. 1667-1672.

[24] M. D. Bellar, T -S. Wu, A. Tchamdjou, J. Mahdavi, and M. Ehsani, "A Review of Soft-Switched DC-AC Converters," *IEEE Transactions on Industry Applications*, Vol. 34, No. 4, July/August 1998, p. 847-860.

[25] R. L. Kirlin, S. F. Legowski, and A. M. Trzynadlowski, "An Optimal Approach to Random Pulse Width Modulation in Power Inverters," *IEEE Power Electronics Specialists Conference (PESC'95)*, Atlanta, USA, June 18-22, 1995, Vol. 1, p. 313-318.

[26] M. Bech, J. K. Pedersen, and F. Blaabjerg, "A Methodology for true Comparison of Analytical and Measured Frequency Domain Spectra in Random PWM Converters," *IEEE Power Electronics Specialists Conference, (PESC-98*), Fukuoka, Japan, May 17-22, 1998, Vol. 2. p. 1408-1414.

[27] J. Holtz, "Pulsewidth Modulation for Electronic Power Conversion," Proceedings of the IEEE, Vol. 82, No.8, p. 1194-1214, 1994.

[28] T. Svensson, *On Modulation and Control of Electronic Power Convertors*, Chalmers University of Technology, Sweden, Technical Report No. 186, 1988.

[29] A. Trzynadlowski and S. Legowski, "Minimum-Loss Vector PWM Strategy for Three-Phase Inverters," *IEEE Transactions on Power Electronics*, Vol. 9, No. 1, January 1994, p. 26-34.

[30] F. R. Walsh, J. F. Moynihan, P. J. Roche, M. G. Egan, J. M. D. Murphy, "Analysis and Influence of Modulation Scheme on the Sizing of the Input Filter in a PWM Rectifier System," *7th European Conference on Power Electronics and Applications (EPE'97)*, Trondheim, Norway, September 8-10, 1997, Vol. 2. p. 929-933.

[31] M. Bojrup, P. Karlsson, M. Alaküla, B. Simonsson, "A Dual Purpose Battery Charger for Electric Vehicles, " *IEEE Power Electronics Specialists Conference, (PESC-98*), Fukuoka, Japan, May 17-22, 1998, Vol. 1, p. 565-570.

[32] S. Hiti, D. Boroyevich, "Small-Signal Modeling of Three-Phase PWM Modulators," *IEEE Power Electronics Specialists Conference (PESC'96)*, Baveno, Italy, June 23-27, 1996, Vol. 1, p. 550-555.

[33] J. K. Pedersen, F. Blaabjerg, J. W. Jensen, P. Thogersen, "An Ideal PWM-VSI Inverter with Feedforward and Feedback Compensation," *5th European Conference on Power Electronics and Applications (EPE'93)*, Brighton, England, September 13-16, 1993, Vol. 5, p. 501-507.

[34] A. M. Hava, R. J. Kerkman, and T. Lipo, "Carrier-Based PWM-VSI Overmodulation Strategies: Analysis, Comparison, and Design," *IEEE Transactions on Power Electronics*, Vol. 13, No. 4, July 1998, p. 674-689.

[35] R. Ottersten and J. Svensson, "Vector Current Controlled Voltage Source Converter – Deadbeat Control and Overmodulation Strategies," 1998 IEEE Nordic Workshop on Power and Industrial Electronics, Espoo, Finland, August 26-27, 1998, Vol. 1, p. 65-70.

[36] J. E. Marshall, *Control of time-delay systems*. IEE Control Engineering Series; 10. Institution of Electrical Engineers, London and New York, 1979.

[37] J. W. Lee, "An Intelligent Current Controller Using Delay Compensation for PWM Converters," *7th European conference on Power Electronics and Applications (EPE'97)*, Trondheim, Norway, September 8-10, 1997, Vol. 1. p. 1342-1346.

[38] T. Kawabata, T. Miyashita, Y. Yamamoto, "Dead Beat Control of Three Phase PWM Inverter," *IEEE Transactions on Power Electronics*, Vol. 5, no. 1, January 1990, p. 21-28.

[39] J. Ollila, "A PWM-Rectifier without Current Measurement," *EPE Journal*, Vol. 4, No. 2, June 1994, p. 14-19.

[40] J -J. Slotine and W. Li, *Applied Nonlinear Control*, Englewood Cliffs, NJ: Prentice-Hall, 1991.

Part II
Appended Publications

Publication A

M. Lindgren, J. Svensson, "Connecting Fast Switching Voltage Source Converters to the Grid — Harmonic Distortion and its Reduction," *IEEE Stockholm Power Tech Conference*, Stockholm, Sweden, June 18-22, 1995, Proceedings of Power Electronics, p. 191-195.

Edited version.

Connecting Fast Switching Voltage-source Converters to the Grid — Harmonic Distortion and its Reduction

Michael Lindgren M. Sc. Jan Svensson M. Sc.

Department of Electrical Machines and Power Electronics
Chalmers University of Technology
S-412 96 Gothenburg, Sweden

Abstract: In this paper, harmonic distortion of fast switching pulse width modulated (PWM) converters connected to the grid is addressed. The origin of harmonic distortion and methods to reduce it are presented. Due to high voltage derivatives, Electro Magnetic Interference (EMI) and insulation stress on the transformer connected to the converter occur. To reduce the distortion, a third order LCL-filter is proposed. It is compared with a first order L-filter. A major advantage of the LCL-filter compared with the L-filter is that the switching frequency of the converter can be significantly decreased. This facilitates reduction of the switching speed of the semiconductor valves, such a step reduces voltage derivatives. In addition, if the plant is to be used for Static Var Compensation (SVC), the system cost can be decreased.

I. Introduction

In converter systems based on fast switching semiconductors, PWM is adopted. In this case, the order of the harmonics injected to the grid can be affected by a proper choice of switching frequency. However, harmonics are still present.

To obtain a sinusoidal current, filters are used. If the converter is connected to the grid by a transformer, the leakage inductance provides filtering. However, to obtain a low current harmonic distortion, the switching frequency has to be set very high, (above 10 kHz). To facilitate this switching frequency, the power semiconductors have to be rapidly switched. This is a drawback since fast switching gives rise to high voltage derivatives in the converter output voltage. High voltage derivatives give rise to electro magnetic interference, (EMI). In addition, if the converter is connected to the transformer by a long cable, the insulation stress is further increased due to reflections [1].

An alternative solution to reduce both voltage- and current harmonic distortion is to use a low-pass LCL-filter [2]. A major advantage of the LCL-filter compared with the L-filter is that a low current harmonic distortion can be obtained at low switching frequencies. This increases the efficiency of the converter and reduces the high frequency distortion caused by the switching of the semiconductors. It is also an advantage in high power applications where it is hard to reach switching frequencies above a few kHz.

II. Origin of Harmonics

In power converters, the semiconductors are used as controlled switches. The component current and voltage are high simultaneously during switching only. This is the principle of PWM. A commonly proposed principle to connect a voltage source converter (VSC) to

the utility grid is illustrated in Fig. 1. The resistive parts have been neglected. L is the filter inductance and L' the equivalent inductance of the grid. The voltages u_{1a}, u_{1b} and u_{1c} are the phase voltages of the converter. The voltages u_{2a}, u_{2b} and u_{2c} are the phase voltages in the so called point of common connection, (PCC). The result of the PWM is displayed in Fig. 2. The fundamental converter phase voltage, u_{1a}, is equal to the phase voltage of the grid, u_{2a}. Consequently, the fundamental current is zero. As displayed, a harmonic current occurs due to the PWM. The switching frequency is 1 kHz and the grid frequency is 50 Hz.

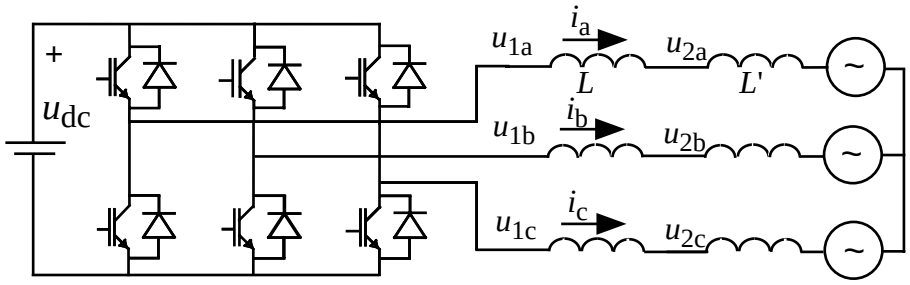

Figure 1: VSC connected to the grid by L-filter.

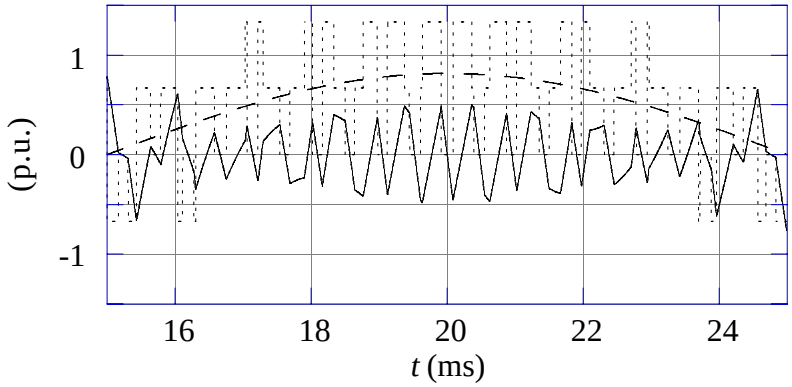

Figure 2: Converter phase voltage (dotted), grid phase voltage (dashed) and resulting phase current (solid).

A. Low and Medium Frequency Harmonics

The harmonic content of the converter output voltage can cause current and voltage harmonic distortion. If an L-filter is used, the voltage harmonic distortion in the point of common connection is determined by

$$\frac{u_2(\mathrm{n})}{u_1(\mathrm{n})} = \frac{L'}{L'+L} \tag{1}$$

This relation is valid below approximately 15 kHz. As well known, the equivalent inductance depends on the short circuit power of the grid. The equivalent reactance of the grid at the low voltage side of the transformer is

$$x_{L2'} = \left(\frac{u_{\mathrm{lo}}{}^2}{S_{\mathrm{KN}}}\right) \tag{2}$$

where u_{lo} is the nominal low voltage of the transformer and S_{KN} is the short circuit power of the grid. The base impedance

$$z_{base} = (\frac{{u_{lo}}^2}{S_{NT}}) \tag{3}$$

where S_{NT} is the rated power of the transformer is used. Thus, the equivalent reactance in p.u. is

$$x_{L_{2'}} = (\frac{S_{NT}}{S_{KN}}) \tag{4}$$

Usually the short circuit power is above 50 MVA. In a converter system installation based on fast switching semiconductors, the power is limited to about 1 MVA. This would give an equivalent grid reactance of 0.02 p.u. Assumed the converter voltage harmonic distortion in Fig. 3, the maximum voltage harmonic distortion is 5.7 %.

In Fig. 3, the ideal harmonic phase voltage spectra of a commonly proposed PWM method, 3rd harmonic injection PWM, is presented. The dc-voltage is $1.5U$, where U is the grid line to line voltage. U is defined as 1 p.u. The modulation index, M is one. M is defined by

$$M = \frac{u(1)}{u(1)_{max}} \tag{5}$$

where $u(1)_{max}$ is the maximum fundamental converter phase voltage. As presented in [3], the voltage harmonics of the lowest frequency occur at frequencies

$$f_{1,2} = (p \pm 2n_1) \tag{6}$$

where p is the frequency ratio defined as

$$p = \frac{f_{mod}}{f_1} \tag{7}$$

and $n_1 = 1,2,3$. Further on, the modulation frequency and fundamental frequency are denoted f_{mod} and f_1. As displayed in Fig. 3, there are also voltage harmonics at frequencies close to multiples of p. The corresponding current harmonic spectra is presented in Fig. 4. The current harmonic distortion is determined by

$$\frac{i_n}{u_{1n}} = \frac{1}{n\omega_1(L' + L)} \tag{8}$$

where $\omega_1 = 2\pi f_1$ rad/s. The inductive reactance of the filter, x_L, is 0.05 p.u. The grid inductance, L', is assumed to be zero (very high ratio of the grid short circuit power and the rated power of the transformer). As displayed, the high order converter phase voltage harmonics are efficiently attenuated.

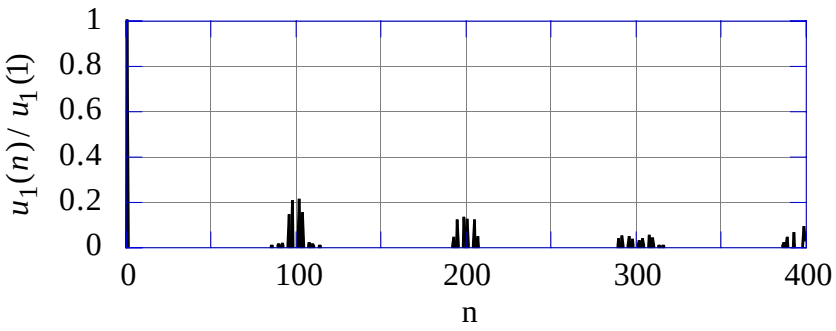

Figure 3: Ideal harmonic phase voltage spectra of 3rd harmonic injection PWM, p= 100 and u_{dc}= 1.5 p.u.

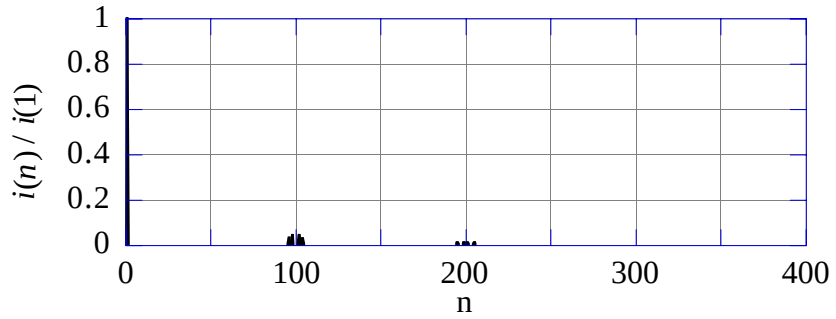

Figure 4: Ideal harmonic current spectra of 3rd harmonic injection PWM. L-filter, x_L= 0.05 p.u., p= 100 and u_{dc}= 1.5 p.u.

Ideally no low order harmonics should occur. In a real system, low order harmonics may occur due to dc-voltage fluctuations and non ideal switching. In Fig. 5, the voltage spectra of an IGBT converter is presented. An analogue Quasine modulator is used and the switching frequency is 4.9 kHz. The properties of Quasine modulation are described in [3]. As displayed, no low order harmonics occur. This is obtained if the commutation time is small in comparison to the period time of the PWM. This usually applies to IGBT converters.

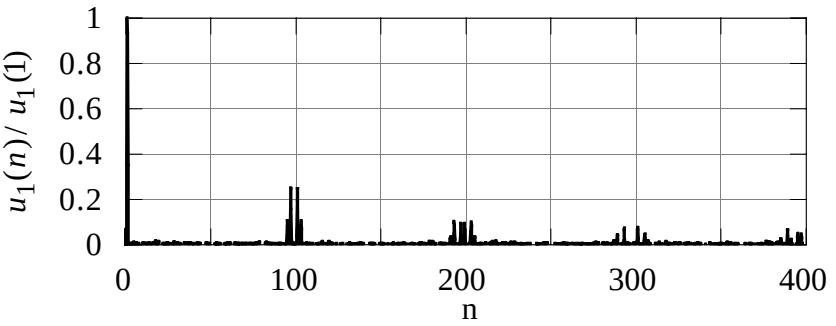

Figure 5: Measured harmonic phase voltage spectra of an IGBT converter, M= 1.

The amplitude of the voltage harmonics in the converter output depends on the ratio of the dc-voltage and the fundamental output voltage. It is thus important to use a PWM-method that can deliver as high output voltage as possible. The method 3rd harmonic injection PWM provides a maximum fundamental line to line voltage of $u_{dc} / \sqrt{2}$ V. Thus, at steady state a dc-voltage of $\sqrt{2}\ U$ is sufficient. However, to obtain high band width the dc-voltage has to be set higher. As presented in [4], the requested dc-voltage depends on the inductance of the grid-filter. The dc-voltage is usually not set above 2*U*.

The dc-voltage influence on current harmonic distortion is displayed in Fig. 6. The current is presented in the rotating *dq*-frame and an L-filter is used. In this frame, a fundamental current is represented as a dot. Consequently, each deviation from the point (0,1) corresponds to a harmonic current. As illustrated, the quadrature ripple is strongly dependent on the dc-voltage. Since quadrature ripple gives rise to active power ripple, the dc-voltage should be set as low as possible. This is also an advantage since the voltage derivative is reduced.

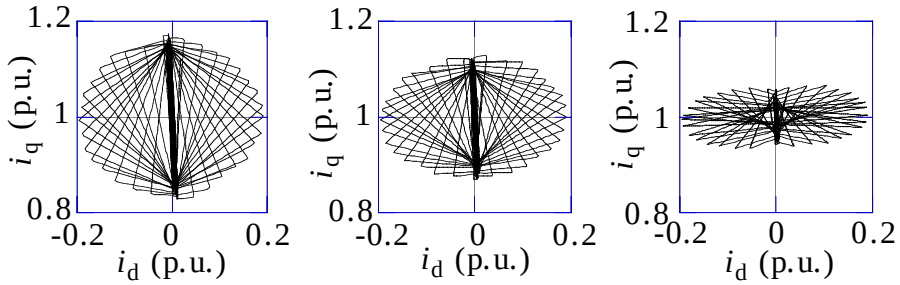

Figure 6: Current vectors at different dc-voltages. i_d is the direct and i_q the quadrature current. u_{dc}= 2.5 p.u. (left), u_{dc}= 2 p.u. (middle) and u_{dc}= 1.5 p.u. (right). L-filter with p= 100 and x_L= 0.05 p.u.

B. Harmonic Distortion above 100 kHz

Harmonic distortion at frequencies above 100 kHz occur due to high voltage derivatives in the converter output voltage. The voltage derivatives give rise to insulation stress and electro magnetic interference (EMI). EMI occur due to each switching and is proportional to the switching frequency. In commercial converters, voltage derivatives are usually limited to reduce these phenomena. Reduction is obtained by slower switching of the semiconductors. Unfortunately, this increases the switching losses. An alternative method often addressed in papers [5] is to perform zero voltage switching (ZVS). Such a step also facilitates increased switching frequency since the switching losses are considerably reduced. Disadvantages are that the dc-link of the converter becomes complex and expensive and the control more advanced.

If long cables are used, reflections may occur at the load connected to the converter. Such reflections are avoided if the voltage pulse rise time is much longer than the wave travelling time on the cable between the converter and the load. In Fig. 7, the equivalent circuit of the converter, cable and the load is displayed.

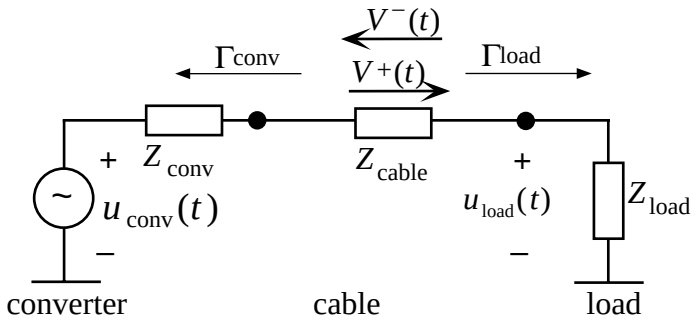

Figure 7: Equivalent circuit of converter, cable and load.

The load reflection coefficient is

$$\Gamma_{load} = \frac{Z_{load} - Z_{cable}}{Z_{load} + Z_{cable}} = \frac{V^-}{V^+} \tag{9}$$

Z_{load} and Z_{conv} denotes the wave impedance of the load and the converter. Z_{cable} is the characteristic impedance of the cable. If the cable is open the Z_{load} is infinite yielding Γ_{load} is 1. The impedance Z_{conv} is almost zero, thus Γ_{conv} is –1. The reflection coefficient is approximately the same for an inductor, induction motor or a transformer. The voltage at a specific point at the cable, for example at the load, can be divided into two travelling voltage waves, V^+ and V^- according to

$$u_{load} = V^+(t) + V^-(t) \tag{10}$$

At each switching of a semiconductor, a voltage travelling wave V^+ occurs. The amplitude of the wave is u_{dc}. Due to the reflection at the load, the load voltage is amplified. The reflected wave changes sign at the converter, thus, after twice the wave travelling time between the load and the converter, τ, the load voltage will start to decrease. The maximum load voltage, $2u_{dc}$ is obtained if the wave travelling time is equal to twice the rise time of the converter voltage. The travelling voltage wave is damped out due to cable losses.

To verify that the combination long cables and fast switching semiconductors give rise to voltage stress on the load connected to the converter, measurements have been carried out. In Fig. 8 a positive line to line voltage pulse at the terminal of the converter is shown. As displayed in Fig. 8, the voltage pulse rise time is approximately 0.35 μs. In Fig. 9, Fig. 10 and Fig. 11, the voltage pulses using open cable and installed motor are displayed at cable length 5, 20 and 32 meters. The wave travelling times are 0.03 μs (5 meter), 0.13 μs (20 meter), 0.20 μs (32 meter).

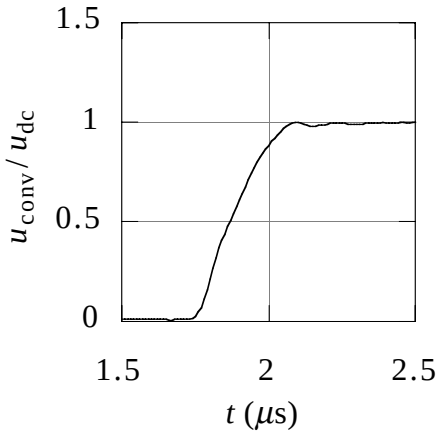

Figure 8: Line to line voltage pulse directly at converter terminals.

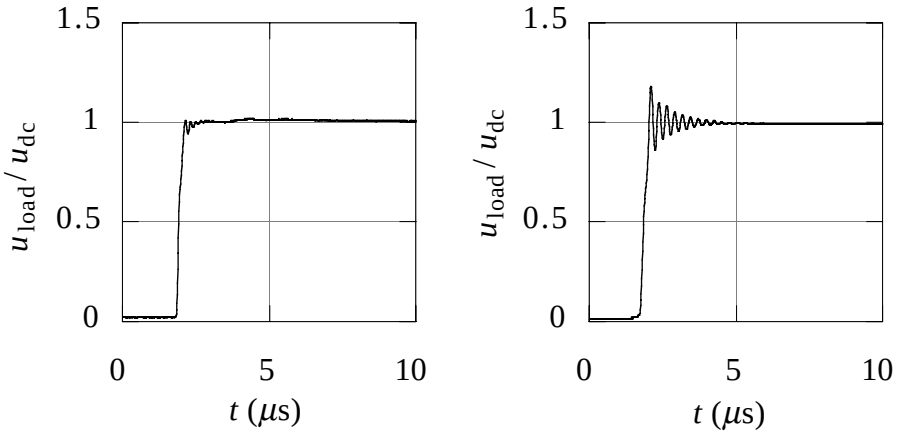

Figure 9: Line to line voltage pulse using a 5 meter cable. Open cable (left) and at machine terminals (right).

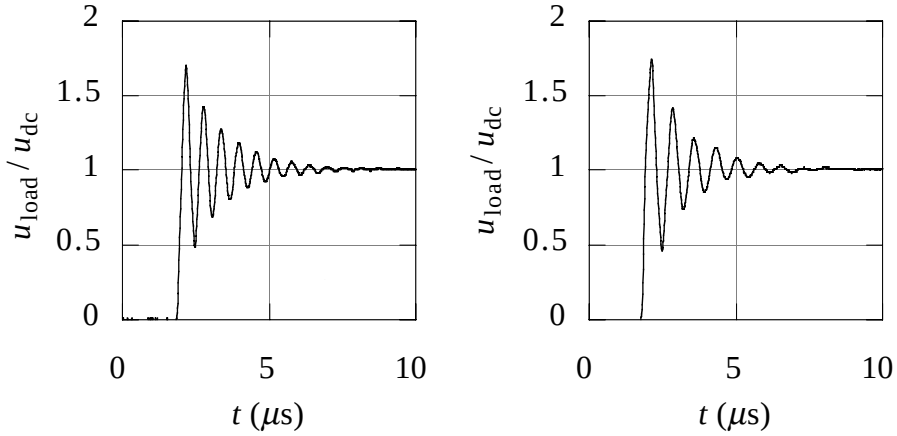

Figure 10: Line to line voltage pulse using a 20 meter cable. Open cable (left) and at machine terminals (right).

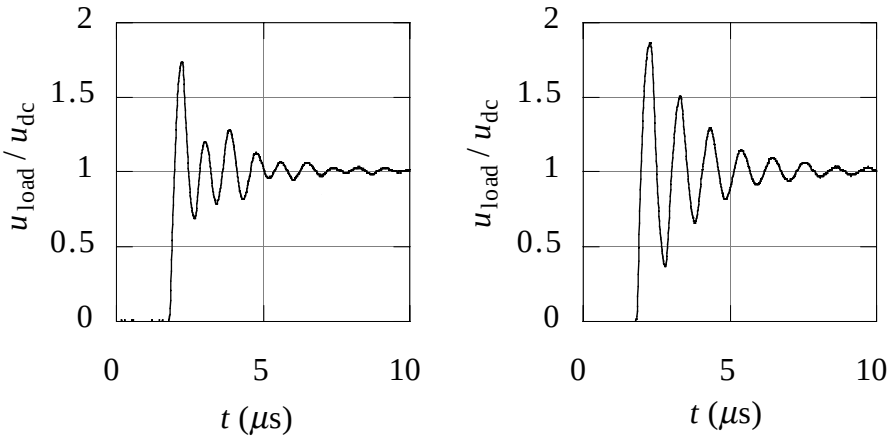

Figure 11: Line to line voltage pulse using a 32 meter cable. Open cable (left) and at machine terminals (right).

In the open cable case, the period time of the resonance frequency corresponds to the wave travelling time. As displayed, the resonance frequency of the load voltage is decreased when the motor is connected compared with an open cable. With motor installed, the reflection occur in the stator winding. This results in increased wave travelling time, thus a lower resonance frequency compared with open cable. The wave velocity is 160 m/µs. The critical cable length is 28 meters, at this length, the peak overvoltage occurs.

III. Filtering Harmonics

Filters are used to reduce the harmonic content of the current injected to the grid. In this section, the L- and the LCL-filter are compared from a filtering point of view. Since the grid always provides inductance, a regular LC-filter becomes an LCL-filter. The configurations are displayed in Fig. 12. As illustrated in Fig. 13, in the LCL-filter case at the resonance frequency, a peak occurs in the transfer function. To assure that the converter does not supply harmonics at the resonance frequency, the PWM has to be accurate.

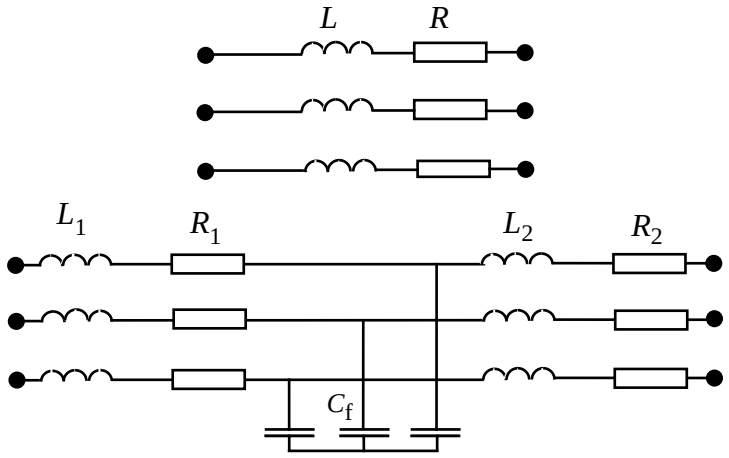

Figure 12: L- and LCL-filter scheme.

In the filters, separate inductors or the transformer leakage inductance can be used. Advantages of including a transformer is that it facilitates supplying non symmetrical loads demanding a zero order current and that it supplies galvanic insulation. If a transformer is included, the inductive reactance is fixed in the range of 4-6 %, here it is assumed to be 5%.

The attenuation of the LCL-filter is determined by the resonance frequency

$$f_{\text{res}} = \frac{1}{2\pi}\sqrt{\frac{L_1 + L_2}{L_1 L_2 C_{\text{f}}}} \tag{11}$$

In Fig. 13, the L- and the LCL-filter attenuation of harmonic distortion is illustrated. The objective is to obtain an attenuation of 20 dB. The total inductive reactance of the L- and LCL-filter are assumed to be 0.075 p.u. The equivalent inductance of the grid is assumed to be a part of the inductance L and L_2 respectively. The capacitive reactance is 10 p.u., thus 0.1 p.u. reactive current is produced by the filter capacitors. If the plant is to be used for SVC, this total cost is decreased compared with switched reactive power. The capacitors should be set to fulfill the average demand for reactive power.

The cross over frequency of the filter is 1258 Hz. As displayed, an attenuation of 20 dB is obtained at frequencies of 7 kHz for the L-filter and 2.4 kHz for the LCL-filter. Consequently, the requested switching frequency is 7 kHz with the L-filter and 2.4 kHz with the LCL-filter. Using these parameters gives the grid current vectors displayed in Fig. 14. In applications where dynamic performance is requested, the voltage has to be set above 1.5 p.u. Here it is assumed to be 2 p.u.

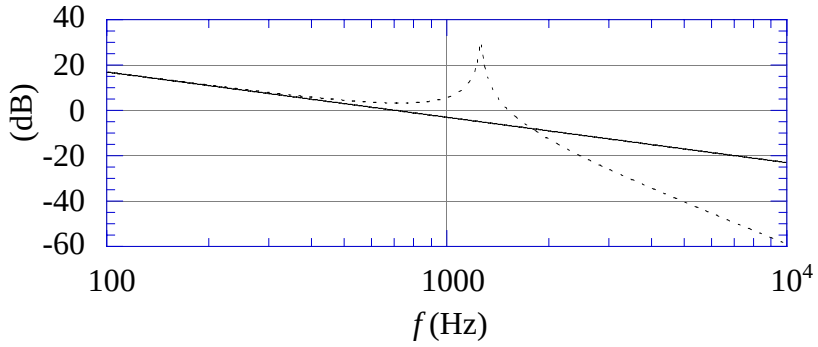

Figure 13: Transfer function from converter phase voltage to line current. L-filter (solid) and LCL-filter (dotted).

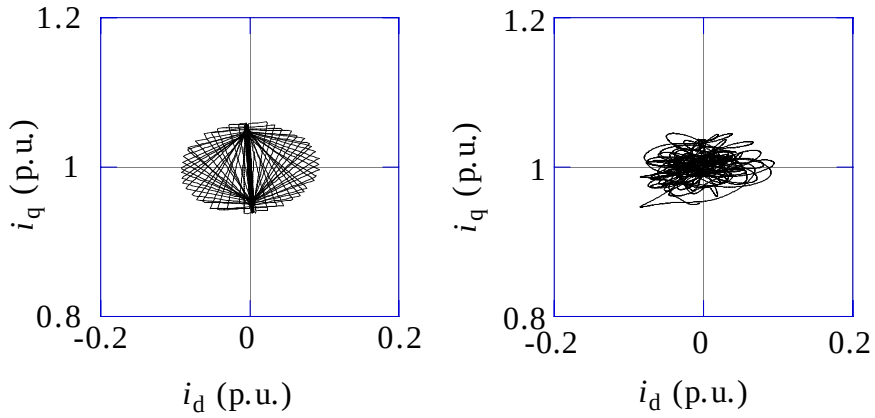

Figure 14: Current vectors. L-filter p= 140 (left) and LCL-filter with p= 48 (right).

IV. Conclusions

Harmonic distortion of fast switching converters is presented. The voltage harmonic distortion in the point of common connection is usually very low. This applies if the converter rated power is low compared with the short circuit power of the grid. If a standard transformer is used for filtering, to obtain sufficiently low current harmonic distortion, the switching frequency has to be set high. This is a drawback since very fast switching is the origin of high voltage derivatives. The voltage derivatives give rise to high frequency harmonic distortion and insulation stress on the load connected to the converter. Reflections measured at the terminal of an induction motor are presented.

To obtain low current- and voltage harmonic distortion at low switching frequencies, a third order low pass filter is proposed. The required switching frequency decreases from 7 kHz with the regular transformer, to 2.4 kHz with the low-pass filter. In addition, if the reactive power produced by the filter capacitors is requested, the cost of the plant can be decreased. This is due to the fact that the converter rated power can be decreased and its efficiency increased due to reduced switching losses. When the switching frequency is decreased, slower switching of the semiconductor valves can be performed. This is a major advantage since the EMI due to voltage derivatives and switching frequency is reduced.

V. References

[1] T. F. Lowery and D. W. Petro, “Application Considerations for PWM Inverter-Fed Low-Voltage Induction Motors,” IEEE Trans. on Industry Application, vol. 30, pp. 286-293, 1994.

[2] J. Ollila, “A PWM rectifier without current measurement,” EPE Journal, vol. 44, pp. 14-19, 1994.

[3] K. Thorborg, Power Electronics -in Theory and Practice. Lund: Stundentlitteratur, 1993.

[4] M. B. Lindgren, “Feed forward- time efficient control of a Voltage source Converter connected to the grid by lowpass filters,” presented at PESC, Atlanta, 1995.

[5] K. Yurugi, H. Yonemori, and M. Nakaogi, “Next generation zero-voltage soft switched PWM three phase Ac-Dc active power converter,” presented at TELESCON, Berlin, 1994.

Publication B

M. Lindgren, "Analysis and Simulation of Digitally Controlled Grid-connected PWM-converters using the Space-vector Average Approximation, " *IEEE 5th Workshop on Computers in Power Electronics*, Portland, USA, August 11-14, 1996, p. 157-162.

Edited version.

Analysis and Simulation of Digitally-controlled Grid-connected PWM-converters Using the Space-vector Average Approximation

Michael B Lindgren M.Sc. Lic of Engineering

Chalmers University of Technology
Department of Electric Power Engineering
Division of Electrical Machines and Power Electronics
S- 412 96 Göteborg Sweden
michael.lindgren@elkraft.chalmers.se

***Abstract*:** A technique to evaluate the dynamic performance of control principles for PWM-converter systems is presented. In the modelling of vector-controlled, grid-flux-oriented control systems, nonlinear switches and time-varying elements due to coordinate transformation occur in the feedback loop. By using space-vector averaging, coordinate transformations and nonlinear switches are avoided. A linear time-invariant analytical model in the grid-flux-oriented dq-frame is derived. Simulations with a switched PWM-model and an analytical model show accurate transient response and frequency response.

I. Introduction

In papers describing control principles, general performance such as frequency response and stability is seldom presented. That is due to the fact that dead-beat control is predominant in power electronics. For a dead-beat controlled system, the small signal dynamic performance is related to the sampling frequency. For the first-order L-filter, dead-beat control of one discretization time is obtained by using vector control. For high-order filters, such as the LC-filter, usually proposed in uninterruptable power supplies (UPS), a principle to obtain dead-beat response in inner and outer loops is presented by Kawabata et al. [1]. By using the technique described in this paper, the dynamic performance of control principles other than dead-beat, such as state feedback with a single control law can be conveniently evaluated.

Multivariable systems are preferably modelled using state-space technique. In this paper, a closed loop discrete state-space equation is derived for a PWM Voltage Source Converter (VSC) with a grid-flux-oriented sampled control system. The space-vector average technique described by Bauer et al. [2] is adopted to model the PWM-converter. In the design and modelling of the control system, the constant gain of the PWM is essential to apply the space-vector average approximation. Transfer functions from a space-vector reference voltage vector to an output voltage vector of the PWM-converter have been shown by Ollila [3]. Constant gain was obtained except for the frequencies where harmonics due to the PWM occur. Here, the result of the transformation of the voltage vectors to the syncronously rotating dq-frame is shown. As presented, the dominant harmonics due to the PWM do not interfer with the frequency response at frequencies of interest in electric power distribution applications such as active filtering.

II. System description

The system to be modelled is displayed in Fig. 1.

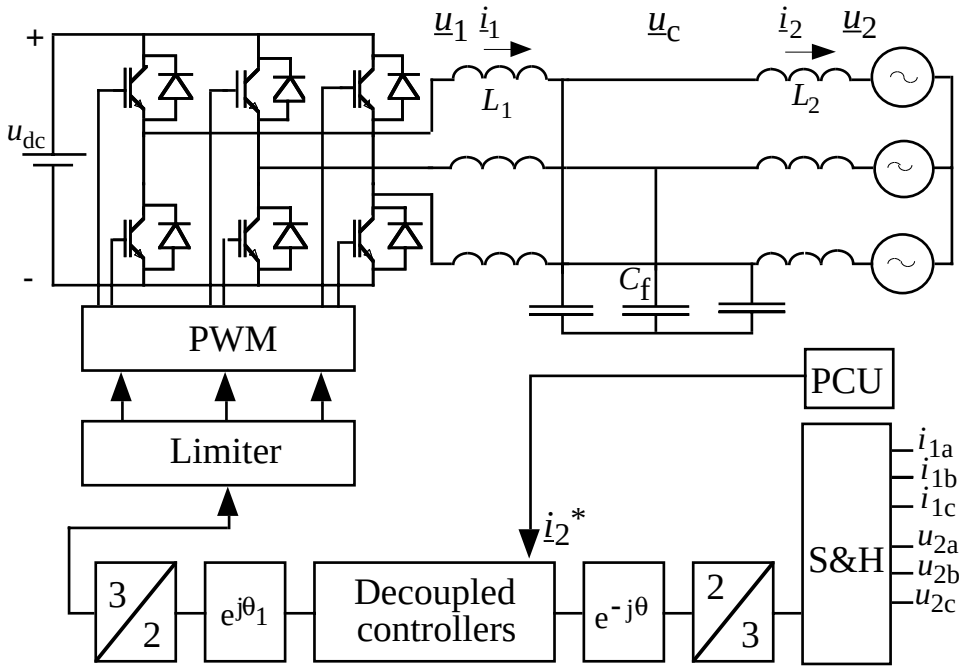

Fig. 1. VSC connected to the grid by LCL-filters.

The parameters used are X_{L1}= 0.05 p.u, X_{L2}= 0.025 p.u, X_C= 10 p.u, sampling frequency,f_S= 9.9 kHz, and switching frequency, f_{SW}= 4.95 kHz. The dc-voltage is 2 p.u. where 1 p.u is defined by the line to line voltage of the grid. Suboscillation 3rd-order harmonic injection PWM is applied. A grid-flux-oriented control system designed to control the current vector $\underline{i}_2$ is used. The control principle is described in [4].

The reference vector of the line current vector is provided by the power controller unit (PCU). The tranformation angle q is the angle of the grid-flux vector at sample k and the transformation angle q_1 is the average angle of the grid-flux vector during the succeding sample interval k+1, k+2.

III. System modeling

The system to be modelled consists of the line filter, the control system, and the converter. The line filter is modelled by a state-space equation, which is linear and time-invariant, assuming that the inductors are designed to avoid saturation and that frequencies below a few kHz are considered. The control system involves transformations between the three-phase and the grid-flux-oriented dq-frame. In addition, a time delay of one sample occurs due to the sampling and evaluation of controller equations. As presented by Holtz [5], in the PWM, a small non-linearity will occur due to non-ideal valves and commutation. In the system modelling, however, ideal valves and commutation are assumed. The space-vector average approximation is performed by setting the converter output vector $\underline{u}_1^{dq}(k)$ equal to its reference voltage vector $\underline{u}_1^{*dq}(k-1)$.

A. Simulation models

In Fig. 2, a SIMULINK^{TM} simulation model with PWM is presented. With the switched PWM-converter, a continuous state-space model of the filter has to be used. The simulation time step should be very short to obtain accurate switching instants. Assuming that 100 time steps are performed during each sample period, the simulation time can be reduced by 100 times if a non switched converter is used. In addition, since transformations are left out, the simulation time is further reduced by 6 times at a Macintosh IIfx. A simulation model with an analytical model of the system is displayed in Fig. 3. The model is defined in the dq-frame exclusively.

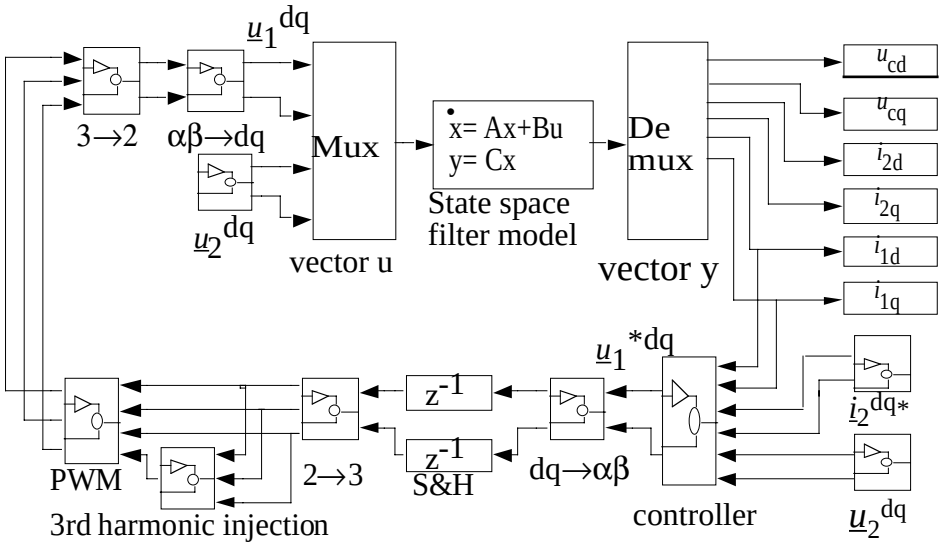

Fig. 2. A Simulink^{TM} simulation model with the switched PWM-converter.

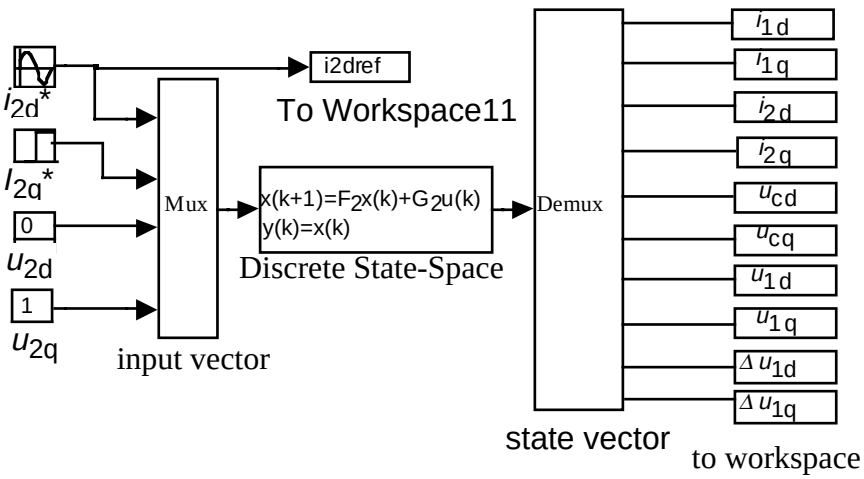

Fig. 3. An analytical state-space model implemented in Simulink^{TM}.

B. Analytical model

A state-space equation of the LCL-filter in the grid-flux oriented dq-system can be formed as

$$\frac{\mathrm{d}\underline{x}}{\mathrm{d}t} = \mathrm{A}\underline{x} + \mathrm{B}\underline{u} \tag{1}$$

where $\underline{x} = (i_{1d}, i_{1q}, i_{2d}, i_{2q}, u_{cd}, u_{cq})^T$ and $\underline{u} = (u_{1d}, u_{1q}, u_{2d}, u_{2q})^T$ are the state and input vector, respectively. The matrices A and B are

$$\mathrm{A} = \begin{bmatrix} -\frac{R_1}{L_1} & \omega & 0 & 0 & -\frac{1}{L_1} & 0 \\ -\omega & -\frac{R_1}{L_1} & 0 & 0 & 0 & -\frac{1}{L_1} \\ 0 & 0 & -\frac{R_2}{L_2} & \omega & -\frac{1}{L_2} & 0 \\ 0 & 0 & -\omega & -\frac{R_2}{L_2} & 0 & \frac{1}{L_2} \\ \frac{1}{C_\mathrm{f}} & 0 & -\frac{1}{C_\mathrm{f}} & 0 & 0 & \omega \\ 0 & \frac{1}{C_\mathrm{f}} & 0 & -\frac{1}{C_\mathrm{f}} & -\omega & 0 \end{bmatrix} \qquad \mathrm{B} = \begin{bmatrix} \frac{1}{L_1} & 0 & 0 & 0 \\ 0 & \frac{1}{L_1} & 0 & 0 \\ 0 & 0 & -\frac{1}{L_2} & 0 \\ 0 & 0 & 0 & -\frac{1}{L_2} \\ 0 & 0 & 0 & 0 \\ 0 & 0 & 0 & 0 \end{bmatrix}$$

Discretization yields the corresponding discrete state-space equation

$$\underline{\mathrm{x}}_1(\mathrm{k}+1) = \mathrm{F}_1\underline{\mathrm{x}}_1(\mathrm{k}) + \mathrm{G}_1\underline{\mathrm{u}}_1(\mathrm{k}) \tag{2}$$

The closed loop state-space equation is obtained by expanding the state-space equation (2) with the controller equations. The time delay of one sample is modelled by introducing the direct and quadrature components of the converter output voltage vector as discrete states. As displayed in matrix F2, the controllers are linear combinations of the state vector and the input vector. In the controllers, delay time compensation is performed. The compensation uses one additional state for each controller. The compensation principle is described in [4]. Since a linear time-invariant control law is adopted, the closed loop system model is also linear and time-invariant. The expanded equation is

$$\underline{\mathrm{x}}_2(\mathrm{k}+1) = \mathrm{F}_2\underline{\mathrm{x}}_2(\mathrm{k}) + \mathrm{G}_2\underline{\mathrm{u}}_2(\mathrm{k}) \tag{3}$$

The new state and input vectors are $\underline{x}_2 = \left(i_{1d}, i_{1q,} i_{2d}, i_{2q,} u_{cd}, u_{cq,}\right)$

and $u_2 = \left(i_{2d}{}^*, i_{2q}{}^*, u_{2d}, u_{2q,}\right)$. The matrices of the closed loop state-space equation are

$$F_2 = \begin{bmatrix} F_{11} & F_{12} & F_{13} & F_{14} & F_{15} & F_{16} & G_{11} & G_{12} & 0 & 0 \\ F_{21} & F_{22} & F_{23} & F_{24} & F_{25} & F_{26} & G_{21} & G_{22} & 0 & 0 \\ F_{31} & F_{32} & F_{33} & F_{34} & F_{35} & F_{36} & G_{31} & G_{32} & 0 & 0 \\ F_{41} & F_{42} & F_{43} & F_{44} & F_{45} & F_{46} & G_{41} & G_{42} & 0 & 0 \\ F_{51} & F_{52} & F_{53} & F_{54} & F_{55} & F_{56} & G_{51} & G_{51} & 0 & 0 \\ F_{61} & F_{62} & F_{63} & F_{64} & F_{65} & F_{66} & G_{61} & G_{62} & 0 & 0 \\ -k_{\mathrm{p}} & 0 & 0 & 0 & 0 & 0 & -1 & 0 & 0 & 0 \\ 0 & -k_{\mathrm{p}} & 0 & 0 & 0 & 0 & 0 & -1 & 0 & 0 \\ -k_{\mathrm{p}} & 0 & 0 & 0 & 0 & 0 & 0 & 0 & -1 & 0 \\ 0 & -k_{\mathrm{p}} & 0 & 0 & 0 & 0 & 0 & 0 & 0 & -1 \end{bmatrix}$$

$$G_2 = \begin{bmatrix} 0 & 0 & G_{13} & G_{14} \\ 0 & 0 & G_{23} & G_{24} \\ 0 & 0 & G_{33} & G_{34} \\ 0 & 0 & G_{43} & G_{44} \\ 0 & 0 & G_{53} & G_{54} \\ 0 & 0 & G_{63} & G_{64} \\ c_1 & -c_2 & c_3 & -c_4 \\ c_2 & c_1 & c_4 & c_3 \\ c_5 & -c_6 & 0 & -c_7 \\ c_6 & c_5 & c_7 & 0 \end{bmatrix}$$

The coefficients introduced are related to the controllers.

IV. Transient response

To illustrate the difference between the simulation model with the switched PWM-model and the analytical model based on space-vector averaging, the transient response can be used. In Fig. 4 and Fig. 5, step responses obtained with the simulation models described in the previous section are displayed. Current steps have to be limited since overmodulation would give rise to a significant deviation between the reference voltage vector and the voltage vector obtained at the converter output. Thus, an analytical model that uses averaging is valid provided that overmodulation does not occur. As illustrated in Fig. 4, harmonics due to the PWM occur in the converter current. The line current is, however, almost sinusoidal. As displayed in Fig. 5, the states simulated with the analytical model lack the harmonics due to the PWM.

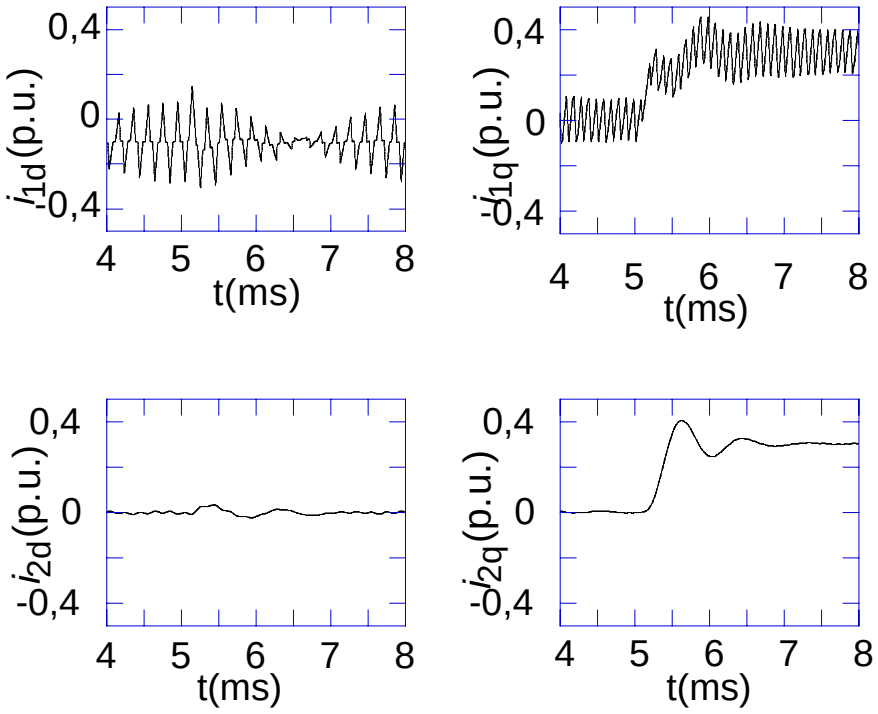

Fig. 4. Simulated transient response with the switched PWM-model in figure 2. Converter currents (upper) and line currents (lower). Direct currents (left) and quadrature currents (right).

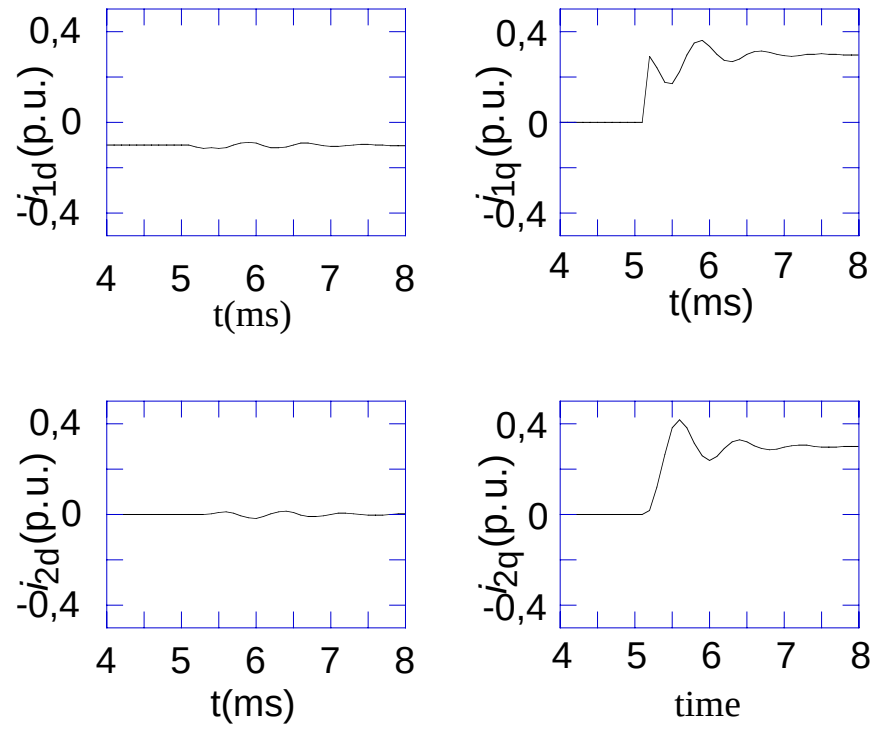

Fig. 5. Simulated transient response with the analytical simulation model in figure 3. Converter currents (upper) and line currents (lower). Direct currents (left) and quadrature currents (right).

V. Frequency response with the switched PWM-converter and with the space-vector average approximation

The voltage harmonics caused by the PWM may give rise to current harmonics that could interact with the frequency response of interest. For a linear system, an input of a specific frequency gives an output at the same frequency. Thus, in the design of the control systems, the accurate transformation of the harmonics to the dq-frame displays whether the harmonics interfere with the frequency response of interest. Usually, the frequency response is not considered at frequencies close to the PWM-frequency, and the analytical model based on the space-vector average approximation can be used to predict the frequency response.

Since the controllers are formed in the grid-flux-oriented reference frame, frequency responses are presented in this frame. The harmonics caused by the PWM can be devided into harmonics due to modulation with a fundamental voltage and harmonics due to modulation with harmonic voltages. The latter case occurs in applications such as active filtering. Thus, voltage harmonics due to the fundamental modulation are constant, and the harmonic spectra due to the harmonic voltage modulation varies with the inductance of the line filter and the amplitude and frequency of the harmonic current supplied by the converter. In this paper, the harmonics due to the fundamental modulation dominate and, as shown, the harmonics due to the harmonic voltage modulation do not affect the result.

The Fourier spectrum of a converter phase voltage is displayed in Fig. 6. In the figure, a fundamental output voltage is supplied by the PWM-converter. As displayed, dominating voltage harmonics occur at frequencies fsw±100 Hz and fsw±200 Hz. By setting the switching frequency to obtain a symmetrical output voltage, even harmonics do not occur in the output voltage. This results in a clearly defined frequency spectrum in the dq-frame. The spectra of the direct and the quadrature voltage components are displayed in Fig. 7 and Fig. 8. As expected, the fundamental voltage is transformed into dc-components in direct and quadrature directions. With a fundamental voltage supplied by the converter, the dc-components of the spectra are equal to the reference voltage in direct and quadrature direction, respectively. Due to the dq-transformation, the order of voltage harmonics of positive order is reduced by one and the order of negative order harmonics is increased by one. In Fig. 7 and Fig. 8, the dominating voltage harmonics occur at frequencies of 4800 Hz and 5100 Hz.

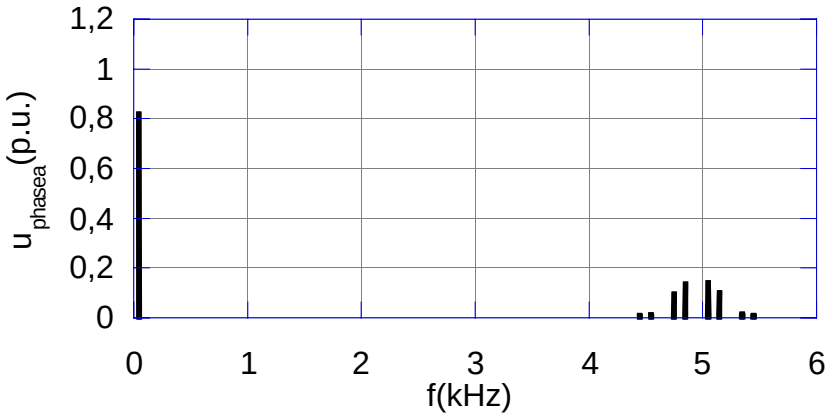

Fig. 6. Fourier spectrum of a converter phase voltage.

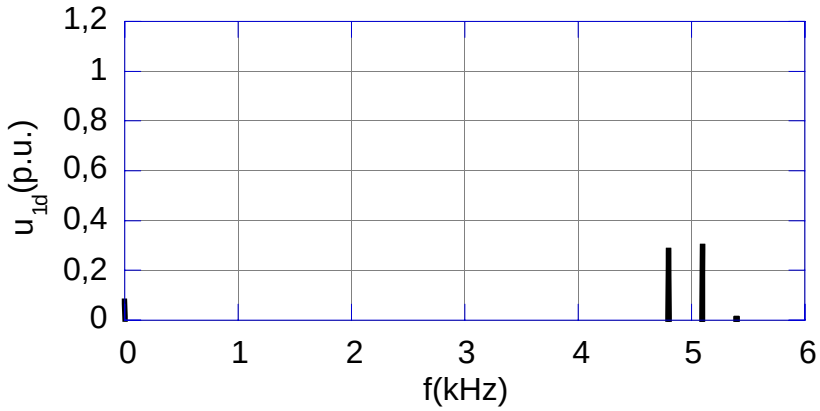

Fig. 7. Fourier spectrum of direct voltage component.

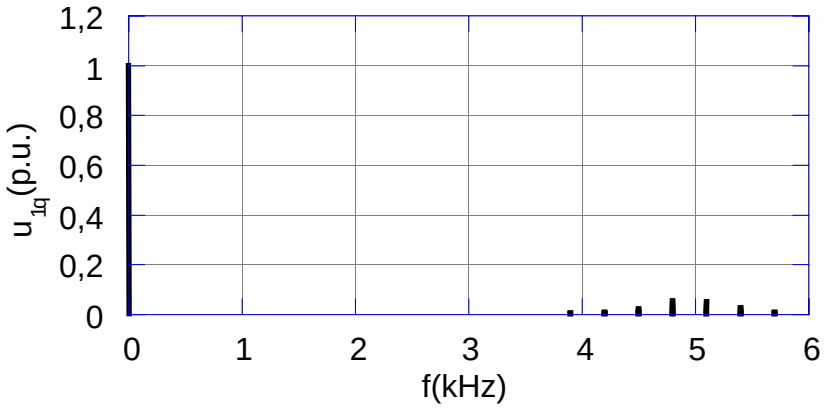

Fig. 8. Fourier spectrum of quadrature voltage component.

In Fig. 9 and Fig. 10, Bode diagrams obtained by the Matlab^{TM} function DBODE(F_2,G_2,Ts) are presented. To verify that the analytical models predicts the frequency response accurately, simulations with the PWM-model and the analytical simulation model are presented at frequencies of 300 Hz and 600 Hz in Fig. 11 and Fig. 12, respectively. These frequencies correspond to harmonics 7 and 5 (±300 Hz), 13 and 11 (±600 Hz). In the simulations with the PWM-model, the current ripple is due to the PWM. The gain and the phase shifts obtained equal the phase shifts predicted by the Bode-diagrams in Fig. 9. As predicted by the Bode-diagram in Fig. 10, the coupling is negligible at 300 Hz. The quadrature current is dominated by the harmonics due to the PWM at 300 Hz, while the Bode-diagram of the coupling can be verified at 600 Hz.

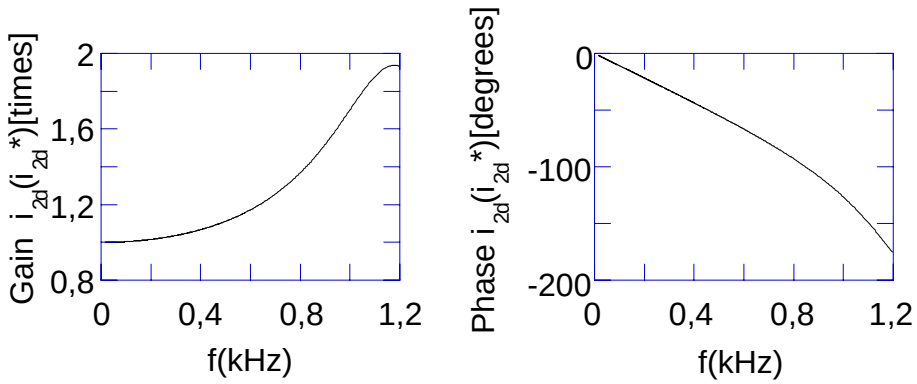

Fig. 9. Bode-diagrams of $i_{2d}(i_{2d}^*)$*. Gain (left) and phase (right).*

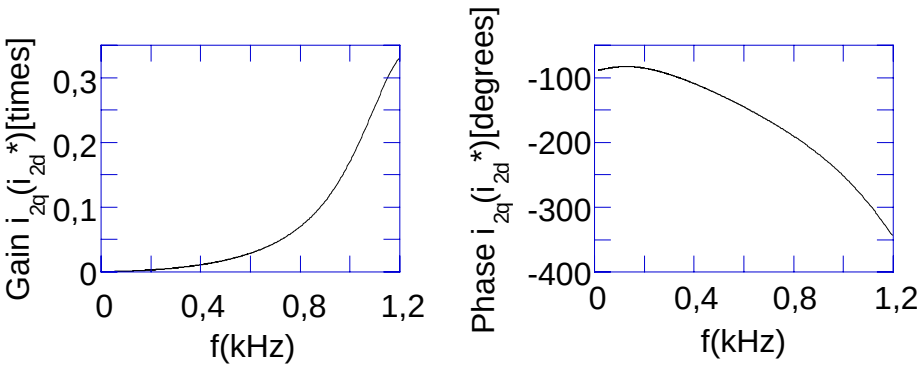

Fig. 10. Bode-diagrams of $i_{2q}(i_{2d}^*)$*. Gain (left) and phase (right).*

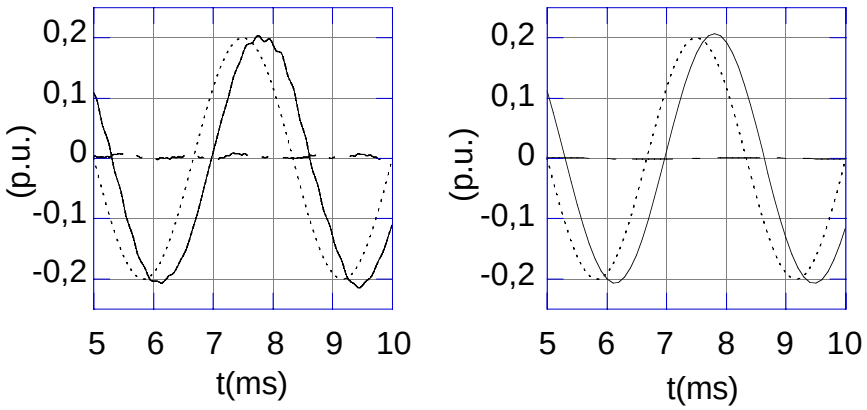

Fig. 11. Simulated frequency response at 300 Hz. PWM-model (left) and analytical model (right). i_{2d}^* *(dotted),* i_{2d} *(solid) and* i_{2q} *(dash-dotted).*

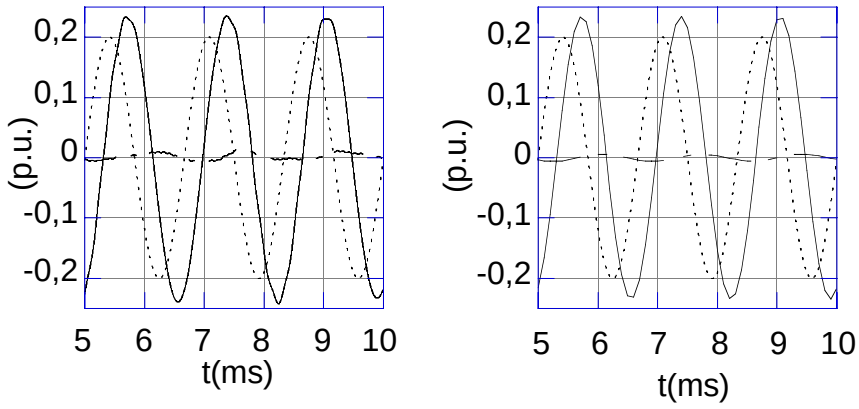

Fig. 12. Simulated frequency response at 600 Hz. PWM-model (left) and analytical model (right). i_{2d}^* *(dotted),* i_{2d} *(solid) and* i_{2q} *(dash-dotted).*

VI. Conclusion

A technique to obtain an analytical model of a digitally controlled grid-connected PWM-converter is presented. The technique is based on discrete state-space modelling and the space-vector average approximation in the dq-frame. The relation between voltage harmonics in the three phase frame and the dq-frame is presented. The dominating harmonics due to the PWM do not interfere with the frequency response of interest in applications such as active filtering. When voltage harmonics are supplied by the converter, additional harmonics occur in the frequency spectrum. These harmonics did not affect the frequency response noticeably. Simulations of transient response and frequency response with a PWM-model and an analytical model display good agreement.

VII. References

[1] T. Kawabata, T. Miyashita, Y. Yamamoto, "Dead Beat Control of Three Phase PWM Inverter". *IEEE Transactions on Power Electronics,* vol. 5, no. 1, January 1990, p. 21-28.

[2] P. Bauer, J. B. Klaassens, "Dynamics and analysis of Three-Phase Ac Power Converters". *European Conference on Power Electronics and Applications (EPE'93)*, Brighton, 13-16 September 1993, Proceedings, vol. 4, pp. 77-81.

[3] J. Ollila, "Analysis of PWM-converters using Space vector theory: application to a voltage source rectifier" Jakko Ollila- Tampere University of Technology, Tampere, 1993.

[4] M. Lindgren, "Feed forward- Time Efficient Control of a Voltage Source Converter Connected to the Grid by Lowpass Filters". *Power Electronics Specialists Conference(PESC'95),* Atlanta, 18-22 June, 1995, Proceedings, vol. 2, p. 1028-1032.

[5] J. Holtz, "Pulsewidth Modulation for Electronic Power Conversion". Proceedings of the IEEE, vol. 82, no.8, pp. 1194-1214, 1994.

Publication C

J. Svensson, M. Lindgren, "Influence of Non-linearities on the Frequency Response of a Grid-Connected Vector-Controlled VSC," to appear in *IEEE Transactions on Industrial Electronics.*

Influence of Non-linearities on the Frequency Response of a Grid-Connected Vector-Controlled VSC

Jan Svensson, *Student Member, IEEE,* and Michael Lindgren, *Student Member, IEEE*

Abstract- In this paper, the small-signal performance of different vector controllers for grid connected voltage source converters is investigated. Losses in the line filter as well as non-linearities due to blanking time and non-ideal valves are usually not modeled in the evaluation of the performance of control principles. A method to compensate for non-linearities due to blanking-time and non-ideal valves is implemented. Furthermore, the influence of the compensation principle on the performance of traditional dead-beat controllers is shown in measured frequency responses. The compensation method reduces the cross-coupling gain and improves the direct-coupling gain. To show the influence of non-linearities, measured frequency responses are compared with responses obtained from analytical models. At high frequencies, the frequency-dependent losses in the line filter should be taken into account to predict the dynamic performance correctly.

Index Terms – Vector current control, Small-signal scheme, Non-linear, Compensation, Voltage source converter, Blanking time, Bode diagram, Transfer function, Valve.

I. Introduction

The discrete-time vector current controller with a sub-oscillating PWM uses a constant switching frequency and harmonics appear at distinct frequencies [1]. This type of controller is sensitive to parameter variations and non-linearities caused by the blanking time and non-ideal semiconductor valves. In steady state and for slowly varying reference values, an integration term in the controller allows some parameter variations and errors due to non-ideal valves. By using feed-forward compensation for parameter variations and errors due to valve non-linearities, the system is able to track the reference values with a higher accuracy. This has been investigated for adjustable-speed drives [2]. In vector current control systems, the cross-coupling between the direct and quadrature current should be low. As shown in [3], cross-coupling and non-linear gain may occur due to the uniform sampling and non-ideal PWM. In the design of high performance vector current control systems for grid-connected VSCs, it is important to take all non-linearities into consideration. In addition to the static characteristics, the dynamic performance of the control system should be studied.

In this paper, the performance of a discrete-time current controller using sub-oscillating PWM for a grid-connected VSC is investigated. Small-signal frequency responses from grid current references to grid currents are determined at an operating point. Frequencies up to the expected bandwidth of 1 kHz are considered. The system is modeled by an analytical discrete state-space equation and the converter is modeled by the average switch model (ASM) technique [4]. The uniform sampling phenomenon is avoided by choosing

a sufficiently high sampling frequency. The controller takes into account the delay-time of one sample due to the computational time. A compensation function is introduced to reduce the influence of the blanking time and non-ideal valves both in steady state and dynamically. Frequency responses obtained from two different analytical models are compared with measured responses. In the first analytical model, the line filter has constant parameters. In the latter model, frequency-dependent losses of the line filter, obtained from measurements, are taken into account. Experimental results are presented for P and PI controllers with and without the compensation function.

II. System Configuration

The system configuration is shown in Fig. 1. The diagram includes the VSC, the line filter and the control system. The control system tracks the active reference current $i_q^*(t)$ and the reactive reference current $i_d^*(t)$. Grid currents and grid voltages are sampled and transformed into the two-axis αβ-coordinate system and then into the rotating *dq*-coordinate system. The *d*-axis of the *dq*-frame is synchronized with the grid flux vector. The reference voltage vector from the controller is transformed into the three-phase system. To take full advantage of the dc-link voltage $u_{dc}(t)$, triplen harmonics are added to the reference voltage values in the block OPT. The last step in controlling the VSC is to transform the reference voltages into a pulse width pattern in the block PWM. The resistance and the inductance of the line filter are denoted by R_s and L_s, respectively. The phase voltages and currents of the grid are denoted by $e_1(t)$, $e_2(t)$ and $e_3(t)$ and $i_1(t)$, $i_2(t)$ and $i_3(t)$, respectively. The phase voltages of the VSC are denoted by $u_1(t)$, $u_2(t)$ and $u_3(t)$.

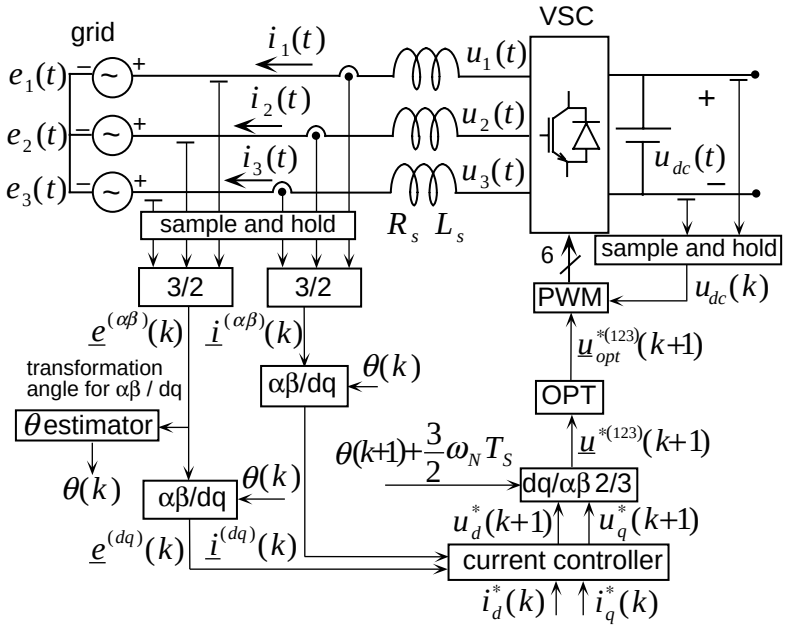

Fig. 1. Overview of the system which includes the VSC, the line filter and the control system.

The experimental system consists of a VSC with IGBT valves (Toshiba MG400Q1US41 1200V, 400A) and a TMS320C30 control computer. The characteristic parameters of the system are displayed in Table 1. The sample frequency f_S is equal to the switching frequency f_{sw}.

TABLE I

CHARACTERISTIC PARAMETERS OF THE SYSTEM.

L_S =0.071 pu	E=1.0 pu	ω_N=100π rad/s	$f_{sw}=f_S$=6 kHz
R_S=0.012 pu	u_{dc}=1.5 pu	T_S=166.7 μs	

The frequency of the grid voltage is 50 Hz, which gives the angular frequency ω_N. All signals are low-pass filtered with the cut-off frequency of 75 kHz before the AD-conversion. The line filter consists of three inductors, one for each phase. The 50 Hz values of the series resistance and inductance of the inductors are used in the current controller. The iron core (UI150) of the inductors is made of 0.5 mm non-oriented laminations (V400-50A), and the core has an air-gap. When the frequency increases, the winding losses increase due to the skin effect, however, the iron losses dominate due to increased eddy-current and hysteresis losses. If the inductor is modeled by a resistance and an inductance in series, these parameters vary, according to measurements, as shown in Figure 2. When the frequency increases from 50 Hz to 1 kHz, which is the expected bandwidth of the system, the resistance increases from 33 mΩ to 1.37 Ω, which is 41 times the 50 Hz value, and the inductance decreases from 1.5 mH to 1.1 mH, which is 78 % of the 50 Hz value.

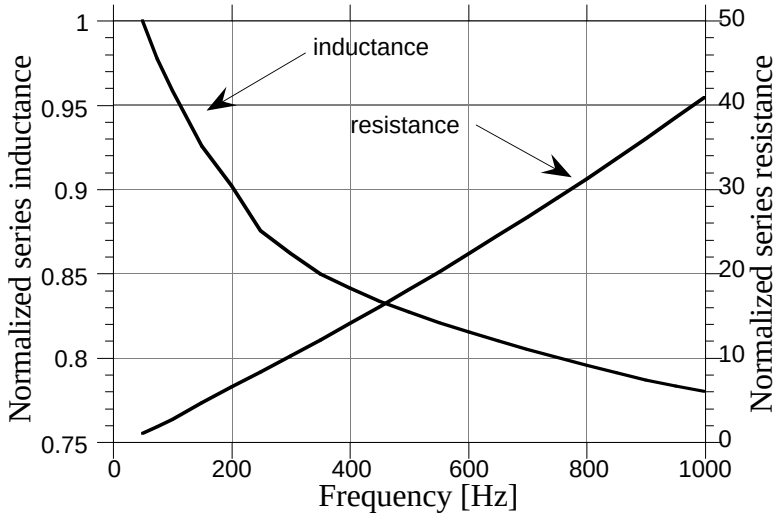

Fig. 2. Measured line filter inductance and resistance as a function of frequency. The values are normalized to 50 Hz values.

III. VSC and Grid Models

The VSC and the grid are modeled as three-phase voltage sources, and the line filter is placed between these sources. The continuous-time state equation for the line filter in the *dq*-coordinate system is

$$\frac{d}{dt}\begin{bmatrix} i_d(t) \\ i_q(t) \end{bmatrix} = \mathbf{A}\begin{bmatrix} i_d(t) \\ i_q(t) \end{bmatrix} + \mathbf{B_u}\begin{bmatrix} u_d(t) \\ u_q(t) \end{bmatrix} + \mathbf{B_e}\begin{bmatrix} e_d(t) \\ e_q(t) \end{bmatrix} \tag{1}$$

where the matrices are given by

$$\mathbf{A} = \begin{bmatrix} -\frac{R_s}{L_s} & \omega_N \\ -\omega_N & -\frac{R_s}{L_s} \end{bmatrix} \mathbf{B_u} = \begin{bmatrix} \frac{1}{L_s} & 0 \\ 0 & \frac{1}{L_s} \end{bmatrix} \mathbf{B_e} = \begin{bmatrix} -\frac{1}{L_s} & 0 \\ 0 & -\frac{1}{L_s} \end{bmatrix}$$

The vector current controller operates in discrete time. To model the closed-loop system, the grid model is transformed into a zero-order held sampled system with the sample time T_s. The state equation is

$$\begin{bmatrix} i_d(k+1) \\ i_q(k+1) \end{bmatrix} = \mathbf{F} \begin{bmatrix} i_d(k) \\ i_q(k) \end{bmatrix} + \mathbf{G_u} \begin{bmatrix} u_d(k) \\ u_q(k) \end{bmatrix} + \mathbf{G_e} \begin{bmatrix} e_d(k) \\ e_q(k) \end{bmatrix} \tag{2}$$

where the matrices are

$$\begin{aligned} \mathbf{F} &= e^{\mathbf{A}T_S} \\ \mathbf{G_u} &= -\mathbf{G_e} = \int_0^{T_S} e^{\mathbf{A}\tau} d\tau \mathbf{B_u} \end{aligned} \tag{3}$$

The VSC is modeled by using the ASM method and the VSC is assumed to provide the requested voltage vector in the *dq*-frame. Thus, the harmonics introduced by the PWM are neglected in the analytical model. The harmonics occur above the frequencies considered in the frequency responses. Ideal valves that commutate according to the PWM pattern are assumed. Thus, the influence of the blanking time between switching valves and the on-state voltage drops in the valves is neglected. Errors due to variations of the grid voltage angle during the sample interval are ignored. For all models, the voltage reference values from the controller must be unsaturated.

It is common in literature that the line filter parameters are assumed to be constant. In this study, two different inductor models are used. In the first model, the inductors have a constant inductance and resistance. In the second one, the influence of the losses on the equivalent series resistance and inductance is taken into account.

IV. Controller and Closed-Loop System Equations

A. The P-controller

The controller is designed to obtain dead-beat current response and to minimize the cross-coupling between *d*- and *q*-direction. The P-controller presented here has partially been adopted from [5]. Equation (1) can be rewritten as

$$u_d(t) = e_d(t) + R_r i_d(t) - \omega_N L_r i_q(t) + L_r \frac{d}{dt} i_d(t) \tag{4}$$

$$u_q(t) = e_q(t) + R_r i_q(t) + \omega_N L_r i_d(t) + L_r \frac{d}{dt} i_q(t) \tag{5}$$

where the inductance and the resistance of the series coil are denoted by subscript *r* to emphasize that the parameters of the controller can differ from the real values. The mean voltages for the sample period *k* to *k*+1 are derived by integrating (4) and (5) from kT_S to $(k+1)T_S$ and dividing by T_S. During one sample period, the current variations are assumed to be linear and the grid voltage components constant. The output reference voltage is delayed by one sample due to the computation time. This delay and the dead-beat gain result in a total delay of two samples for the current response. A time delay compensation term is included in the dead-beat controller to avoid current oscillations. The controller equations are

$$u_d^*(k+1) = e_d(k) + R_r i_d(k) - \omega_N L_r i_q(k) + k_P\left(i_d^*(k) - i_d(k)\right) - \Delta u_d(k) \tag{6}$$

$$u_q^*(k+1) = e_q(k) + R_r i_q(k) + \omega_N L_r i_d(k) + k_P\left(i_q^*(k) - i_q(k)\right) - \Delta u_q(k) \tag{7}$$

where the gain for the dead-beat current response is

$$k_P = \frac{L_r}{T_s} + \frac{R_r}{2} \tag{8}$$

To compensate for the delay of one sample, the method described in [6] is used. The compensation is obtained by adding the factors

$$\Delta u_d(k) = k_p\left(i_d^*(k-1) - i_d(k-1)\right) - \Delta u_d(k-1) \tag{9}$$

$$\Delta u_q(k) = k_p\left(i_q^*(k-1) - i_q(k-1)\right) - \Delta u_q(k-1) \tag{10}$$

to the controllers. The closed-loop state equation for the system with the P-controller can be written as

$$\begin{bmatrix} i_d(k+1) \\ i_q(k+1) \\ u_d^*(k+1) \\ u_q^*(k+1) \\ \Delta u_d(k+1) \\ \Delta u_q(k+1) \end{bmatrix} = \mathbf{F_{CLP}} \begin{bmatrix} i_d(k) \\ i_q(k) \\ u_d^*(k) \\ u_q^*(k) \\ \Delta u_d(k) \\ \Delta u_q(k) \end{bmatrix} + \mathbf{G_{CLP}} \begin{bmatrix} i_d^*(k) \\ i_q^*(k) \\ e_d(k) \\ e_q(k) \end{bmatrix} \tag{11}$$

B. The PI-controller

The integral part of the PI-controller is introduced to avoid static errors caused by non-linearities, noisy measurements and non-ideal components. The proportional part is the same as for the P-controller. The equations of the PI-controller can be written as

$$u_d^*(k+1) = e_d(k) + R_r i_d(k) - \omega_N L_r i_q(k) + k_P\left(i_d^*(k) - i_d(k)\right) - \Delta u_d(k) + \Delta u_{Id}(k) \tag{12}$$

$$u_q^*(k+1) = e_q(k) + R_r i_q(k) + \omega_N L_r i_d(k) + k_P\left(i_q^*(k) - i_q(k)\right) - \Delta u_q(k) + \Delta u_{Iq}(k) \tag{13}$$

The integration term is a sum of the current errors and can be written as

$$\begin{bmatrix}\Delta u_{Id}(k+1)\\ \Delta u_{Iq}(k+1)\end{bmatrix}=\begin{bmatrix}\Delta u_{Id}(k)\\ \Delta u_{Iq}(k)\end{bmatrix}+k_I\begin{bmatrix}i_d^*(k-2)\\ i_q^*(k-2)\end{bmatrix}-k_I\begin{bmatrix}i_d(k)\\ i_q(k)\end{bmatrix} \tag{14}$$

where the response time of two samples is taken into account. The integration constant is defined by $k_I = T_S k_P R_r / L_r$. The closed-loop state equation with the PI-controller becomes

$$\mathbf{x}(k+1) = \mathbf{F}_{\mathbf{CLPI}}\mathbf{x}(k) + \mathbf{G}_{\mathbf{CLPI}}\left[i_d^*(k)\ i_q^*(k)\ e_d(k)\ e_q(k)\right]^T \tag{15}$$

where the state vector $\mathbf{x}(k)$ has 12 states.

V. System Linearization at an Operating Point

A small-signal analysis is generally performed by analyzing the linearized system around an operating point. Perturbations around the operating point are denoted by Δ. In this paper, a linear model of the system is used. However, due to non-linearities in the PWM and the non-linear line-filter parameters, the result is assumed to be valid only at the operating point.

The operating point of the system is determined by the reference values of grid currents, grid voltages and the DC-link voltage. When using a PI-controller, grid currents become equal to their reference values in steady state. The controller output becomes

$$\begin{aligned} u_{d0}^* &= e_{d0} + R_r i_{d0} - \omega_N L_r i_{q0}^* \\ u_{q0}^* &= e_{q0} + R_r i_{q0} + \omega_N L_r i_{d0}^* \end{aligned} \tag{16}$$

where the operating point is denoted by the subscript 0. The output voltage of the converter is equal to the reference voltage of the converter. The steady-state grid current is obtained from (2) as

$$\begin{bmatrix}i_{d0}\\ i_{q0}\end{bmatrix} = (I-\mathbf{F})^{-1}\left(\mathbf{G_u}\begin{bmatrix}u_{d0}\\ u_{q0}\end{bmatrix}+\mathbf{G_e}\begin{bmatrix}e_{d0}\\ e_{q0}\end{bmatrix}\right) \tag{17}$$

VI. Valve Compensation Function

To reduce the influence of the non-linearities caused by the PWM and the valves, a valve compensation function for the valve parameters has been developed. Non-linearities occur due to two different phenomena: blanking time and on-state voltage drop. To avoid short-circuiting the dc-link, each commutation is divided into two steps. First, the valve which is in on-state is turned off. After the blanking time, the other valve in the phase leg is turned on. If the transistor is conducting in the valve that is turned off, the diode in the valve that is to be turned on starts to conduct as soon as the transistor is turned off. Thus, the switching time instant is not influenced by the blanking time. If the sign of the current is not changed, the next commutation will be delayed by the blanking time since a commutation from a diode to a transistor occurs. Consequently, the average phase voltage deviates from that requested by the PWM modulator.

The influence of blanking time and on-state voltage drop can be reduced by adding compensation voltages Δu^* to the reference phase voltages u^*, i.e., by introducing a valve compensation function. The equations (18), (19) and (20) are used for compensating phase 1. Equation (18) compensates only for the blanking time. Equations (19) and (20) compensate also for the voltage drop across the valves in the on-state, for positive and negative phase currents, respectively.

$$\Delta u^*_{1,Tb}(k) = u_{dc}\,\mathrm{sign}\big(i_1(k)\big)T_b \,/\, T_S \tag{18}$$

$$u^*_{1,comp}(k) = \Delta u^*_{1,Tb}(k) + D_1 u_{onT1} + \big(1-D_1\big)u_{onD2} + u^*_1(k) \tag{19}$$

$$u^*_{1,comp}(k) = \Delta u^*_{1,Tb}(k) - \big(1-D_1\big)u_{onT2} - D_1 u_{onD1} + u^*_1(k) \tag{20}$$

The blanking time and the sampling time are denoted by T_b and T_S. The phase 1 duty ratio is $D_1 = 2u^*_1 / u_{dc}$. Voltage drops across the transistor and the diode are denoted by u_{onT} and u_{onD}. These voltage drops have been measured and are displayed in Table 2. The voltage drops consist of a constant term u_0 and a current-dependent term $R_{on}i$. As discussed above, the compensation is only valid when the current is positive or negative during a whole sample period. The valve compensation is not included when the amplitude of the sampled phase current is smaller than the amplitude of the current ripple.

TABLE II

MEASURED PARAMETERS FOR THE VALVE COMPENSATION FUNCTION.

u_{0T}=1.08 V	u_{0D}=1.05 V	T_S=166.7 µs
R_{onT}=12 mΩ	R_{onD} =10 mΩ	T_b=1.4 µs

VII. Analytical and Experimental Frequency Response Analysis

The frequency responses around the operating point were both measured and calculated by means of the analytical models. The operating point (i^*_{d0}=0.22 pu and i^*_{q0}=–0.67 pu) was selected to represent the operation of a grid friendly rectifier in an adjustable speed drive. Measurements have shown that small differences occur due to different operation points. Slightly better results have been obtained in rectifying operations compared with inverter operations. Theoretically a bandwidth of half the sample frequency can be expected. However, due to non-modeled losses in the line filter and other non-linearities, a bandwidth of approximately 1 kHz was expected. Four different controllers were used in the experimental investigation. They are denoted by the following symbols:

M(p) P-controller without valve compensation function

M(pi) PI-controller without valve compensation function

M(p,c) P-controller with valve compensation function

M(pi,c) PI-controller with valve compensation function

Theoretical frequency responses were obtained for four models, all without compensation functions:

A(p) P-controller with constant line filter parameters

A(pi) PI-controller with constant line filter parameters

B(p) P-controller with frequency-dependent line filter parameters

B(pi) PI-controller with frequency-dependent line filter parameters

In the measurements, a sinusoidal small-signal current reference Δi^* of 0.1 pu was added to one of the two reference current components at the operating point. For instance, the current reference Δi^* is applied in *q*-direction to obtain the transfer function (TF) of the direct-coupling in *q*-direction and the TF of the cross-coupling from *q*- to *d*-direction. Measurements were performed at 27 different frequencies between 10 Hz and 1200 Hz. The reference currents as well as the *d*- and *q*-currents were sampled. A sample frequency of 10 kHz and anti-alias filters with a cut-off frequency of 3 kHz were used in the data acquisition system. In the analysis of the measured results, the FFT-algorithm was used to evaluate the gain and phase shift between the sinusoidal reference current Δi_d^* or Δi_q^* and the measured currents Δi_d and Δi_q. The signals were filtered by a flat-top window before the FFT.

A. Direct coupling in q-direction

As shown in Fig. 3, the theoretical gain of the controllers A(·) from Δi_q^* to Δi_q is approximately 0 dB over the whole frequency span. The measured gain of the controllers M(·) is close to 0 dB at low frequencies. When the frequency increases above approximately 400 Hz, the gain increases for all controllers. At 1 kHz, the gain is approximately 1 dB, which corresponds to a 12 % increase. The measured gain can be predicted by including the frequency-dependent line filter parameters according to models B(·). The gain characteristics are very similar for all controller types. The analytical models A(·) give a slightly larger phase lag than the measured one, but the analytical models B(·) track the measured phase correctly.

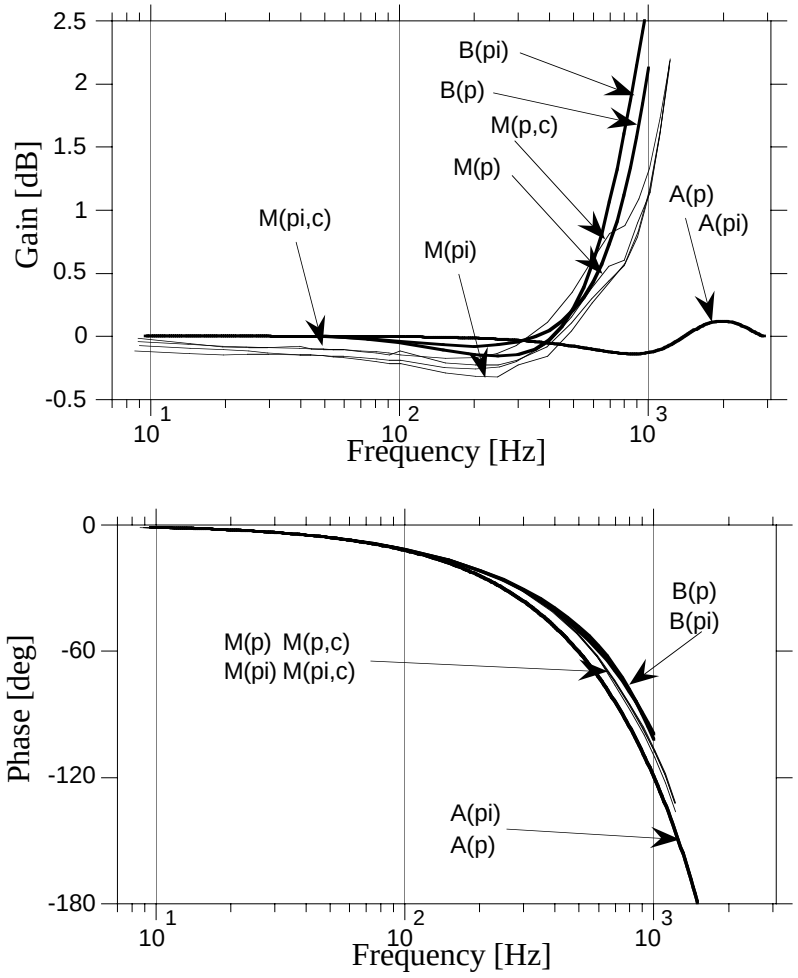

Fig. 3. Bode diagrams for the reference q*-current* Δi_q^* *to the* q*-current* Δi_q.

B. Cross-coupling from q-direction to d-direction

As shown in Fig. 4, the theoretical gains of the controllers A(·) from Δi_q^* to Δi_d are low at low frequencies. The gain increases with frequency and reaches a maximum of –18 dB at 1.8 kHz. Compared with the direct-coupled TF from Δi_q^* to Δi_q, the gains and phase-shifts of the cross-coupling TFs have slightly different characteristics. At low frequencies from 10 to 40 Hz, the measured gain of controller M(p) is higher than the gain of M(pi); –40 dB compared to –45 dB. At higher frequencies, the gains increase with frequency and converge. The gains of the controllers with compensation, M(p,c) and M(pi,c), are lower and have a minimum of –70 dB at 55 Hz. From 55 Hz and upwards, the gain increases and at 1.2 kHz, the gain is –20 dB. Valve compensation reduces the cross-coupling gain. The theoretical gains of the models B(·) are slightly higher than those of the models A(·) but lower than the measured gains. The valve compensation function results in a phase-shift change from 0° to 180° at 55 Hz.

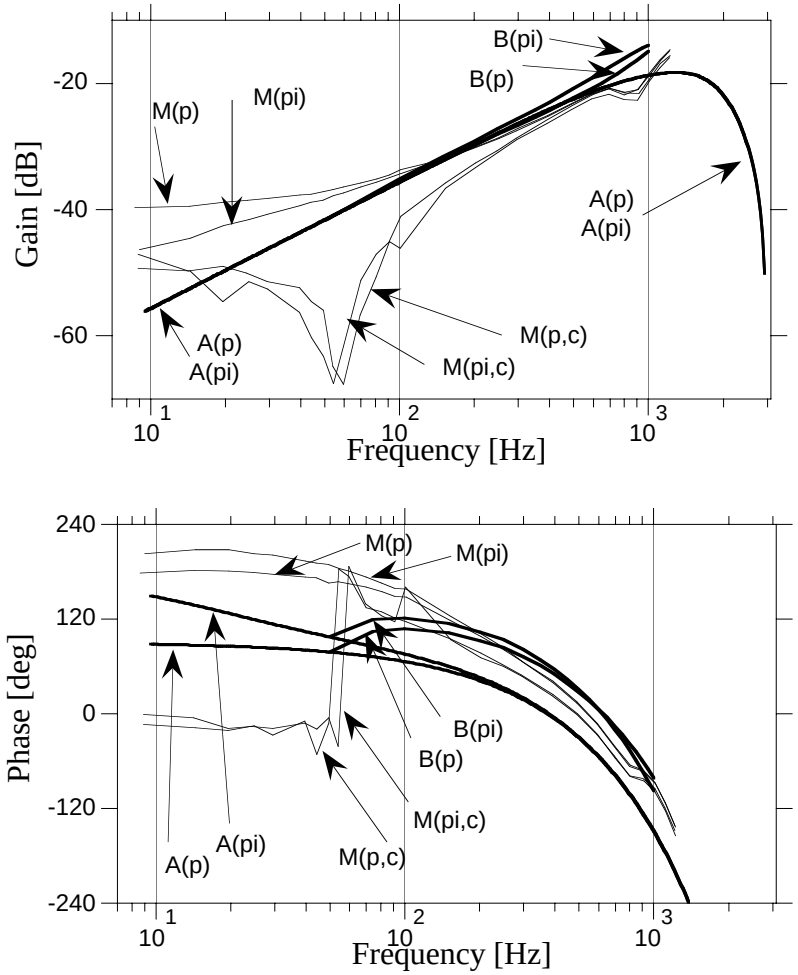

Fig. 4. Bode diagrams for the reference q-*current* Δi_q^* *to the* d-*current* Δi_d.

C. Direct coupling in d-direction

According to Fig. 5, the gain of the TF Δi_d^* to Δi_d is close to 0 dB for the theoretical models A(·). The measured gain characteristics can be divided into two groups: with and without valve compensation; the integration term does not affect the responses. Without valve compensation, the gains are constant, approximately –0.3 dB, up to 750 Hz where the gains drop down to a minimum of –0.8 dB at 900 Hz before increasing again. At 1200 Hz, the gains are 1 dB. With valve compensation, the gains with the controllers M(p,c) and M(pi,c) are approximately 0 dB for frequencies up to 750 Hz. Above 750 Hz, the gains are similar both with and without compensation. The gains of the theoretical TFs B(p) and B(pi) do not have a gain dip at 900 Hz, instead the gain is 0 dB at low frequencies and starts to increase at a frequency of 500 Hz. The phase-shifts of the measured frequency responses follow the theoretical phase-shifts B(p), B(pi), which have a smaller phase lag than the models A(p) and A(pi).

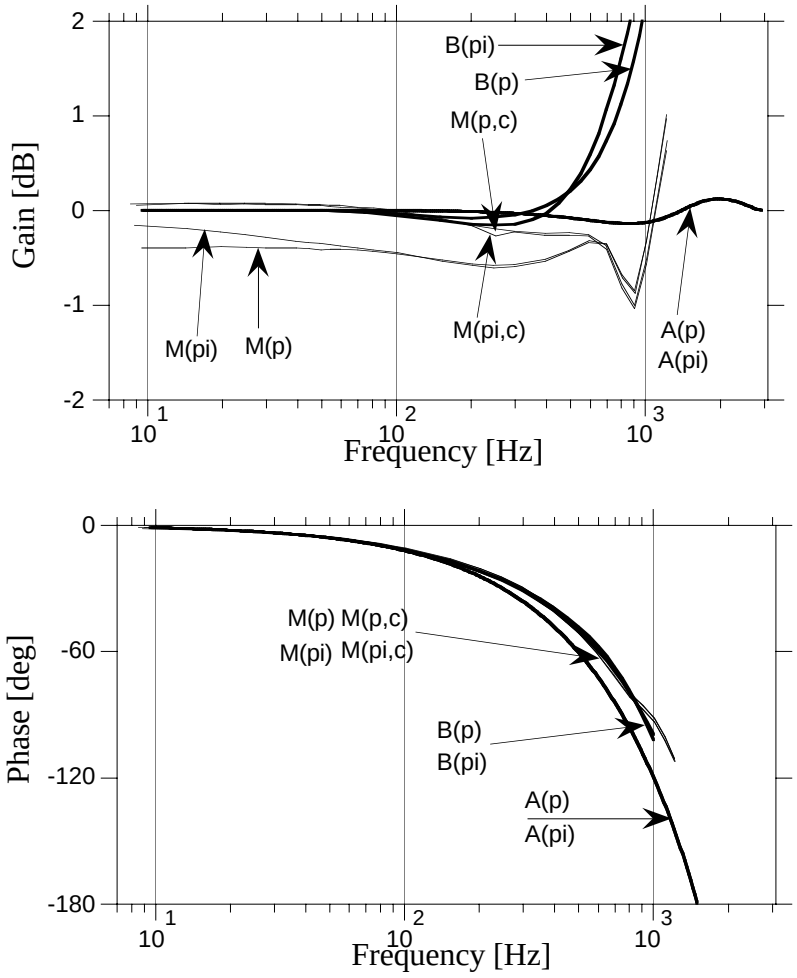

Fig. 5. Bode diagrams for the reference d-*current* Δi_d^* *to the* d-*current* Δi_d.

D. Cross-coupling from d-direction to q-direction

The theoretical TFs A(p) and A(pi) from Δi_d^* to Δi_q have a low gain at low frequencies, as shown in Fig. 6. The gain increases with frequency and reaches a maximum of –18 dB at 1.8 kHz. The measured gains can be divided into two groups: with and without valve compensation; the integration term does not influence the gain. When using valve compensation, the gain is almost constant (–34 dB) up to 100 Hz, which can be compared with –30 dB without compensation. From approximately 150 Hz, the gain characteristics are the same both with and without valve compensation. At 1200 Hz, the gains are –12 dB. The gains of the analytical TFs B(p) and B(pi) are higher than the gains of the TFs A(p) and A(pi) but lower than the measured gains.

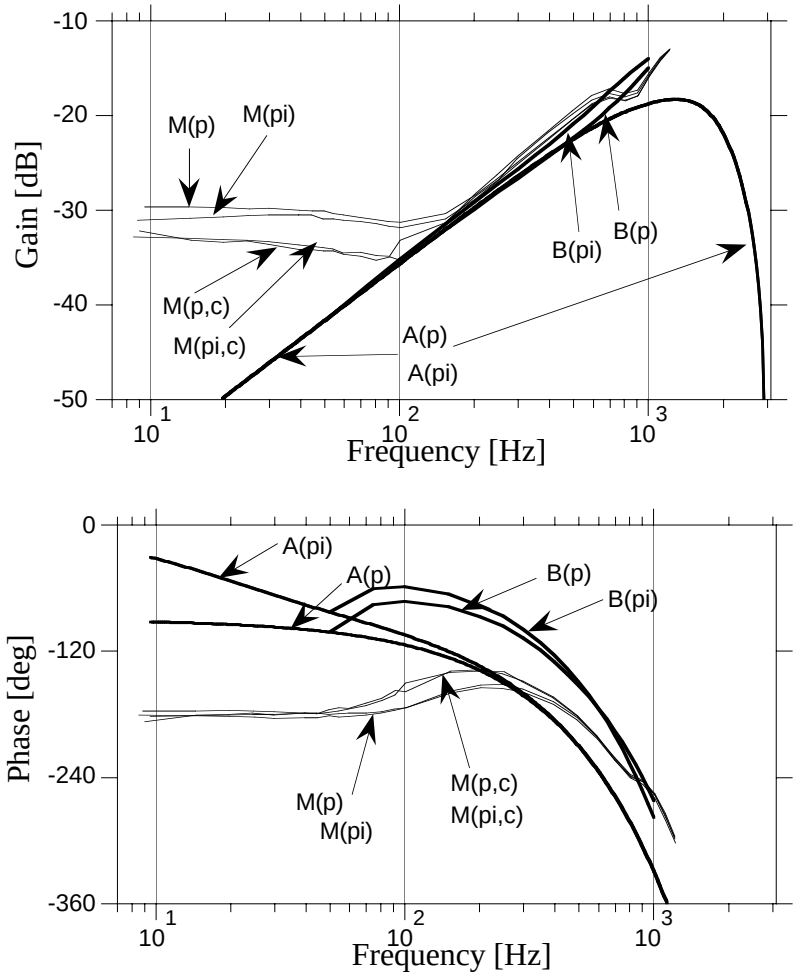

Fig. 6. Bode diagrams for the reference d*-current* Δi_d^* *to the* q*-current* Δi_q.

VIII. Summary of Transfer Function Analysis

A. Low-frequency responses

The compensation function for the non-ideal valves and blanking time results in more accurate steady-state values of the *d*- and *q*-currents. The compensation acts as a feedforward term whereas an integration term can be characterized as a feedback term. The gain characteristics for the direct coupling in *d*-direction is improved. Furthermore, the gain of the cross-coupled TF from the reference *q*-current to the *d*-current is reduced by approximately 10 dB. The direct gain in *q*-direction is close to 0 dB both with and without the compensation function. Finally, the gain of the cross-coupled TF from the reference *d*-current to the *q*-current is reduced by approximately 10 dB.

B. High-frequency responses

At high frequencies, from approximately 500 Hz and upwards, the influence of the line filter parameter variations with frequency dominates over the influence of the valves. Thus, it is difficult to evaluate the performance of the valve compensation function. For the directly-coupled TFs, the gain increases with frequency. For the cross-coupled TFs, a deviation occurs between theoretical and measured gains. The deviation can be partly predicted by including the losses according to models B(·).

IX. Conclusion

In this paper, the current frequency response of a grid-connected VSC using a vector current controller is investigated to determine the performance of different current controllers. The measured transfer functions show that the steady-state performance is improved by adding a valve compensation function to the controller. The valve compensation should be used because the cross-coupling gain is reduced at low frequencies and the direct-coupling gain is closer to one. The integration part of the controller has a minor influence on the dynamic performance. The compensation function reduces the coupling between the *q*-direction to the *d*-direction. At high frequencies, i.e., from 500 Hz and upwards, frequency responses are affected by frequency dependent losses in the line filter. The gain and the cross-coupling increase in all measured transfer functions. This can partly be predicted by using a frequency-dependent model of the line filter.

X. References

[1] J. Holtz, "Pulsewidth Modulation for Electronic Power Conversion," *Proc. of IEEE*, Vol. 82, No. 8, pp. 1194-1214, August 1994.

[2] J. K. Pedersen, F. Blaabjerg, J. W. Jensen, P. Thogersen, "An Ideal PWM-VSI Inverter with Feedforward and Feedback Compensation," *5th European Conference on Power Electronics and Applications (EPE'93)*, Brighton, England, 13-16 September 1993, pp. 501-507.

[3] S. Hiti, D. Boroyevich, "Small-Signal Modeling of Three-Phase PWM Modulators," *Power Electronics Specialists Conference (PESC'96)*, Baveno Italy, 23-27 June, 1996, pp. 550-555.

[4] R. Kagalwala, S. S. Venkata, P. O. Lauritzen, "A Transient Behavioral Model (TBM) for Power Converters," *5th Workshop on Computers in Power Electronics*, IEEE Power Electronics Society, Portland USA, 11-14 August, 1996.

[5] J. Svensson, "Inclusion of Dead-Time and Parameter Variations in VSC Modelling for Predicting Responses of Grid Voltage Harmonics." *7th European Conference on Power Electronics and Applications (EPE'97)*, Trondheim, Norway, 8-10 September 1997, Proceedings, Vol. 3, pp. 216-221.

[6] M. Lindgren, "Feed forward – Time Efficient Control of a Voltage Source Converter Connected to the Grid by Lowpass Filters." *Power Electronics Specialists Conference (PESC'95)*, Atlanta, USA, 18-22 June 1995, Vol. 2, pp. 1028-1032.

Publication D

J. Svensson, M. Lindgren, "Vector Current Controlled Grid Connected Voltage Source Converter — Influence of Non-linearities on the Performance," *IEEE Power Electronics Specialists Conference (PESC 98*), Fukuoka, Japan, May 17-22, 1998, Vol. 1, p. 531-537.

Edited version.

Vector Current Controlled Grid Connected Voltage Source Converter— Influence of Non-Linearities on the Performance

Jan Svensson Michael Lindgren

Department of Electric Power Engineering
Chalmers University of Technology
S-412 96 Göteborg, Sweden

***Abstract*—** In the literature, the influence of non-linearities occurring due to the effects of blanking time, the valves and the non-ideal grid filter on the dynamic performance of current controlling are usually not described. In this paper, small-signal analysis is used to study the influence of non-linearities for a vector current controlled VSC connected to a grid. To show the influence of non-linearities, measured frequency responses are compared with responses from analytical models. Measured responses are presented for operation in rectifier and inverter operation as well as static VAr operation. As displayed, the frequency dependent losses in the grid filter affect the dynamic performance at high frequencies. A method for compensating for non-linearities due to blanking-time and non-ideal valves is implemented. The compensation method improves the performance.

I. Introduction

In the evaluation of control systems for voltage source converters (VSCs) connected to an AC grid, the dynamic performance of the system should be studied. The discrete-time vector current controller with a sub-oscillating PWM [1] uses feedforward and is sensitive to parameter variations and non-linearities. In VSCs, a blanking time is introduced to avoid short-circuiting the dc-link voltage. This blanking time gives rise to a non-linearity in the PWM. In addition, a voltage drop occurs across the valves when the valves are conducting. These effects introduce non-linearities into the system.

In steady-state and for slowly varying reference values, an integration term in the controller allows some parameter variations and non-linearities. The performance of the current control system can be improved by using feedforward compensation for errors due to the blanking time and non-linearities of the valves. This has been investigated for adjustable-speed drives [2].

In addition to errors caused by the valves, the PWM-method may introduce non-linearities. The linearity of an analog control system performing continuous natural sampling in the PWM has been investigated in [3]. Constant gain was obtained except for frequencies in which harmonics due to the PWM occur. In [4], both natural sampling and uniform sampling were considered. As displayed, natural sampling is linear. With uniform sampling, the amplitude of the fundamental output is a function of the frequency ratio. In [3] and [4], transfer functions in the fixed $\alpha\beta$-frame were considered. In flux-oriented control systems, errors may be introduced by coordinate transformations. Since uniform sampling is performed, a piecewise constant angle is used in the transformation from the fixed frame to the rotating frame. Due to the rotation of the *dq*-frame during the sample, a non-linear gain and coupling between *d*- and *q*-directions may occur if low

sampling frequencies are used. As displayed in [5], cross-coupling and non-linear gain may occur due to uniform sampling and non-ideal PWM.

The influence of valve compensation dynamically, i.e., in the frequency domain, has not been focused on before for a grid-connected VSC. Moreover, the influence of the frequency dependent parameters of the grid filter on the current controller and the effect of the operating point on the small-signal performance is an important aspect which has not been studied before.

In this paper, the performance of a discrete-time vector current controller using a sub-oscillating PWM is investigated. To reduce the influence of the valves both in steady state and dynamically, a compensation function is introduced. The dynamic performance of the control system is studied in the frequency domain. To evaluate the performance of P and PI-controllers and the influence of the compensation function for the non-linearities, measured frequency responses are compared with responses from analytical models. In the first analytical model, the grid filter has constant parameters. In the latter model, measured frequency-dependent losses of the filter are taken into account. To display the influence of the losses in the grid-filter inductors, two different inductors are used. Measured responses are also shown at four different operating points.

II. System Configuration

The system configuration of the VSC connected to the grid by an L-type grid filter is shown in Fig. 1. The controller tracks the reference active current $i_q^*(t)$ and the reference reactive current $i_d^*(t)$. The grid currents and the grid voltages are sampled and transformed into the two-axis αβ-coordinate system and then into the rotating *dq*-coordinate system. The *d*-axis of the *dq*-frame is synchronized with the grid flux vector. The reference voltage vector from the controller is transformed back into the three-phase system. To take full advantage of the dc-link voltage $u_{dc}(t)$, triplen harmonics are added to the reference voltage values in the block OPT.

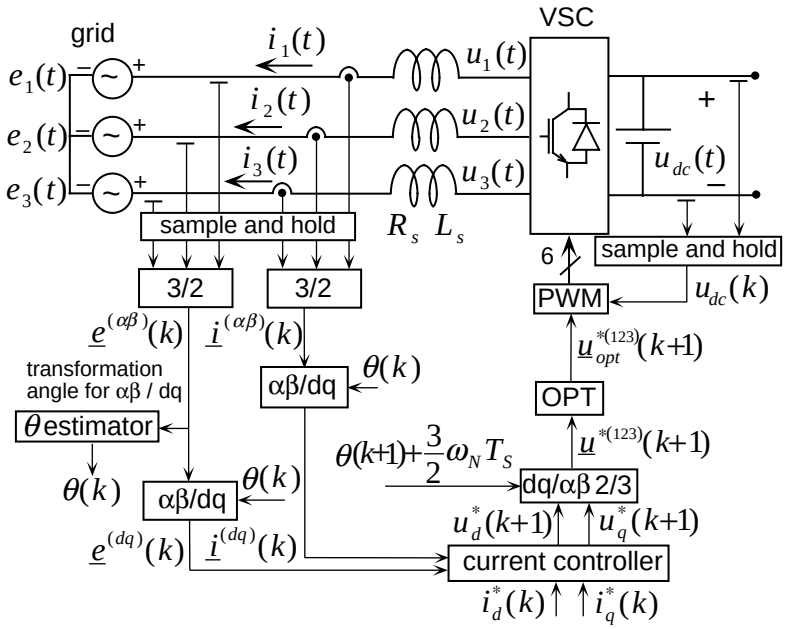

Fig. 1. Overview of the system, which contains the VSC, the grid filter and the controller.

The reference voltages for the VSC are transformed into a pulsewidth pattern in the block PWM. The resistance and the inductance of the grid filter are denoted by R_S and L_S, respectively. The phase voltages and currents of the grid are denoted by $e_1(t)$, $e_2(t)$ and $e_3(t)$ and $i_1(t)$, $i_2(t)$ and $i_3(t)$, respectively. The phase voltages of the VSC are denoted by $u_1(t)$, $u_2(t)$ and $u_3(t)$. The experimental system consists of a VSC with IGBT valves (Toshiba MG400Q1US41 1200V, 400A) and a TMS320C30 control computer. The characteristic parameters of the system are displayed in Table 1. The sample frequency, f_S, is equal to the switching frequency, f_{SW}. The sample time is denoted by T_S. The frequency of the grid voltages is 50 Hz, which gives the angular frequency ω_g in Table 1. The base impedance is denoted by Z_{base}. In the measurements of the currents, LEM LA50-S/SP1 modules are applied. In the inputs to the DSP-system, first-order, low-pass filters with a crossover frequency of 75 kHz are used. In the optical fibers between the control system and the drive circuits of the valves, a time delay of 0.5 μs is introduced. Finally, a time-delay of 3 μs occurs in the gate circuits of the valves.

TABLE I

CHARACTERISTIC PARAMETERS OF THE SYSTEM.

L_S =0.071 pu	E =1.0 pu	ω_g=100π rad/s	f_{sw} =6 kHz
R_S=0.012 pu	u_{dc}=1.5 pu	T_S=166.7 μs	Z_{base}=6.28 Ω

III. VSC and Grid Models

To evaluate the performance of the vector-control system, measured small-signal responses are compared with responses from analytical models. By forming state-space models in the rotating *dq*-frame, time-invariant models of the closed-loop system are obtained. The valves in the converter are modelled as ideal switches by the use of the average switch model (ASM) technique [6]. Due to the harmonic content in the converter output voltages, analytical models based on averaging predict the states of the system accurately only at the sampling instants .

A. Grid Filter and Converter Models

The continuous-time state equation for the grid filter in the *dq*-coordinate system is

$$\frac{d}{dt}\begin{bmatrix} i_d(t) \\ i_q(t) \end{bmatrix} = \mathbf{A}\begin{bmatrix} i_d(t) \\ i_q(t) \end{bmatrix} + \mathbf{B_u}\begin{bmatrix} u_d(t) \\ u_q(t) \end{bmatrix} + \mathbf{B_e}\begin{bmatrix} e_d(t) \\ e_q(t) \end{bmatrix} \tag{1}$$

where the matrices are given by

$$\mathbf{A} = \begin{bmatrix} -\frac{R_s}{L_s} & \omega_N \\ -\omega_N & -\frac{R_s}{L_s} \end{bmatrix} \mathbf{B_u} = \begin{bmatrix} \frac{1}{L_s} & 0 \\ 0 & \frac{1}{L_s} \end{bmatrix} \mathbf{B_e} = \begin{bmatrix} -\frac{1}{L_s} & 0 \\ 0 & -\frac{1}{L_s} \end{bmatrix}$$

The vector current controller operates in discrete time. To model the closed-loop system, the grid model is transformed into a zero-order held sampled system with the sample time T_S. The state equation is

$$\begin{bmatrix} i_d(k+1) \\ i_q(k+1) \end{bmatrix} = \mathbf{F}\begin{bmatrix} i_d(k) \\ i_q(k) \end{bmatrix} + \mathbf{G_u}\begin{bmatrix} u_d(k) \\ u_q(k) \end{bmatrix} + \mathbf{G_e}\begin{bmatrix} e_d(k) \\ e_q(k) \end{bmatrix} \tag{2}$$

where the matrices are

$$\mathbf{F} = \mathrm{e}^{\mathbf{A}T_S}$$
$$\mathbf{G_u} = -\mathbf{G_e} = \int_0^{T_S} \mathrm{e}^{\mathbf{A}\tau} d\tau \mathbf{B_u} \tag{3}$$

The VSC is modelled by using the ASM method and is assumed to provide the requested voltage vector in the *dq*-frame. Two different inductor models are used. In the first model, the inductors have a constant inductance and resistance. In the second one, the influence of the losses on the equivalent series resistance and inductance is taken into account.

B. Controllers and Closed-loop Models

The controller presented here has partially been adopted from [7]. The integration part of the PI-controller is introduced to compensate for static errors caused by non-linearities, noisy measurements and non-ideal components. Eq. (1) can be rewritten as

$$u_d(t) = e_d(t) + R_r i_d(t) - \omega_g L_r i_q(t) + L_r \frac{d}{dt} i_d(t) \tag{4}$$

$$u_q(t) = e_q(t) + R_r i_q(t) + \omega_g L_r i_d(t) + L_r \frac{d}{dt} i_q(t) \tag{5}$$

where the inductance and the resistance of the series coil, which is used in the controller is denoted by subscript *r* to emphasize that the parameters of the controller can differ from the real values. The mean voltages over the sample period *k* to *k*+1 are derived by integrating (4) and (5) from kT_S to $(k+1)T_S$ and dividing by T_S. Dead-beat control is used. During one sample period, the current variations are assumed to be linear and the grid voltage components constant. The output reference voltages are delayed one sample due to the computer calculation time. A time delay compensation term is included in the dead-beat controller to avoid current oscillations. When using dead-beat control, it takes two samples before the grid currents are equal to the reference values of the current. The equations of the controller can be written as

$$\begin{aligned} u_d^*(k+1) &= e_d(k) + R_r i_d(k) - \omega_g L_r i_q(k) \\ &+ k_P\left(i_d^*(k) - i_d(k)\right) + \Delta u_{Id}(k) - \Delta u_d(k) \end{aligned} \tag{6}$$

$$\begin{aligned} u_q^*(k+1) &= e_q(k) + R_r i_q(k) + \omega_g L_r i_d(k) \\ &+ k_P\left(i_q^*(k) - i_q(k)\right) + \Delta u_{Iq}(k) - \Delta u_q(k) \end{aligned} \tag{7}$$

where the gain for the dead-beat control is

$$k_P = \frac{L_r}{T_s} + \frac{R_r}{2} \tag{8}$$

The compensation terms for one-sample time delay [8] are

$$\Delta u_d(k) = k_p\left(i_d^*(k-1) - i_d(k-1)\right) - \Delta u_d(k-1) \tag{9}$$

$$\Delta u_q(k) = k_p\left(i_q^*(k-1) - i_q(k-1)\right) - \Delta u_q(k-1) \tag{10}$$

The integration term of the PI-controller is a sum of the current errors for all the old samples and can be written as

$$\begin{bmatrix}\Delta u_{Id}(k+1)\\ \Delta u_{Iq}(k+1)\end{bmatrix} = \begin{bmatrix}\Delta u_{Id}(k)\\ \Delta u_{Iq}(k)\end{bmatrix} + k_I\begin{bmatrix}i_d^*(k-2)\\ i_q^*(k-2)\end{bmatrix} - k_I\begin{bmatrix}i_d(k)\\ i_q(k)\end{bmatrix} \tag{11}$$

where the integration constant is defined as $k_I = T_S k_P R_r / L_r$. The closed-loop state equation with the PI-controller becomes

$$\mathbf{x}(k+1) = \mathbf{F}_{\mathbf{CLPI}}\mathbf{x}(k) + \mathbf{G}_{\mathbf{CLPI}}\left[i_d^*(k)\ i_q^*(k)\ e_d(k)\ e_q(k)\right]^T \tag{12}$$

where the state vector $\mathbf{x}(k)$ has 12 states.

IV. System Linearization and Influence of Non-linearities

Since most systems are non-linear, a small-signal analysis is generally performed by analysing the linearized system around an operating point denoted by the subscript 0. Perturbations around the operating point are denoted as Δ. In this paper, a linear model of the system is used. However, due to non-linearities in the PWM and non-linear grid-filter parameters, the result is assumed to be valid only at the operating point.

A. Parameters of the Grid Filter

The grid filter consists of an inductor in each phase. The 50 Hz values of the series resistance and inductance of the inductor are used in the current controller. To display the influence of the frequency dependent losses in the grid filter on the dynamic performance, two different inductors are used. The iron core of inductor 1, is made of 0.5 mm non-oriented laminations, and the iron core of inductor 2 is made of 0.35 mm oriented laminations. Both cores have air-gaps. When the frequency increases, the I^2R losses increase due to the skin effect, but the iron losses will dominate due to increased eddy-current and hysteresis losses. If the inductors are modelled by equivalent series resistance and inductance in the frequency domain, the equivalent series parameters vary, according to measurements, as shown in Fig. 2. Both inductors have similar total losses. By using thinner and oriented iron in the core, the hysteresis losses and eddy current losses in the iron are reduced and a more constant series inductance is obtained. The I^2R losses are similar with both filters.

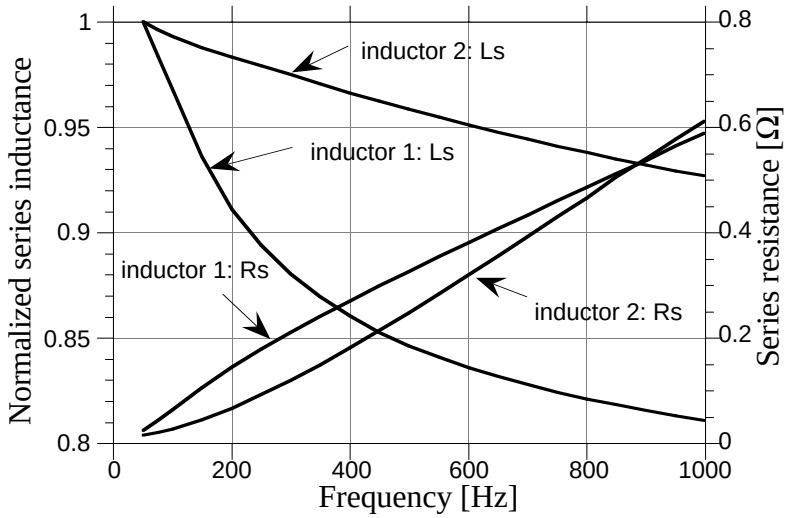

Fig. 2. The measured grid filter inductance and resistance as a function of the frequency for two different inductors.

B. Non-linear Valves and Valve Compensation Function

The non-linearities of the valves and PWM occur due to two different phenomena: blanking time and on-state voltage drop. To avoid short-circuiting the dc-link, each commutation is divided into two steps. First, the conducting valve is turned off. After the blanking time, the other valve in the phase leg is turned on. If the transistor is conducting in the valve that is turned off, the diode in the valve that is to be turned on starts to conduct as soon as the transistor is turned off. Thus, the switching time instant is not influenced by the blanking time. If the sign of the current is not changed, the next commutation is delayed by the blanking time since a commutation from a diode to a transistor occurs. Consequently, the average phase voltage deviates from that requested by the PWM modulator.

The influence of the blanking time and the on-state voltage drop can be reduced by adding compensation voltages Δu^* to the reference phase voltages u^*, i.e., by introducing a valve compensation function. The equations for the compensation of phase 1 are

$$\Delta u^*_{1,Tb}(k) = \text{sign}\left[i_1(k)\right] T_b \,/\, T_S \tag{13}$$

$$u^*_{1,comp}(k) = \Delta u^*_{1,Tb}(k) + D_1 u_{onT1} + \left(1 - D_1\right) u_{onD2} + u^*_1(k) \tag{14}$$

$$u^*_{1,comp}(k) = \Delta u^*_{1,Tb}(k) - \left(1 - D_1\right) u_{onT2} - D_1 u_{onD1} + u^*_1(k) \tag{15}$$

Equation (13) compensates only for the blanking time. Equations (14) and (15) also compensate for the voltage drop across the valves in the on-state for positive and negative current, respectively. The blanking time and the sampling time are denoted as T_b and T_S, respectively. The phase 1 duty ratio is $D_1 = 2u^*_1 / u_{dc}$. The transistor and diode voltage drops are denoted as u_{onT} and u_{onD}. These voltage drops have been measured and are displayed in Table II.

The voltage drops consist of a constant term u_0 and a current-dependent term $R_{on}i$. As discussed above, the compensation is only valid when the current is positive or negative during a whole sample period. When the amplitude of the phase current sample is smaller than the amplitude of the current ripple, the valve compensation is not included.

TABLE II

MEASURED PARAMETERS FOR THE VALVE COMPENSATION FUNCTION.

u_{0T}=1.08 V	u_{0D}=1.05 V	T_S=166.7 μs
R_{onT}=12 mΩ	R_{onD} =10 mΩ	T_b=1.4 μs

V. Analysis of Frequency Responses

To examine the influence of the non-linearities on the dynamic performance of the system, small-signal frequency responses have been measured at different operating points. The influence of the non-linear valves is described by displaying responses with and without the valve compensation function. In section A, the influence of the losses in the grid-filter inductors is described by comparing measured responses with different inductors at a selected operating point. The frequency responses in section A were both measured and calculated by means of analytical models. The objective in section B is to verify that the linear model of the system is valid both in the rectifier operation and the inverter operation, as well as static VAr compensation. In section B, responses measured at four different operating points are presented.

Four different controllers are used. Measured responses are denoted as:

- M(p) P-controller
- M(pi) PI-controller
- M(p,c) P-controller with valve compensation
- M(pi,c) PI-controller with valve compensation

The corresponding responses from the analytical models, all without compensation functions, are denoted as:

- A(p) P-controller with constant parameters
- A(pi) PI-controller with constant parameters
- B(p) P-controller with frequency-dependent grid filter parameters
- B(pi) PI-controller with frequency-dependent grid filter parameters

In the measurements, a sinusoidal small-signal current Δi^* of 0.1 pu was added to one of the reference currents at the operating point. Measurements were performed at 27 different frequencies between 10 Hz and 1200 Hz. The reference currents as well as the *d*- and *q*-currents were sampled at 10 kHz. Anti-alias filters with a crossover frequency of 3 kHz were used. In the analysis of the measured results, the FFT-algorithm was used to evaluate the amplitude gain and phase shift between the sinusoidal reference current Δi_d^* or Δi_q^* and the measured currents Δi_d and Δi_q.

A. Responses with Different Grid Filter Inductors

In this section, the influence of the losses in the grid-filter inductors is described. The measured transfer functions are obtained at the operating point i_{d0}^{*}=0.22 pu and i_{q0}^{*}= –0.67 pu. Responses for inductors with high iron-losses are denoted as M1(·) and responses for inductors with low iron losses are denoted as M2(·). The Bode-diagrams below are scaled in dB. The gains 1 dB and 2 dB correspond to 12 % and 26 %, respectively.

Direct Coupling in q-direction

The gain characteristics of the direct coupling in the q-direction are very similar for all controller types. As shown in Fig. 3, the gain of the response M1(·) is close to 0 dB at low frequencies. However, when the frequency exceeds about 400 Hz, the gain is increased for all controllers M1(·). However, at 1 kHz the gain is 2 dB, which corresponds to an error of 26 %. Thus, the gain deviates from the gain predicted by the linear analytical models A(·). As displayed, the increase in the gain can be predicted by using models B(·). In the responses M2(·), the gain is much closer to the ideal response at all frequencies. The analytical models A(·) give a slightly larger phase lag than the measured one, but the analytical models B(·) track the measured phase correctly.

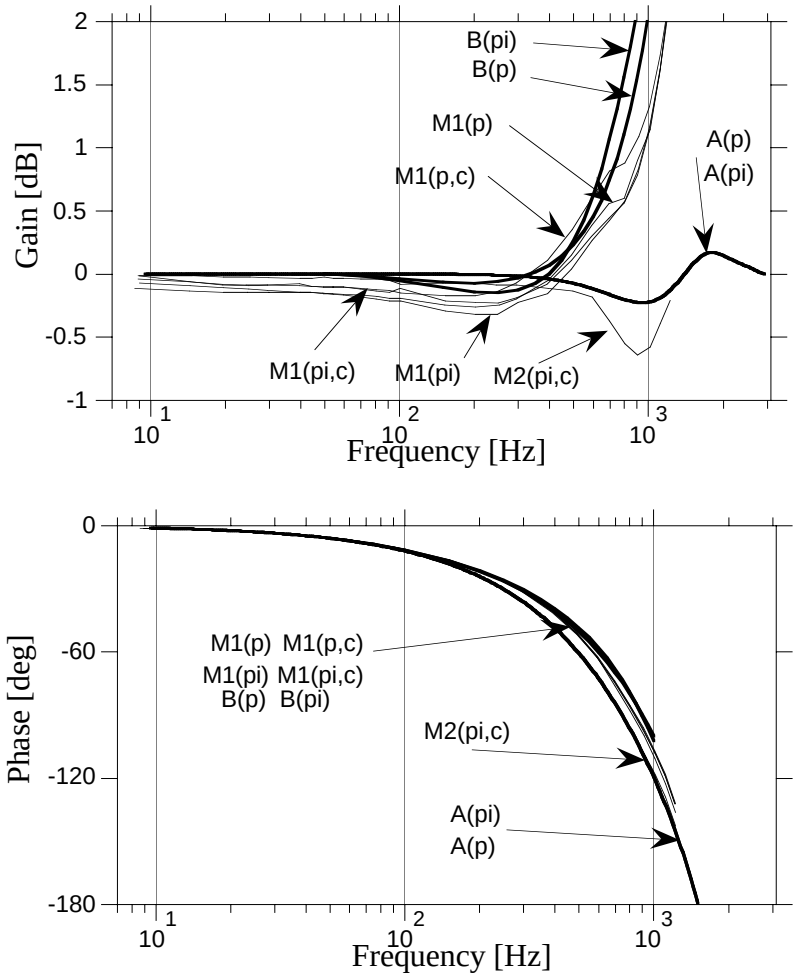

Fig. 3. The Bode diagram from the reference q-current Δi_q^* *to the q-current* Δi_q.

Cross Coupling from q-direction to d-direction

In Fig. 4, the gains of the cross coupling from the *q*-direction to the *d*-direction are shown. The gains for the responses obtained from measurements with compensation for the non-linear valves M1(p,c) and M1(pi,c) are lower than the measured gains without compensation, M1(p) and M1(pi). Consequently, the valve compensation decreases the cross-coupling. The theoretical gains with models B(·) are slightly higher than those of models A(·) but lower than the measured gains. The cross-coupling is significantly affected by the losses in the inductor only at high frequencies, where lower coupling is displayed in the response M2(pi,c). There is also a deviation at low frequencies but very low coupling is obtained with both inductors.

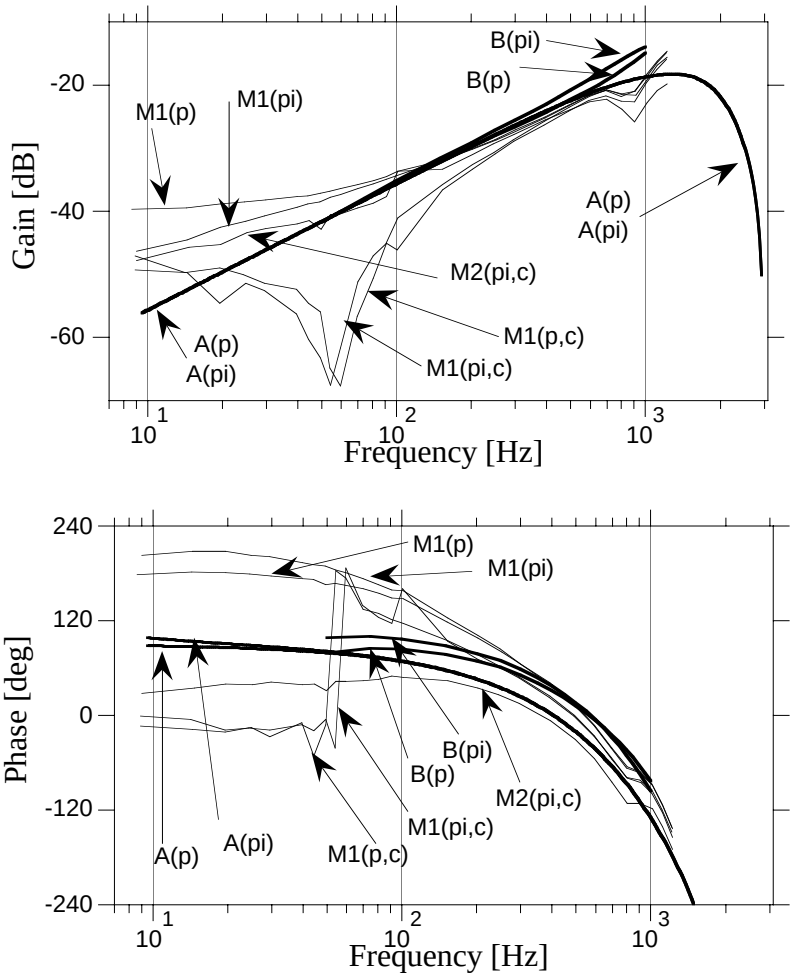

Fig. 4. The Bode diagram from the reference q-current Δi_q^* *to the d-current* Δi_d.

Direct Coupling in d-direction

Direct coupling in the *d*-direction is displayed in Fig. 5. At low frequencies, the responses with the compensation function follow the analytical responses most accurately. At high frequencies, the measured responses do not follow the responses from any of the analytical models. This is due to a non-modelled error in the converter system at high frequencies. In the responses M1(·), the frequency dependent losses in the inductor cause an error that partly cancels the error caused by the converter system. In the measured response M2(pi,c), the gain is reduced at high frequencies. The phase-shifts of the measured frequency responses follow the theoretical phase-shifts B(p), B(pi), which have a smaller phase lag than the models A(p) and A(pi).

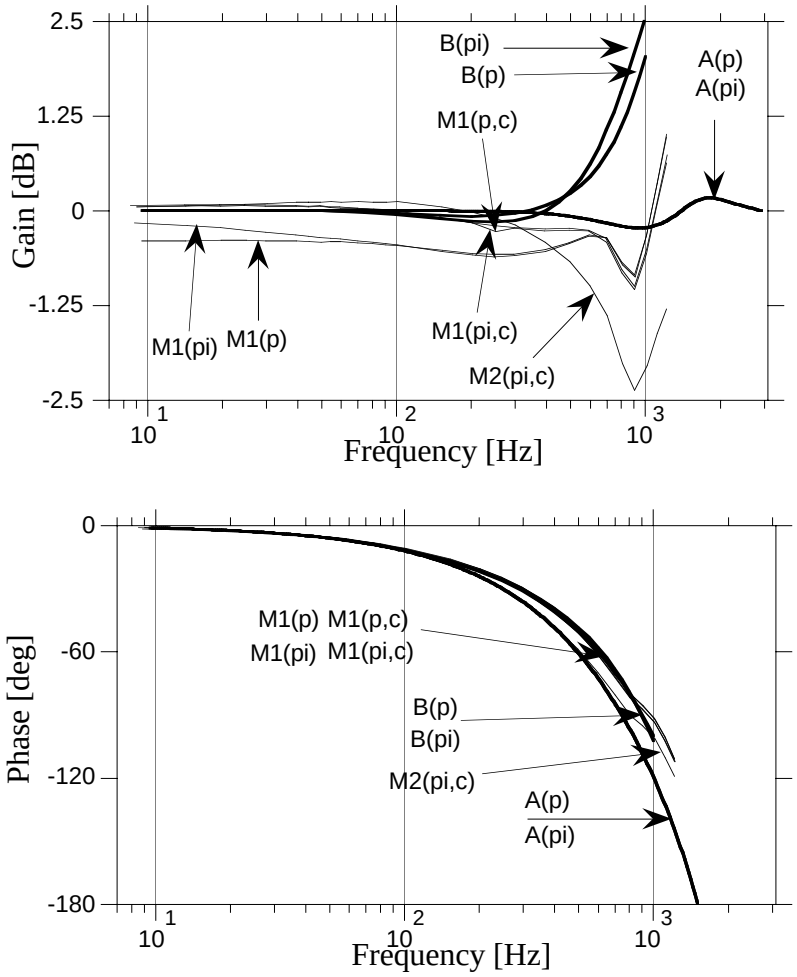

Fig. 5. The Bode diagram from the reference d-current Δi_d^* *to the d-current* Δi_d.

Cross Coupling from d-direction to q-direction

Figure 6 shows that cross coupling from the *d*-direction to the *q*-direction is reduced by using the valve compensation function in responses M1(·). However, at low frequencies, low coupling is obtained for both inductors. The coupling at high frequencies is lower in M2(pi,c) in comparison with M1(·).

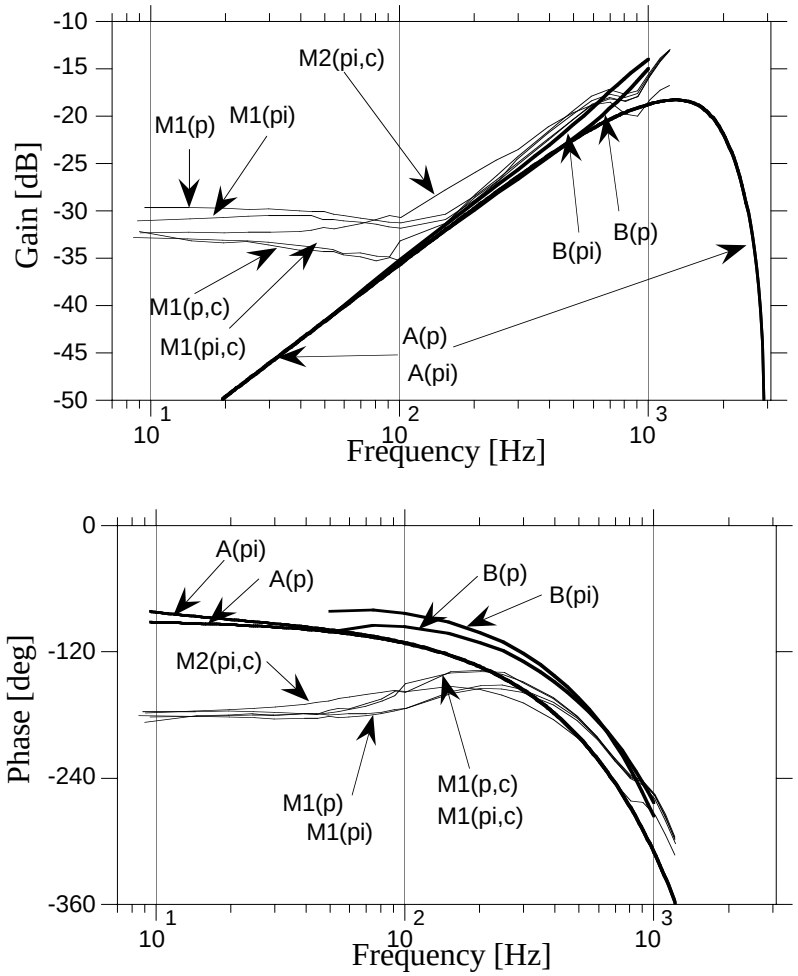

Fig. 6. The Bode diagram from the reference d-current Δi_d^* *to the q-current* Δi_q.

B. Responses at Different Operating Points

The objective in this section is to examine the influence of the operating point on the dynamic performance. The inductor with low iron-losses is used. To illustrate the influence of the non-linearities caused by the valves, measurements with and without the valve compensation function are displayed. As shown in the responses in the previous section, the phase is usually predicted well by a linear analytical model. The phase-shifts are, thus, not displayed. At each operating point, responses to sinusoidal perturbations in the *d*- and *q*-directions are presented. Responses for rectifier and inverter operations are displayed in Figs. 7 to 10. Moreover, responses for reactive power compensation are shown in Figs. 11 to 14. In all cases, the Bode-diagrams are scaled in dB. The gains of 1 dB and 2 dB correspond to 12 % and 26 %, respectively.

Responses in Rectifier and Inverter Operations

The operating points corresponding to rectifier and inverter operations are: i_{d0}^{*}=0.22 pu, i_{q0}^{*} = –0.67 pu, denoted as –P; and i_{d0}^{*} = –0.22 pu, i_{q0}^{*} = 0.67 pu, denoted as P.

In Fig. 7, responses from the *q*- to *q*-direction are displayed. The best responses are obtained in the rectifier operation. At low frequencies, similar performances are obtained. At high frequencies, the best results are obtained without the compensation function.

According to Fig. 8, similar couplings from the *q*- to *d*-direction are obtained at both operating points. At low frequencies, without compensation, the highest coupling occurs in the inverter operation. At high frequencies, the same coupling is obtained at both operating points. The valve compensation function reduces the coupling at frequencies above 100 Hz.

As illustrated in Fig. 9, almost exactly the same responses from the *d*- to *d*-direction are obtained for both operating points. The valve compensation function improves the performance at low frequencies. The best responses are obtained without compensation at frequencies from 600 Hz to 900 Hz.

The coupling from the *d*-to *q*-direction is displayed in Fig. 10. In the inverter operation, a significant difference between responses with and without the valve compensation function is obtained at low frequencies. However, a very low coupling is obtained in the inverter operation. At 1 kHz, the lowest coupling is obtained without the valve compensation function at both operating points.

Responses in Reactive Power Compensation Modes

Reactive power compensation corresponds to the points: i_{d0}^{*} = –0.67 pu and i_{q0}^{*} = 0.22 pu, denoted as –Q; i_{d0}^{*} = 0.67 pu, i_{q0}^{*} = –0.22 pu denoted as Q.

As displayed in Fig. 11, at low frequencies, the response from the *q*- to *q*-direction is significantly improved by using valve compensation. The best responses are obtained without the compensation function in the frequency range from 600 Hz to 1100 Hz.

In Fig. 12, the coupling from the *q*- to *d*-direction is displayed. The influence of the compensation function varies with the frequency. At low frequencies and with a positive reactive current, the lowest coupling occurs without the valve compensation function. At the other operating point, the most effective compensation is obtained at low frequencies. The opposite effect is displayed at frequencies from 600 Hz to 1 kHz.

In the responses plotted in Fig. 13, approximately the same responses from the *d*- to *d*-direction are obtained in both operating points. The valve compensation function improves the performance below 600 Hz.

As illustrated in Fig. 14, the lowest coupling from the *d*-direction to the *q*-direction occurs with the negative reactive current. At this operating point, the compensation function yields very low coupling at low frequencies and improves performance below 600 Hz. At the operating point with the positive reactive current, the coupling is reduced below 300 Hz. At higher frequencies, a similar coupling is obtained with and without compensation.

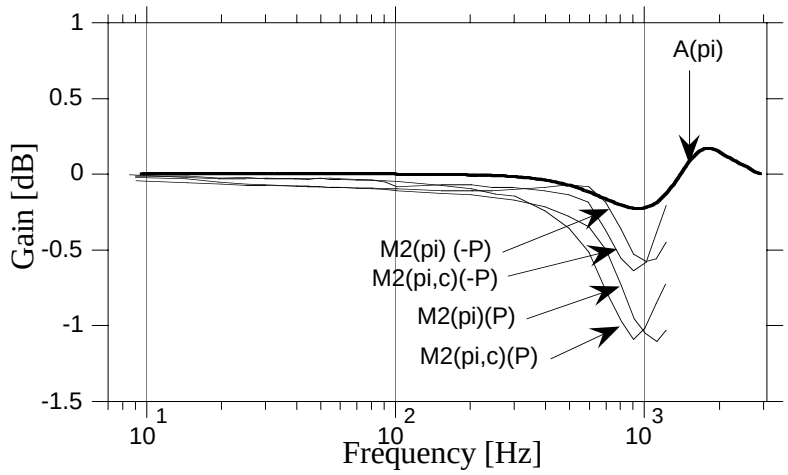

Fig. 7. The frequency response gain from the reference q-current Δi_q^* *to the q-current* Δi_q.

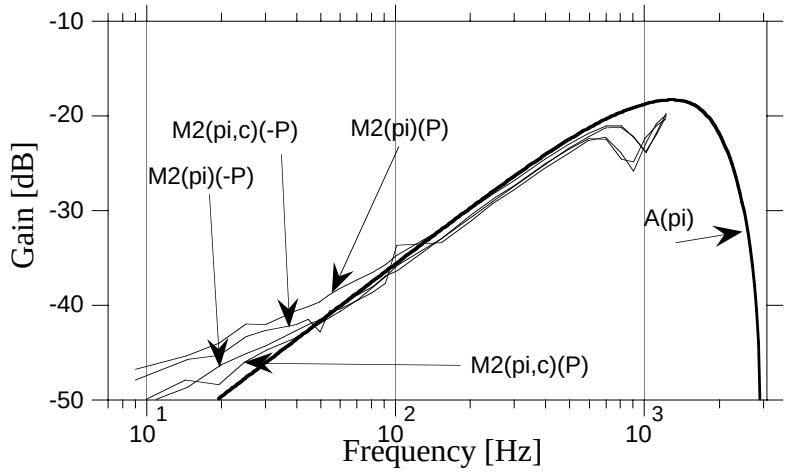

Fig. 8. The frequency response gain from the reference q-current Δi_q^* *to the d-current* Δi_d.

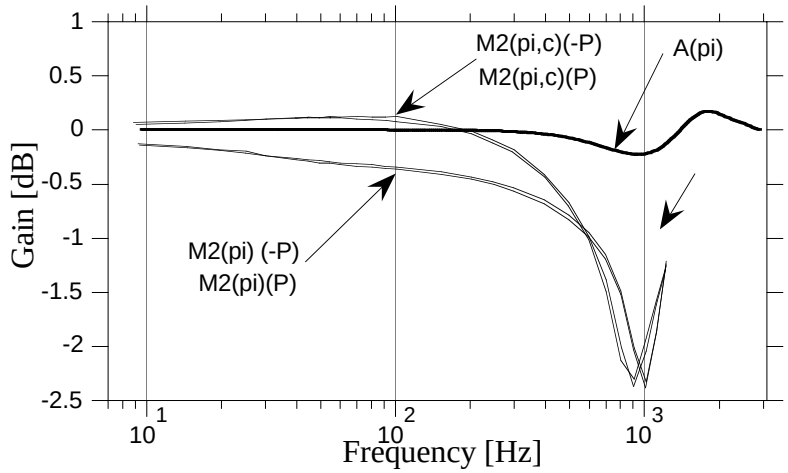

Fig. 9. The frequency response gain from the reference d-current Δi_d^* *to the d-current* Δi_d.

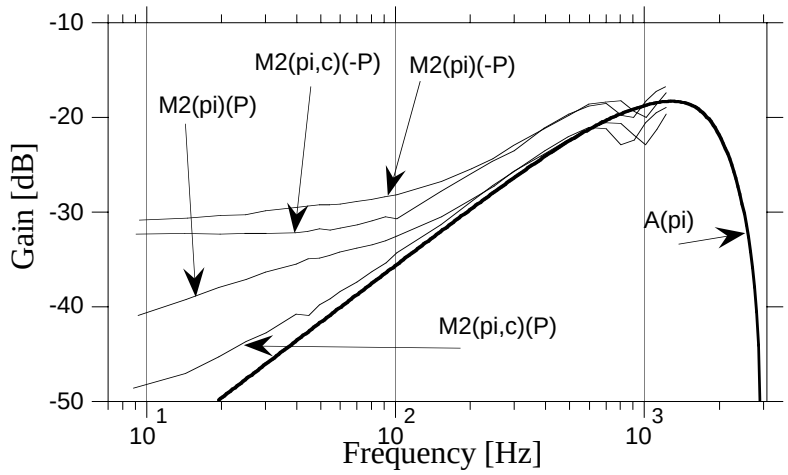

Fig. 10. The frequency response gain from the reference d-current Δi_d^* *to the q-current* Δi_q.

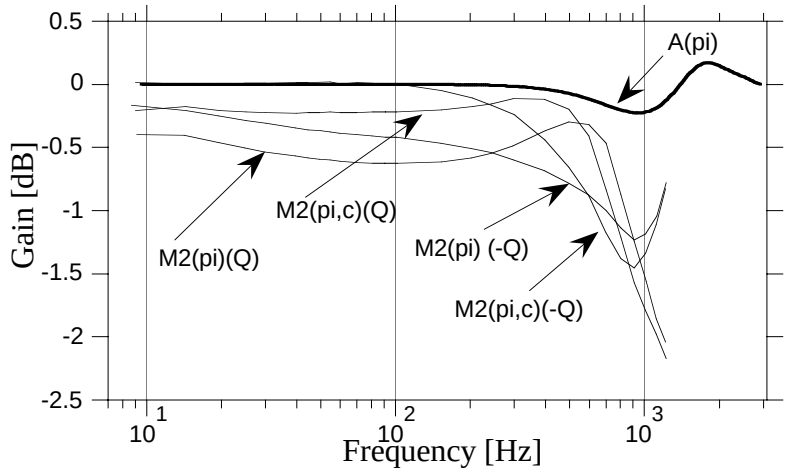

Fig. 11. The frequency response gain from the reference q-current Δi_q^* *to the q-current* Δi_q.

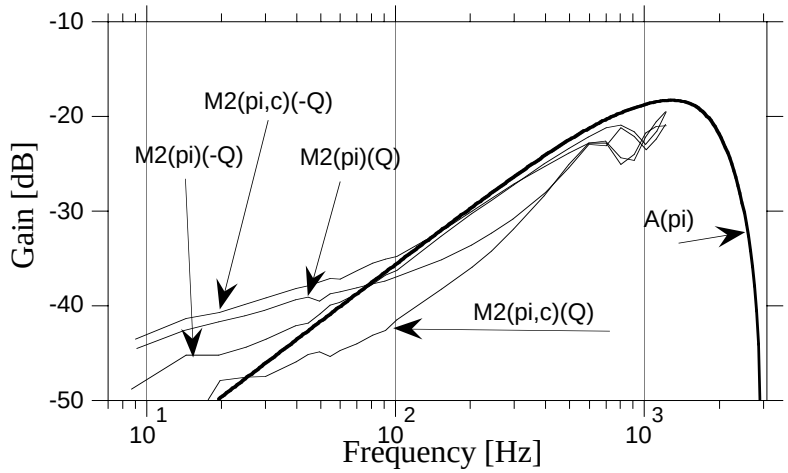

Fig. 12. The frequency response gain from the reference q-current Δi_q^* *to the d-current* Δi_d.

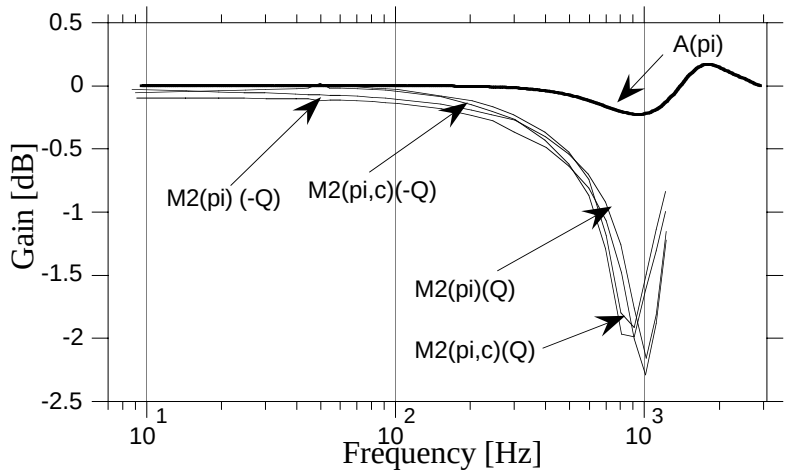

Fig. 13. The frequency response gain from the reference d-current Δi_d^* *to the d-current* Δi_d.

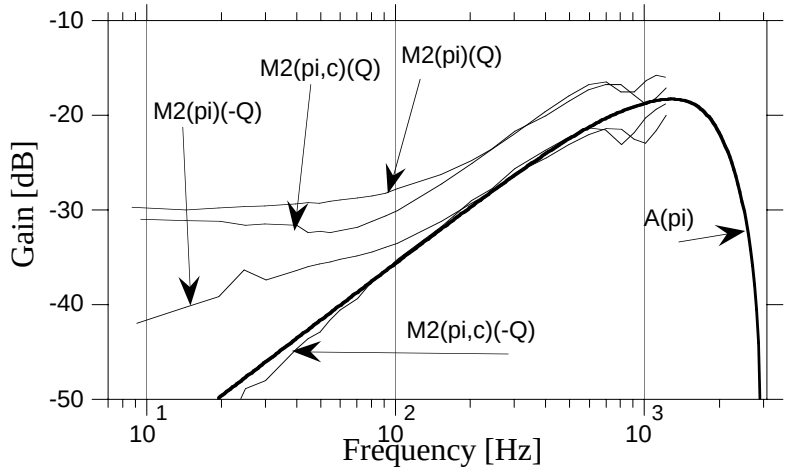

Fig. 14. The frequency response gain from the reference d-current Δi_d^* *to the q-current* Δi_q.

C. Summary of the Frequency Response Analysis

To determine the influence of non-linearities on dynamic performance, small signal frequency responses are determined. In section A, the influence of the losses in the inductors are in focus. As shown, the measured responses in the *q*-direction for inductors with high losses deviate from the responses obtained from the linear analytical model at high frequencies. This deviation can be predicted by including the frequency dependent losses of the grid filter in the analytical model. In the *d*-direction, the deviation does not appear. According to the analytical model with the losses included, a deviation should also occur in the *d*-direction. This indicates that the converter system introduces an error in the *d*-direction. The responses obtained with inductors with low losses show that the response in the *q*-direction is considerably improved. However, the deviation is increased in the *d*-direction. Thus, an error is displayed in the *d*-direction. The conclusion is that the dynamic performance is improved by using inductors with low losses. This is predicted by analytical models and also verified in the *q*-direction. In the *d*-direction, the responses are distorted due to a non-modelled error due to the time delay between the PWM circuit and the switching of the valves in the converter system.

In section B, the influences of the compensation for the non-linearities are displayed at different operating points. The objective is to show that the performance is improved by using the compensation method proposed. The responses are improved at all operating points at low frequencies. At high frequencies, the best results are obtained however, without the compensation function. This should be the result of the non-modelled error mentioned above. The distortion could also be the result of non-ideal sampling. However, the errors occur in the *d*-direction. In the *d*-direction, the sampling can actually be shifted several μs since the current is not changed in the *d*-direction when the voltage vectors 000 and 111 are active. Thus, the error should be due to the time delay between the PWM circuit and the switching of the valves.

VI. Conclusion

The obtained frequency responses correspond well to the analytical model. However, the focus has been on the small deviations in the gains and in the phases from their presumed values. The influence of non-linearities caused by non-ideal valves and grid filter inductors on the frequency response of a vector controlled grid connected VSC are investigated. Non-linearities caused by losses in the grid filter, by blanking time and by non-ideal IGBT-valves are described and their influence on the frequency responses are verified by measurements. By using a compensation function for non-linearities caused by the blanking time and the valves, the frequency responses are improved at frequencies up to about 600 Hz. At higher frequencies, the best results are often obtained without the compensation function. This may be a result of the time delay between the PWM-circuit and the switching of the valves. The non-linearities result in different responses at different operating points.

VII. References

[1] J. Holtz, "Pulsewidth Modulation for Electronic Power Conversion," Proc. of IEEE, Vol. 82, No. 8, August 1994, pp. 1194-1214.

[2] J. K. Pedersen, F. Blaabjerg, J. W. Jensen, P. Thogersen, "An Ideal PWM-VSI Inverter with Feedforward and Feedback Compensation," *5th European Conference on Power Electronics and Applications (EPE'93)*, Brighton, England, 13-16 September 1993, pp. 501-507.

[3] J. Ollila, "Analysis of PWM-converters Using Space Vector Theory: Application to a Voltage Source Rectifier," Doctoral Thesis, Tampere University of Technology, Tampere, Finland, 1993.

[4] S. R. Bowes, "New Sinusoidal Pulsewidth-modulator Inverter," Proc. IEE, Vol. 122, No. 11, November 1975.

[5] S. Hiti, D. Boroyevich, "Small-Signal Modeling of Three-Phase PWM Modulators," *Power Electronics Specialists Conference (PESC'96)*, Baveno Italy, 23-27 June 1996, pp. 550-555.

[6] R. Kagalwala, S. S. Venkata, P. O. Lauritzen, "A Transient Behavioral Model (TBM) for Power Converters," *5th Workshop on Computers in Power Electronics*, IEEE Power Electronics Society, Portland USA, 11-14 August 1996, pp. 18-24.

[7] J. Svensson, "Inclusion of Dead-Time and Parameter Variations in VSC Modelling for Predicting Responses of Grid Voltage Harmonics." *7th European Conference on Power Electronics and Applications (EPE'97)*, Trondheim, Norway, 8-10 September 1997, Proceedings, Vol. 3, pp. 216-221.

[8] M. Lindgren, "Feed forward – Time Efficient Control of a Voltage Source Converter Connected to the Grid by Lowpass Filters," *Power Electronics Specialists Conference (PESC'95)*, Atlanta, 18-22 June 1995, Vol. 2, pp. 1028-1032.

Publication E

M. Lindgren, J. Svensson, "A Method to Compensate for Non-ideal Commutation and Valves in PWM-systems with High Ripple Currents," *1998 IEEE Nordic Workshop on Power and Industrial Electronics* (*NORPIE/98*), Espoo, Finland, August 26-27, 1998, p. 147-152.

Edited version.

A Method to Compensate for Errors Caused by the Blanking Time in PWM Systems with High Ripple Currents

Michael Lindgren Jan Svensson

Chalmers University of Technology
Department of Electric Power Engineering
S-412 96 Göteborg, Sweden
michael.lindgren@elkraft.chalmers.se, jan.svensson@elkraft.chalmers.se

Abstract— In PWM converters, the non-linearity caused by the blanking time depends on the direction of the phase current at the commutations. Previous principles for compensating for non-linearities have been based on the sign of the phase current at the sampling instants, and are not able to compensate if the phase current changes sign between the sampling instant and the commutations. At a low power level, such a change of sign occurs for a large part of the line period when PWM converters are connected to the grid. This paper describes a method to solve the problem by predicting the sign of the phase currents at the commutations. Experimental results are presented for a three-phase grid-connected PWM converter controlled by a discrete vector-current controller. The method makes the compensation possible also at low power levels and in systems with small line filters or low sampling frequencies.

I. Introduction

The performance of PWM converters connected to an ac grid, and PWM inverters in adjustable speed drives (ASDs) is affected by non-linearities that are introduced by non-ideal semiconductor valves and by the blanking time that is used to avoid short-circuiting the dc link of the converter. The non-linearities influence the dynamic performance, as well as the harmonic distortion.

Vector controlled systems using IGBT converters usually operate at high switching frequencies. In such a system, a significant voltage error is caused by the blanking time. This error depends on the sign of the phase currents at the commutations. In ASDs using IGBT valves, the current ripple caused by the PWM is usually low due to high switching frequencies and due to the leakage inductance of the machine. At low ripple currents, the compensation can be based on the sign of the phase current at the sampling instants. When PWM converters are connected to the grid, however, the current ripple caused by the PWM may be high. The current ripple becomes high when line filters with a low inductance are used, especially for high order line filters, such as the LCL-filter [1]. In systems with a high current ripple, the sign of the phase currents at the commutations may be the opposite of the sign at the sampling instant. In such a system, previous compensation methods cannot be used.

The errors caused by the non-linearities and methods to reduce their influence in PWM inverters for ASDs have been described in several publications [2-4]. In [2], methods for reducing the harmonic distortion of the phase currents of machines in ASDs are described and compared. Similar results are also shown for an inductive load in [3]. In [4], a

compensation method for space vector modulation (SVM) PWM that is able to take into account the individual turn-on and turn-off times of the valves is described. Until now, the influence of non-ideal valves and the blanking time on the performance of grid-connected PWM converters has not been in focus.

As described in [5], the dynamic performance of grid-connected vector controlled voltage source converters (VSCs) can be increased by compensating for non-linearities caused by the non-ideal valves and the blanking time. As with previous compensation methods, the compensation was based on the sign of the phase currents at the sampling instants. The compensation function was disconnected at low currents to avoid erroneous compensation due to the high current ripple.

In this paper, an improved compensation method based on predicting the sign of the phase currents at the commutations that occur during each sampling interval is introduced. The method is implemented for a grid-connected vector-controlled converter using a sub-oscillation PWM method. Measurements are presented with and without the compensation method at high and low phase currents.

II. System Description

The system configuration of the VSC connected to the grid by an L-type line filter is shown in Fig. 1. The resistance and the inductance of the line filter are denoted by R_s and L_s, respectively. The phase voltages and currents of the grid are denoted by $e_1(t)$, $e_2(t)$ and $e_3(t)$ and $i_1(t)$, $i_2(t)$ and $i_3(t)$, respectively. The phase voltages of the VSC are denoted by $u_1(t)$, $u_2(t)$ and $u_3(t)$. The grid currents and the grid voltages are sampled and transformed into vectors in the fixed two-axis $\alpha\beta$–coordinate system and then into the rotating *dq*-coordinate system. The *d*-axis of the *dq*-frame is synchronized with the grid flux vector. A predictive discrete dead-beat vector controller tracks the references for the active current $i_q^*(t)$ and the reactive current $i_d^*(t)$. The reference voltage vector from the controller is transformed into the three-phase system. To take full advantage of the dc-link voltage $u_{dc}(t)$, triplen harmonics are added to the reference voltage values in the block OPT. The compensation function for the blanking time and non-ideal valves is represented by the block COMP. The reference voltages for the VSC are transformed into a pulse pattern in the block PWM.

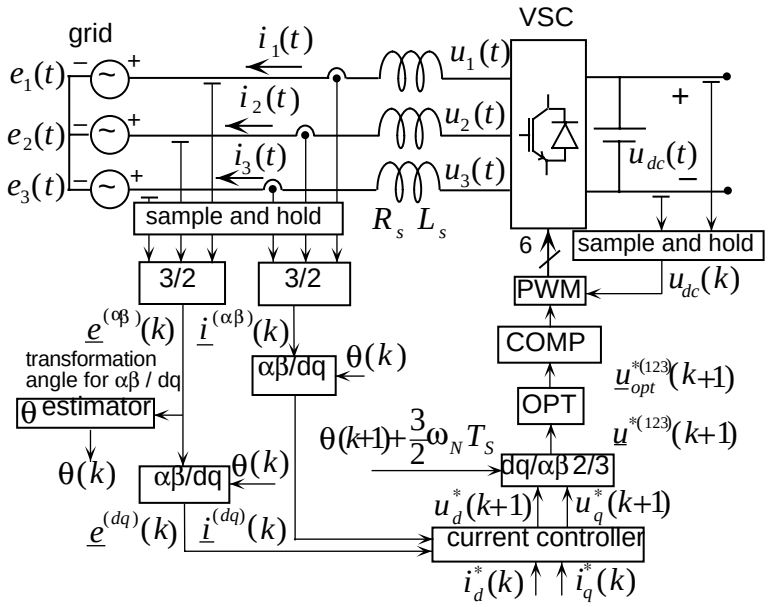

Fig. 1. Overview of the converter system.

The experimental system consists of a VSC with IGBT valves (Toshiba MG400Q1US41 1200V, 400A) and a TMS320C30 control computer. The characteristic parameters of the system are displayed in Table I. The line-to-line voltage of the grid, E, is 400 V rms and the rated phase current is 35 A rms. The switching frequency f_{sw} is equal to the sampling frequency f_s. The sampling time is denoted by T_s. The angular frequency of the grid voltages is denoted by ω_{grid}. The grid frequency is 50 Hz. In the measurements of the currents, LEM LA50-S/SP1 modules are used. First-order, low-pass filters with a crossover frequency of 75 kHz are used at the inputs to the DSP-system. In the optical fibers between the control system and the control circuits of the valves, a time delay of 0.5 μs is introduced, and a time delay of 3 μs is introduced by the gate circuits and the capacitive gates of the valves.

TABLE I
CHARACTERISTIC PARAMETERS OF THE SYSTEM.

L_S=0.071 p.u.	E=1.0 p.u.	ω_{grid}=100π rad/s	f_{sw}=6 kHz
R_S=0.012 p.u.	u_{dc}=1.63 p.u.	T_S=166.7 μs	

III. Errors Caused by Blanking Time and Non-ideal Valves

In this section, errors introduced by non-ideal commutations and non-ideal valves are presented. Two commutations are assumed to take place in each phase leg of the converter during each sampling interval. This is the case when the sampling frequency is equal to the switching frequency assuming that overmodulation does not occur.

During each sampling interval, the lower valve conducts in the beginning of the interval. At the first commutation, the upper valve is turned on. The commutation is delayed by the blanking time if the current is positive, since the diode conducts in this case. Thus, the error is introduced at the commutation from a diode to a transistor, since the diode in the conducting valve is not affected by the gate of the valve. A time delay T_{blank} of the first commutation reduces the average phase voltage during the sampling interval by

$$\Delta u_{blank} = u_{dc} \frac{T_{blank}}{T_s} \tag{1}$$

At the second commutation during the sampling interval, the lower valve is turned on. The commutation from the upper valve to the lower valve is delayed by the blanking time if the current is negative. If the current is negative at the second commutation, the average phase voltage during the sampling interval is increased by Δu_{blank} defined by (1).

Thus, the first commutation is delayed by the blanking time if the current is positive at the first commutation and the second commutation is delayed by the blanking time if the current is negative at the second commutation. The first commutation introduces a negative error and the second commutation introduces a positive error. As a result, the average voltage during the sampling interval is reduced by Δu_{blank} if the current is positive at both commutations and increased by Δu_{blank} if the current is negative at both commutations. If the current is positive at the first commutation and negative at the second commutation, errors of different signs occur and the total error is zero. The same applies if the current is negative at the first commutation and positive at the second commutation. Consequently, no error occurs if the phase current has different signs at the two commutations during a sampling interval. The blanking time T_{blank} of the experimental system is $1.4\ \mu s$ and a positive or negative error of $5.5\ V$ in the average phase voltage occurs if the phase current has the same sign at both commutations during a sampling interval.

In the investigated system, the time delay of $3\ \mu s$ introduced by the gate circuits and the capacitive gate of the valves is approximately the same at the turn-off and the turn-on of a transistor. The average phase voltages are not affected since a turn-on and a turn-off of a transistor occur during each sampling interval. The influence of different turn-on and turn-off times is described in [4].

The forward voltages across the valves for the diode and for the transistor are defined as

$$u_{onD} = U_{D0} + R_{onD} i \tag{2}$$

$$u_{onT} = U_{T0} + R_{onT} i \tag{3}$$

respectively, where U_{D0} and U_{T0} are the no-load voltage drop of the diode and the transistor, respectively. R_{onD} and R_{onT} are the resistances of the diode and the transistor. These parameters have been determined from measurements and are listed in Table II. The forward voltages have been measured for phase currents from 0 to 50 A.

The on-state voltage across the valves results in an error Δu_{on} in the average phase voltage during each sampling interval. Δu_{on} depends on the sign of the phase current. The errors for a positive phase current, and for a negative phase current for phase 1 are

$$\Delta u_{1oni+} = -D_1 u_{onT} - (1 - D_1) u_{onD} \tag{4}$$

$$\Delta u_{1oni-} = (1 - D_1) u_{onT} + D_1 u_{onD} \tag{5}$$

respectively, where the duty ratio is defined as

$$D_1 = \frac{2u_1^*}{u_{dc}} \tag{6}$$

TABLE II
MEASURED PARAMETERS OF IGBT VALVES

U_{D0} = 1.05 V	U_{T0} = 1.08 V	R_{onD} = 10 mΩ	R_{onT} = 12 mΩ

IV. The Compensation Method with Prediction

To compensate for the errors due to the blanking time and the on-state voltage drop, the reference phase voltages to the PWM-circuit are adjusted by adding compensation voltages to the reference voltages from the current controllers. The reference voltage of phase 1 during the sampling interval from *k*+1 to *k*+2 is compensated by

$$u_{1comp}^*(k+1) = u_1^*(k+1) + \Delta u_1(k+1) \tag{7}$$

where

$$\Delta u_1(k+1) = \text{sign}(i_1(k+1))\Delta u_{blank}\zeta_1 - \Delta u_{on} \tag{8}$$

The parameter ζ_1 is determined by the prediction algorithm, and is set to zero if the phase current is going to have different signs at the two commutations which occur during the sampling interval from *k*+1 to *k*+2.

To evaluate if the signs of the phase current in each phase are different at the two commutations during each sampling interval, the sampling interval is divided into 7 segments as illustrated in Fig. 2. During each segment, a linearized equation is used to evaluate the change of the phase current. The phase with the highest reference voltage, $u_{\max}^*$, is commutated first and last during the sampling interval; these time instants are denoted by t_1 and t_6. The phase with the median reference voltage, u_{mid}^*, is commutated at the time instants t_2 and t_5, and the phase with the lowest reference voltage, $u_{\min}^*$, is commutated at the time instants t_3 and t_4. Consequently, assumed that the reference voltage of phase 1 is highest, the current at the first commutation is

$$i_1(t_1) = i_1(k+1) + \Delta i_{1,I} \tag{9}$$

where $\Delta i_{1,I}$ denotes the change of the current during the first segment. The current at the second commutation occurs at the time instant t_6 as

$$i_1(t_6) = i_1(t_1) + \Delta i_{1,II} + \Delta i_{1,III} + \Delta i_{1,IV} + \Delta i_{1,V} + \Delta i_{1,VI} \tag{10}$$

where Δi_{II} to Δi_{VI} denotes the change of the current for segments *II* to *VI*. The parameter ζ_1 of phase 1 is set to zero if

$$i_1(t_1)i_1(t_6) \le 0$$

The linearized equation used for phase 1 is

$$\Delta i_1 = \frac{v_1 - v_o - e_1(k+1) - R_s i_1(k+1)}{L_s} \Delta t \tag{11}$$

where v_0 is the potential of the neutral point and v_1 is the potential in phase 1 of the converter.

To compensate for the time delay of one sample from the sampling until the sampling interval where the voltage compensator is effective, the first order predictors

$$i_1(k+1) = 2i_1(k) - i_1(k-1) \tag{12}$$

$$e_1(k+1) = 2e_1(k) - e_1(k-1) \tag{13}$$

are used to predict the phase current and the phase voltage at the sampling instant *k*+1.

The phase current and the phase voltage in (11) are assumed to be constant during the sampling interval from *k*+1 to *k*+2. v_1 is determined from the reference voltages of phase 1. The voltage drop of the valve is neglected and v_1 is set to $u_{dc}/2$ for the segments where the upper valve is conducting, and to $-u_{dc}/2$ when the lower valve is conducting. v_0 is unambiguously determined during each of the seven segments of the sampling interval, since v_0 is equal to the average of the three phase potentials of the converter. This applies assuming that the sum of the phase currents and the sum of the phase voltages of the grid are zero. The sum of the phase currents is zero, since no neutral conductor is connected to the dc link. In practice, the sum of the phase voltages is not zero. This unsymmetry introduces an error of a few volts into the evaluation of v_0. This error is neglected in this paper.

The reference voltages of the PWM and the corresponding output vectors of the converter are illustrated in Fig. 2. In the sampling interval that is described in the figure, the reference value of phase 1 is highest, the reference value of phase 2 is the median and the reference value of phase 3 is the lowest phase voltage. Each of the three reference voltages are compared with the triangular wave. The upper valve in each phase conducts when the reference voltage is higher than the triangular wave, and the lower valve conducts when the reference voltage is lower than the triangular wave. A voltage vector $\underline{u}$= 000 denotes that the lower valve is conducing in all three phases and a voltage vector $\underline{u}$= 111 denotes that the upper valve is conducing in all three phases. For the first and the last intervals, the output vector $\underline{u}$= 000 is used, and the voltage in the neutral point is, consequently, $-u_{dc}/2$. For the interval t_3 to t_4, the vector $\underline{u}$= 111 is active, and v_0 is $u_{dc}/2$. During the intervals t_1 to t_2 and t_5 to t_6, one of the vectors $\underline{u}$= 100, $\underline{u}$= 010, or $\underline{u}$= 001 are output (depending on the angle of the grid-flux vector). The neutral point voltage is $-u_{dc}/6$. Finally, during the intervals from t_2 to t_3 and from t_4 to t_5, one of the vectors $\underline{u}$= 011, $\underline{u}$= 101, or $\underline{u}$= 110 are output, and the neutral point voltage is $u_{dc}/6$.

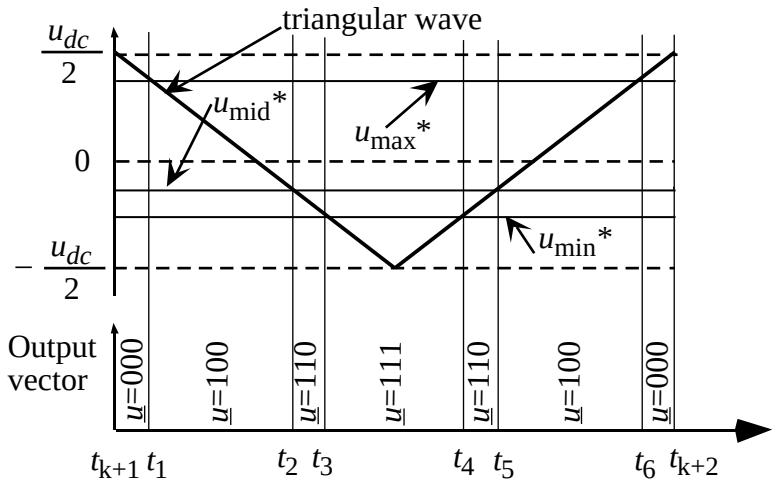

Fig. 2. Triangular sub-oscillating PWM and the output vectors of the VCS during one sampling interval.

The times that are used in the prediction algorithm are obtained from the reference voltages of the PWM as

$$t_1 = \frac{T_s}{2}\left(\frac{1}{2} - \frac{u_{\text{max}}^*}{u_{dc}}\right) \tag{14}$$

$$t_6 = T_s - t_1 \tag{15}$$

$$t_2 = \frac{T_s}{2}\left(\frac{1}{2} - \frac{u_{mid}^*}{u_{dc}}\right) \tag{16}$$

$$t_5 = T_s - t_2 \tag{17}$$

$$t_3 = \frac{T_s}{2}\left(\frac{1}{2} - \frac{u_{\text{min}}^*}{u_{dc}}\right) \tag{18}$$

$$t_4 = T_s - t_3 \tag{19}$$

V. Experimental results

In this section, the performance of the current control system is displayed with and without any compensation for the non-linearities caused by the on-state voltage drop and the blanking time. The performance is illustrated in steady state. In order to verify that the compensation function reduces the errors, no integration is used in the controller. The errors are functions of the power factor, as described in [3]. In Figs. 3 to 6, rectifier operations at a current of 0.1 p.u. are displayed. Figs. 7 to 10 show the currents when a reactive current of 0.1 p.u. is supplied by the converter. Finally, Figs. 11 to 14 show the rectifier operation at 0.8 p.u. Observe that each plot has been measured by a digital oscilloscope at different time instants.

As described in Figs. 3, 4, 7 and 8, the phase current commutates at different signs for approximately half the period at a phase current of 0.1 p.u. Consequently, during each sampling interval, there is always one phase that commutates at different signs. As a

result, the converter voltage in the *dq*-frame would not be accurate during any sampling interval without a compensation based on prediction. In principle, the harmonic distortion should be reduced by the compensation. However, due to a voltage harmonic distortion on the grid, a similar distortion of the phase current is obtained with and without the compensation. The current harmonic distortion is also reduced by the current control system.

As shown in Figs. 5 and 13, there are only minor static errors in the *d*-direction when the converter operates in a pure rectifier operation and the *d*-reference is zero. As displayed in Fig. 9, a static error occurs in the *d*-direction when the converter supplies a current only in the *d*-direction. The static error is effectively reduced when the compensation method is used.

Fig. 10 shows that only a minor error occurs in the *q*-direction when a current is supplied in the *d*-direction. In Figs. 6 and 14, it is shown that a significant error occurs in the *q*-direction when a current reference in the *q*-direction is applied. The errors are significantly reduced by the compensation function.

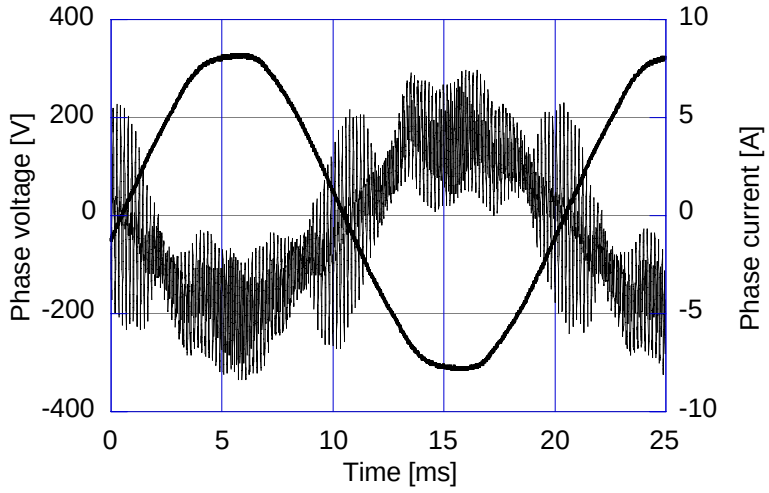

Fig. 3. Line current and line voltage without compensation at a reference current of –0.1 p.u. active current (rectifier operation).

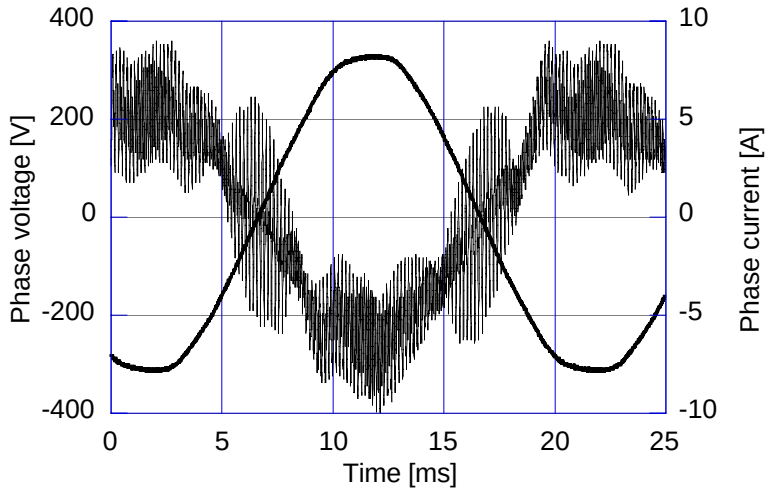

Fig. 4. Line current and line voltage with compensation at a reference current of –0.1 p.u. active current (rectifier operation).

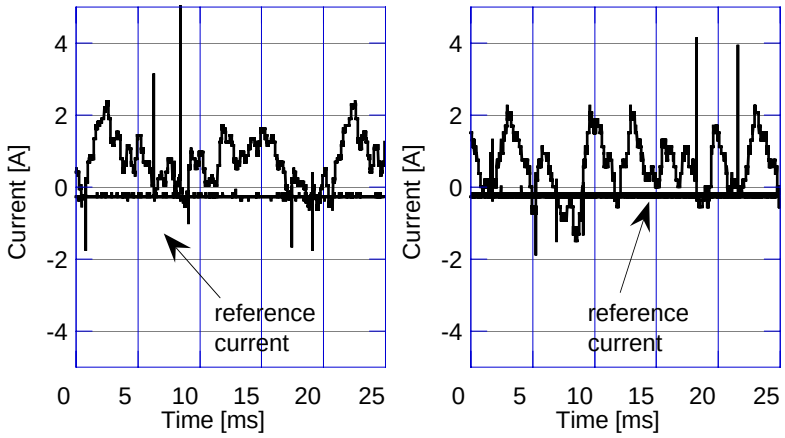

Fig. 5. Reference d-current and resulting d-current of line current at a reference current of –0.1 p.u. active current (rectifier operation). Without compensation (left) and with compensation (right).

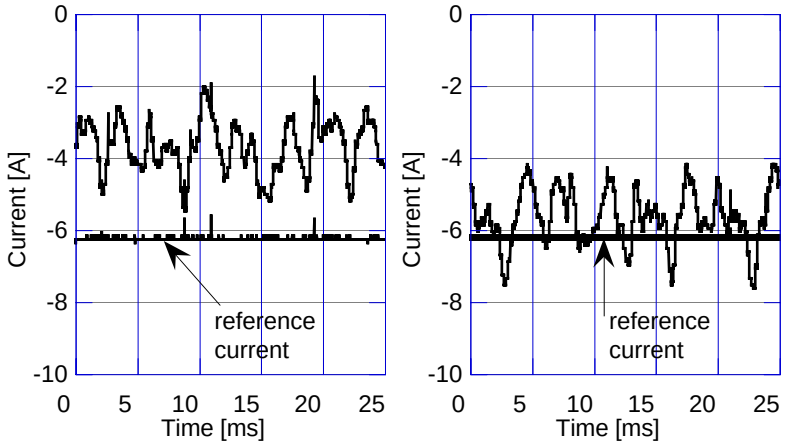

Fig. 6. Reference q-current and resulting q-current of line current at a reference current of –0.1 p.u. active current (rectifier operation). Without compensation (left) and with compensation (right).

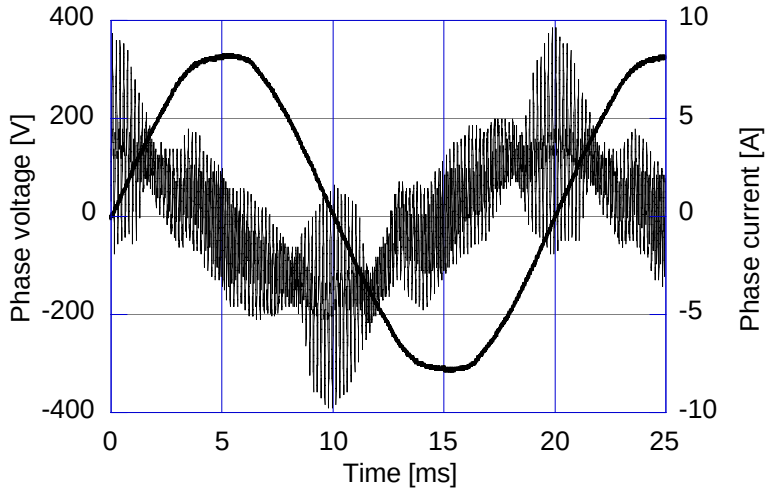

Fig. 7. Line current and line voltage without compensation at a reference current of 0.1 p.u. reactive current (reactive power generation operation).

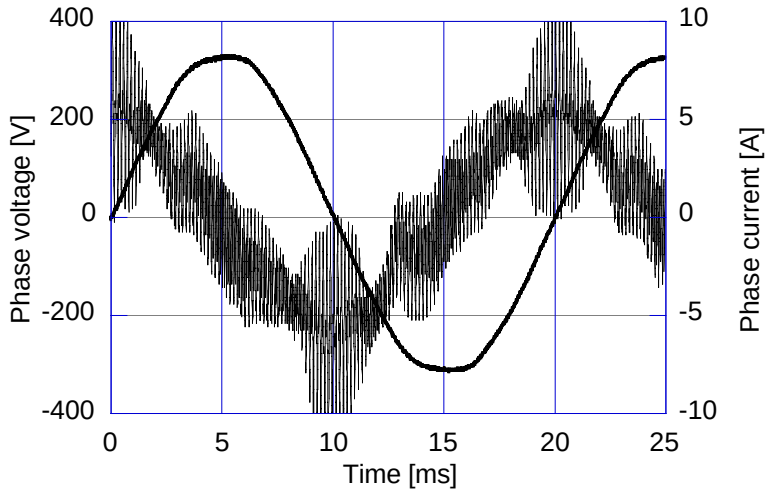

Fig. 8. Line current and line voltage with compensation at a reference current of 0.1 p.u. reactive current (reactive power generation operation).

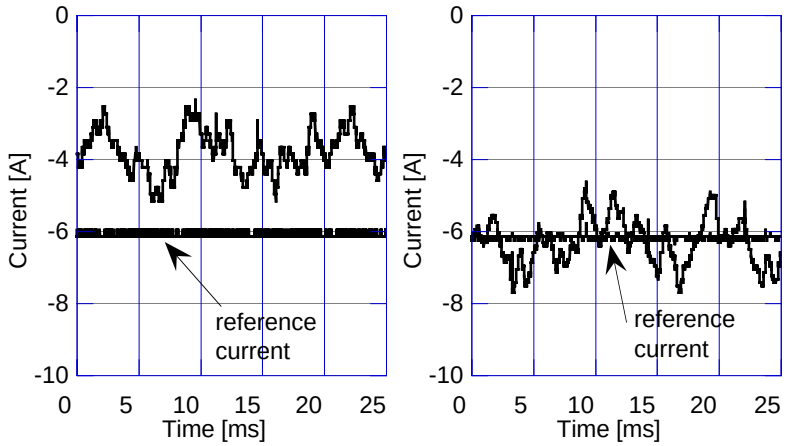

Fig. 9. Reference d-current and resulting d-current of line current at a reference current of 0.1 p.u. reactive current (reactive power generation operation). Without compensation (left) and with compensation (right).

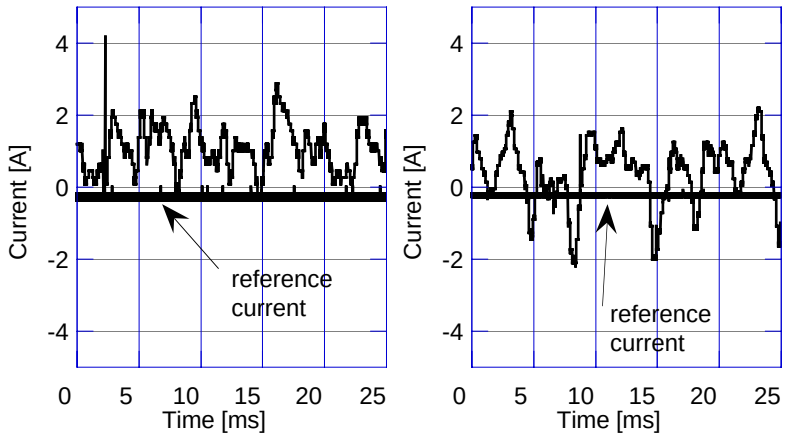

Fig. 10. Reference q-current and resulting q-current of line current at a reference current of 0.1. p.u. reactive current (reactive power generation operation). Without compensation (left) and with compensation (right).

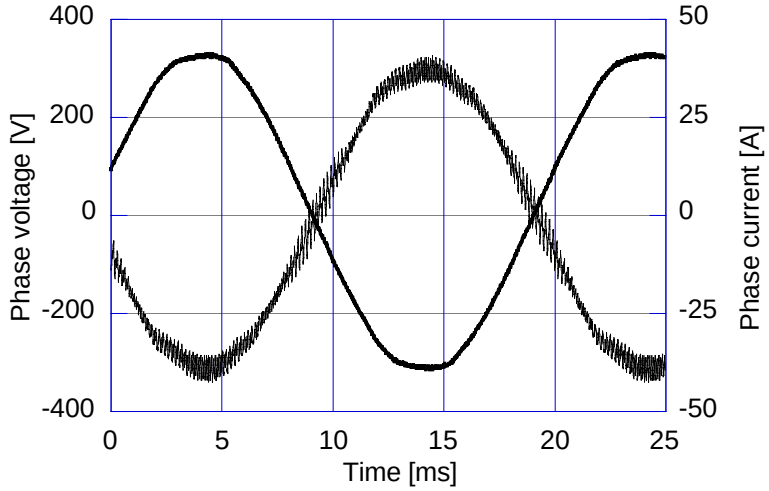

Fig. 11. Line current and line voltage without compensation at a reference current of –0.8 p.u. active current (rectifier operation).

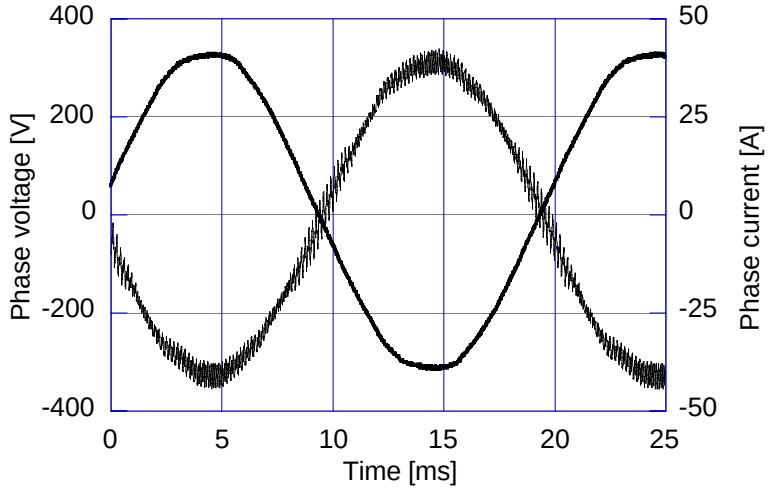

Fig. 12. Line current and line voltage with compensation at a reference current of –0.8 p.u. active current (rectifier operation).

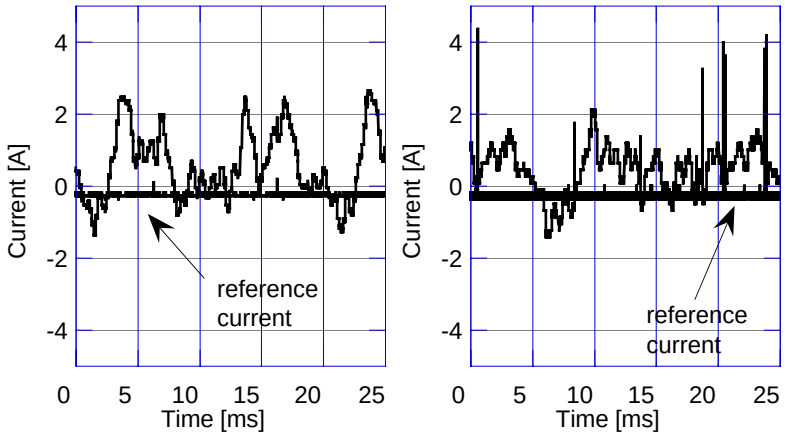

Fig. 13. Reference d-current and resulting d-current of the line current at a reference current of –0.8 p.u. active current (rectifier operation). Without compensation (left) and with compensation (right).

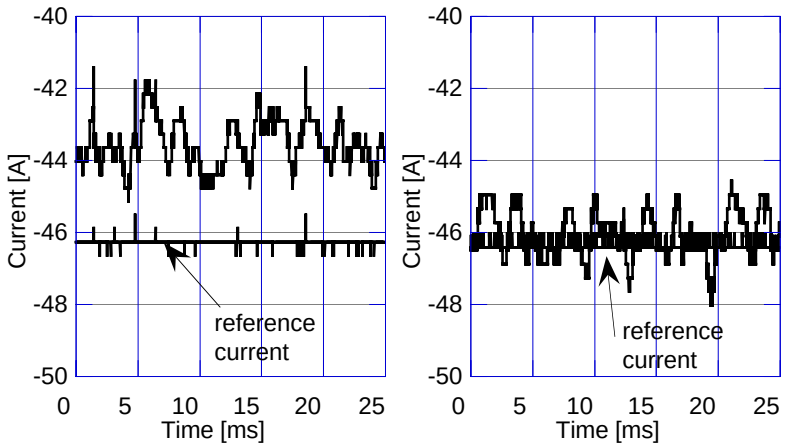

Fig. 14. Reference q-current and resulting q-current of the line current at a reference current of –0.8 p.u. active current (rectifier operation). Without compensation (left) and with compensation (right).

VI. Conclusion

A method of compensating for errors caused by the on-state voltage drop and the blanking time in grid-connected VSCs is described. In grid-connected PWM converters, a significant current ripple occurs in the phase currents. It is shown here that it is necessary to predict the sign of the phase currents at the commutation instants during the sampling intervals in order to compensate accurately. A prediction method is described for a vector-current controlled grid-connected three-phase VSC and experimental results are presented. As shown, the static errors of the vector control system vary with the power factor. The static errors are effectively reduced by the compensation function. The current harmonic distortion of the phase current is not significantly reduced by the compensation function. This is partly due to a voltage harmonic distortion of the grid during the measurements and partly due to the fact that harmonic distortion is reduced by the current control system. The main advantage of the compensation method is that a more ideal operation of a vector control system is obtained.

Acknowledgment

The project was financed by Sydkraft AB's research foundation and by the Swedish National Board for Industrial and Technical Development.

References

[1] M. Bojrup, P. Karlsson, M. Alaküla, B. Simonsson. "A Dual Purpose Battery Charger for Electric Vehicles," *IEEE Power Electronics Specialists Conference (PESC-98*), Fukuoka, Japan, May 17-22, 1998, pp. 565 - 570.

[2] J. K. Pedersen, F. Blaabjerg, J. W. Jensen, P. Thogersen, "An Ideal PWM-VSI Inverter with Feedforward and Feedback Compensation," *5th European Conference on Power Electronics and Applications (EPE'93),* Brighton, England, 13-16 September 1993, pp. 501 - 507.

[3] S. Jeong, M. Park, "The Analysis and Compensation of Dead-Time Effects in PWM Inverters," *IEEE Transactions on Industrial Electronics,* Vol. 38, No. 2, April 1991, pp. 108 - 114.

[4] J. Choi, S. Young, S. Sul, "Inverter Output Voltage Synthesis Using Novel Dead Time Compensation," *IEEE Applied Power Electronics Conference* (*APEC-94*), Vol. 1, 1994 pp. 100 -106.

[5] J. Svensson, M. Lindgren. "Vector Current Controlled Grid Connected Voltage-source Converter. Influence of Non-linearities on the Performance," *IEEE Power Electronics Specialists Conference (PESC-98*), Fukuoka, Japan, May 17-22, 1998, pp. 531–537.

Publication F

M. Lindgren, "Feed forward — Time Efficient Control of a Voltage Source Converter Connected to the Grid by Lowpass filters," *IEEE Power Electronics Specialists Conference (PESC 95)*, Atlanta, USA, June 18-22, 1995, Vol. 2, p. 1028-1032.

Edited version.

Some of the equations have been corrected as compared with the original paper.

Feed forward — Time Efficient Control of a Voltage Source Converter Connected to the Grid by Lowpass Filters

Michael B Lindgren M.Sc.
Chalmers University of Technology
Department of Electrical Machines and Power Electronics
S- 412 96 Gothenburg Sweden
michaell@emke.chalmers.se

***Abstract*—** To reduce the number of measurements in digitally controlled converter systems, observers are often proposed. This gives complicated controller equations and to obtain sufficient sampling frequency, DSPs are often proposed. In this paper, a control principle avoiding measurements by using feed forward of steady state vectors is introduced. Only one state out of three is measured. The time efficient controllers facilitates using a low cost control system.

I. INTRODUCTION

Recent increase in the power rating of fast switching power semiconductors facilitates performing load levelling, UPS, SVC, active filtering and sinusoidal rectifying at increasing power rates. Compared to line commutated converters, the harmonic distortion is considerably reduced. Nevertheless, harmonics are still present. Today research activities are addressing the problem of reducing the switching losses and Electro Magnetic Interference (EMI) by performing soft switching of the power semiconductors using resonant converters [1]. This allows increased switching frequency, thus reduced current harmonics injected to the grid. An alternative solution is to use low pass filters between the converter and the grid. This provides low harmonic distortion at moderate switching frequencies. Compared to the regular series choke filter (L-filter), the switching frequency can be considerably reduced "in press" [2]. Compared to resonant converters, the complexity of the control system is significantly reduced. A control system measuring all variables results in an expensive system and a high time consumption for the AD conversion. An alternative is to feed back some of the state variable, and to estimate other states by using observers. Observers result in time consuming controller equations. To limit the delay time, DSP based systems are often proposed [3]. Compared to micro controller systems, this increases the system cost and complexity.

In this paper, a control principle based on feed forward is presented. Major advantages of the control principle are that only one state out of three have to be measured and that the controller equations are time efficient. In applications where stable operation is sufficient it is possible to omit the feedback. An variant of it adapted for rectifier operation is presented in [4]. In digital control of PWM-converters, the delay time is related to the switching frequency. To obtain high dynamic performance, the switching frequency has to be set high. A method using increased sampling frequency during transient response is introduced.The method provides high dynamic performance and low semiconductor losses.

II. SYSTEM DESCRIPTION

The system layout is presented in Fig. 1

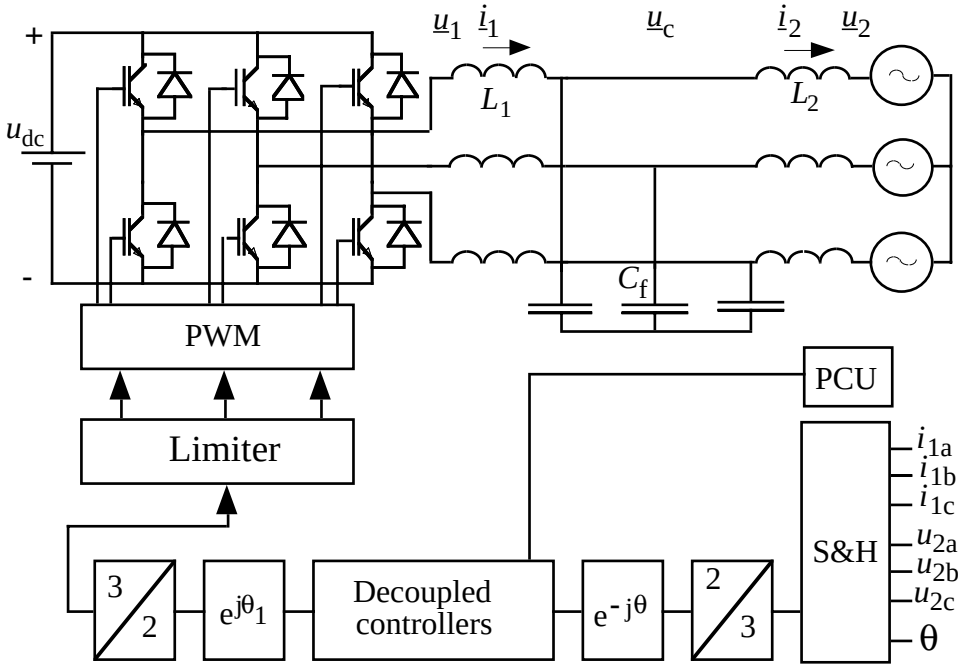

Fig. 1. VSI connected to the grid by LCL-filters.

All vector variables are defined in the synchronously rotating dq- reference frame. The transformation angle θ is the angle of the grid flux in phase a. θ_1 is the average angle of the succeeding sample interval. The parameters are: x_{l1}=0.05 p.u. x_{l2}= 0.025 p.u. x_c= 10 p.u. R_1= R_2= 0.005 p.u. u_{dc}= 2 p.u. u_{base}= 400 V, i_{base}= 10 A, z_{base}= 40 Ω.

L_1 is the leakage inductance of a transformer and L_2 is the inductance of a series inductor. By installing the transformer at this side of the capacitors, the reactive current produced by the capacitors is not loading the transformer. PCU denotes power controller unit. In this paper, the PCU is assumed to be an outer loop. The dc-voltage u_{dc} is assumed to be constant.

A. Attenuation of harmonics

To obtain appropriate attenuation of harmonics, an attenuation of 20 dB is sufficient. As displayed in Fig. 2, this is obtained at 2.5 kHz. Thus, a switching frequency of 2.5 kHz is sufficient from harmonic distortion point of wiev. Suboscillation third harmonic injection PWM is performed. The sampling frequency is equal to twice the switching frequency.

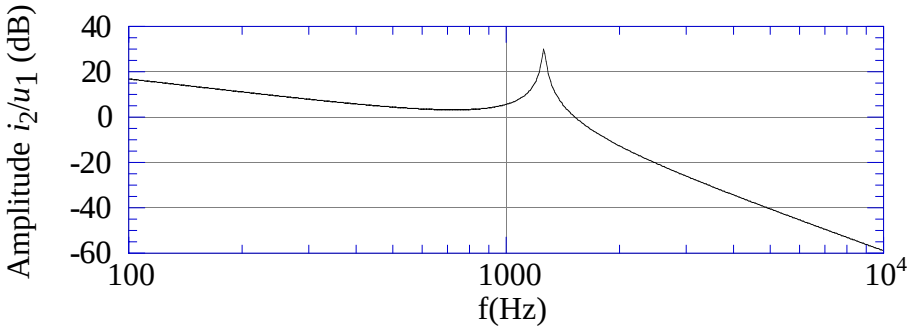

Fig. 2. Transfer function from converter phase voltage to line current.

B. Control

To achieve high dynamic performance the control is performed in the synchronously rotating dq- reference frame. It is based on feed forward of reference values and proportional control of the converter current vector according to (1). In addition, delay time compensation is performed. This is described in section III. The controller equation is

$$\underline{u}_1^* = \underline{u}_2 + (R_2 + \mathrm{j}\omega L_2)\underline{i}_2^* + (R_1 + \mathrm{j}\omega L_1)\underline{i}_1^* + k_\mathrm{p}(\underline{i}_1^* - \underline{i}_1) \tag{1}$$

$\underline{u}_1^*$ is the converter voltage reference vector. $\underline{i}_2^*$ is the grid current reference vector to be supplied by the PCU. The corresponding converter current reference vector, $\underline{i}_1^*$, is determined by using steady state relations.

The steady state relations between converter and grid reference currents are

$$i_{1\mathrm{d}}^\bullet = (1-\omega^2 L_2 C_\mathrm{f}) i_{2\mathrm{d}}^\bullet - R_2 \omega C_\mathrm{f} i_{2\mathrm{q}}^\bullet - \omega C_\mathrm{f} u_{2\mathrm{q}} \tag{2}$$

$$i_{1\mathrm{q}}^\bullet = (1-\omega^2 L_2 C_\mathrm{f}) i_{2\mathrm{q}}^\bullet + R_2 \omega C_\mathrm{f} i_{2\mathrm{d}}^\bullet + \omega C_\mathrm{f} u_{2\mathrm{d}} \tag{3}$$

Using these relations the controllers can be expressed

$$u_{1\mathrm{d}}^\bullet(k+1) = -k_p i_{1\mathrm{d}} + \mathrm{c}_1 i_{2\mathrm{d}}^\bullet - \mathrm{c}_2 i_{2\mathrm{q}}^\bullet + \mathrm{c}_3 u_{2\mathrm{d}} - \mathrm{c}_4 u_{2\mathrm{q}} \tag{4}$$

$$u_{1\mathrm{q}}^\bullet(k+1) = -k_p i_{1\mathrm{q}} + \mathrm{c}_2 i_{2\mathrm{d}}^\bullet + \mathrm{c}_1 i_{2\mathrm{q}}^\bullet + \mathrm{c}_4 u_{2\mathrm{d}} + \mathrm{c}_3 u_{2\mathrm{q}} \tag{5}$$

The coefficient used are

$$\mathrm{c}_1 = (R_1 + k_\mathrm{p})(1-\omega^2 L_2 C_\mathrm{f}) + R_2(1-\omega^2 L_1 C_\mathrm{f}) \tag{6}$$

$$\mathrm{c}_2 = \omega L_2 + (R_1 + k_\mathrm{p}) R_2 \omega C_\mathrm{f} + \omega L_1 (1-\omega^2 L_2 C_\mathrm{f}) \tag{7}$$

$$\mathrm{c}_3 = 1-\omega^2 L_1 C_\mathrm{f} \tag{8}$$

$$\mathrm{c}_4 = (R_1 + k_\mathrm{p})\omega C_\mathrm{f} \tag{9}$$

III. ANALYTICAL SYSTEM MODELING

A converter system using digital control is a mixed signal system with a statistical time delay caused by the PWM. Thus, analysis can be performed in the discrete or continuous plane. In this paper, discrete modelling of the system is used. A major advantage of the discrete analysis is that the delay time caused by the sample and hold is easily modelled. In a system based on vector control, analytical modelling is preferably performed in the dq-reference frame. Still, to perform PWM, the feed back loop includes cordinate transformations. When dynamics and stability are to be analysed, the converter can be modelled as an ideal voltage source in the dq-frame. This implies that the analysis can be performed exclusively in the dq-frame. To model the system, state space technique is used.

A. Open loop state space equation

From Fig. 1, the open loop state space equation

$$\frac{\mathrm{d}}{\mathrm{dt}}\underline{x}_1 = \mathrm{A}\underline{x}_1 + \mathrm{B}\underline{u}_1 \tag{10}$$

can be formed. A and B are the system- and input matrix respectively and $\underline{x}_1$ and $\underline{u}_1$ are the state- and input vector. $\underline{x}_1 = (i_{1d}, i_{1q}, i_{2q}, i_{2q}, u_{cd}, u_{cq})$ and $\underline{u}_1 = (u_{1d}, u_{1q}, u_{2d}, u_{2q})$. The matrixes are

$$\mathrm{A} = \begin{bmatrix} -\frac{R_1}{L_1} & \omega & 0 & 0 & -\frac{1}{L_1} & 0 \\ -\omega & -\frac{R_1}{L_1} & 0 & 0 & 0 & -\frac{1}{L_1} \\ 0 & 0 & -\frac{R_2}{L_2} & \omega & -\frac{1}{L_2} & 0 \\ 0 & 0 & -\omega & -\frac{R_2}{L_2} & 0 & \frac{1}{L_2} \\ \frac{1}{C_\mathrm{f}} & 0 & -\frac{1}{C_\mathrm{f}} & 0 & 0 & \omega \\ 0 & \frac{1}{C_\mathrm{f}} & 0 & -\frac{1}{C_\mathrm{f}} & -\omega & 0 \end{bmatrix}$$

$$\mathrm{B} = \begin{bmatrix} \frac{1}{L_1} & 0 & 0 & 0 \\ 0 & \frac{1}{L_1} & 0 & 0 \\ 0 & 0 & -\frac{1}{L_2} & 0 \\ 0 & 0 & 0 & -\frac{1}{L_2} \\ 0 & 0 & 0 & 0 \\ 0 & 0 & 0 & 0 \end{bmatrix} \quad \mathrm{C} = \begin{bmatrix} 1 & 0 & 0 & 0 & 0 & 0 \\ 0 & 1 & 0 & 0 & 0 & 0 \\ 0 & 0 & 1 & 0 & 0 & 0 \\ 0 & 0 & 0 & 1 & 0 & 0 \\ 0 & 0 & 0 & 0 & 1 & 0 \\ 0 & 0 & 0 & 0 & 0 & 1 \end{bmatrix}$$

Discretization yields the corresponding discrete state space equation

$$\underline{x}_1(k+1) = F_1 \underline{x}_1(k) + G_1 \underline{u}_1(k) \tag{11}$$

B. Closed *loop state space equation*

To evaluate the dynamic performance, the closed loop state space model is formed. Due to the sampling and evaluation of controller equations, a delay of one sampling period occurs in the feedback loop. The closed loop state space equation is obtained by expanding the state space equation (11) with the controller equations. In the controllers, delay time compensation is performed. This conciderably improves the dynamic performance. Delay time compensation is obtained by adding a compensation term in each controller equation according to

$$u_{1d}{}^{*}(k) = u_{1d}{}^{*}(k) - \Delta u_{1d}{}^{*}(k) \tag{12}$$

$$u_{1q}{}^{*}(k) = u_{1q}{}^{*}(k) - \Delta u_{1q}{}^{*}(k) \tag{13}$$

where

$$\Delta u_{1d}{}^{\bullet}(k) = k_p\left[i_{1d}{}^{\bullet}(k-1) - i_{1d}(k-1)\right] - \Delta u_{1d}{}^{\bullet}(k-1) \tag{14}$$

$$\Delta u_{1q}{}^{\bullet}(k) = k_p\left[i_{1q}{}^{\bullet}(k-1) - i_{1q}(k-1)\right] - \Delta u_{1q}{}^{\bullet}(k-1) \tag{15}$$

The expanded equation is

$$\underline{x}_2(k+1) = F_2 \underline{x}_2(k) + G_2 \underline{u}_2(k) \tag{16}$$

The new vectors are $\underline{x}_2 = (i_{1d}, i_{1q}, i_{2d}, i_{2q}, u_{cd}, u_{cq}, u_{1d}, u_{1q}, \Delta u_{1d}, \Delta u_{1q})$ and $\underline{u}_2 = (i_{2d}{}^{*}, i_{2q}{}^{*}, u_{2d}, u_{2q})$. The matrices are

$$F_2 = \begin{bmatrix} F_{11} & F_{12} & F_{13} & F_{14} & F_{15} & F_{16} & G_{11} & G_{12} & 0 & 0 \\ F_{21} & F_{22} & F_{23} & F_{24} & F_{25} & F_{26} & G_{21} & G_{22} & 0 & 0 \\ F_{31} & F_{32} & F_{33} & F_{34} & F_{35} & F_{36} & G_{31} & G_{32} & 0 & 0 \\ F_{41} & F_{42} & F_{43} & F_{44} & F_{45} & F_{46} & G_{41} & G_{42} & 0 & 0 \\ F_{51} & F_{52} & F_{53} & F_{54} & F_{55} & F_{56} & G_{51} & G_{51} & 0 & 0 \\ F_{61} & F_{62} & F_{63} & F_{64} & F_{65} & F_{66} & G_{61} & G_{62} & 0 & 0 \\ -k_p & 0 & 0 & 0 & 0 & 0 & -1 & 0 & 0 & 0 \\ 0 & -k_p & 0 & 0 & 0 & 0 & 0 & -1 & 0 & 0 \\ -k_p & 0 & 0 & 0 & 0 & 0 & 0 & 0 & -1 & 0 \\ 0 & -k_p & 0 & 0 & 0 & 0 & 0 & 0 & 0 & -1 \end{bmatrix}$$

$$G_2 = \begin{bmatrix} 0 & 0 & G_{13} & G_{14} \\ 0 & 0 & G_{23} & G_{24} \\ 0 & 0 & G_{33} & G_{34} \\ 0 & 0 & G_{43} & G_{44} \\ 0 & 0 & G_{53} & G_{54} \\ 0 & 0 & G_{63} & G_{64} \\ c_1 & -c_2 & c_3 & -c_4 \\ c_2 & c_1 & c_4 & c_3 \\ c_5 & -c_6 & 0 & -c_7 \\ c_6 & c_5 & c_7 & 0 \end{bmatrix}$$

where the following coefficients are introduced

$$c_5 = k_p(1-\omega^2 L_2 C_f) \tag{17}$$

$$c_6 = k_p R_2 \omega C_f \tag{18}$$

$$c_7 = k_p \omega C_f \tag{19}$$

IV. DYNAMIC PERFORMANCE

To set the controller gain and analyse the dynamic performance, the root loci of the closed loop state equation are analysed.The closed loop state equation is of tenth order, thus five complex conjugated poles occur. The gain is varied from zero to k_{pd} where

$$k_{pd} = \frac{x_{l1}}{\omega T_s}. \tag{20}$$

A. Time delay influence

In Fig. 3, the frequency ratio is 50. As displayed, the system is at the stability limit at k_p= 0. This corresponds to open loop operation. As displayed, the stability limit is exceeded if the gain is increased. In Fig. 4 and Fig. 5, the frequency ratios are 75 and 100 respectively. This corresponds to delay times of 133 µS (p= 75) and 100 µS (p=100). The arrows point out the pole location at the gains selected; k_p= 1.09k_{pd} (p= 75) and k_p= 1.06k_{pd} (p= 100). Every fifth pole location is plotted. The difference in gain between two poles is k_{pd}/9 (p= 75) and k_{pd}/12 (p= 100).

In Fig. 6 and Fig. 7, the converter- and grid-current vector components obtained at the gains selected are displayed. As displayed, the current ripple is reduced if the frequency ratio is increased. In addition, the coupling is low. The step responses are almost equal, this is due to saturated controllers. At p= 100 saturation occurs at positive quadrature current errors above 0.3 p.u. At p= 75, due to lower gain, saturation occurs at errors above 0.4 p.u.

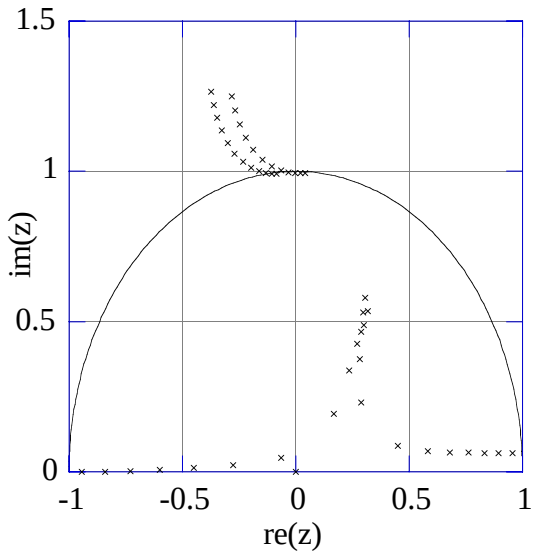

Fig. 3. Root loci at p= 50. k_p goes from zero to $2k_{pd}$.

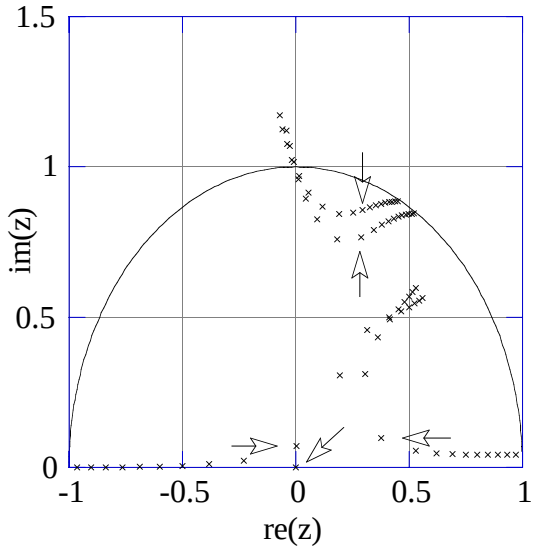

Fig. 4. Root loci at p= 75. k_p goes from zero to $2k_{pd}$.

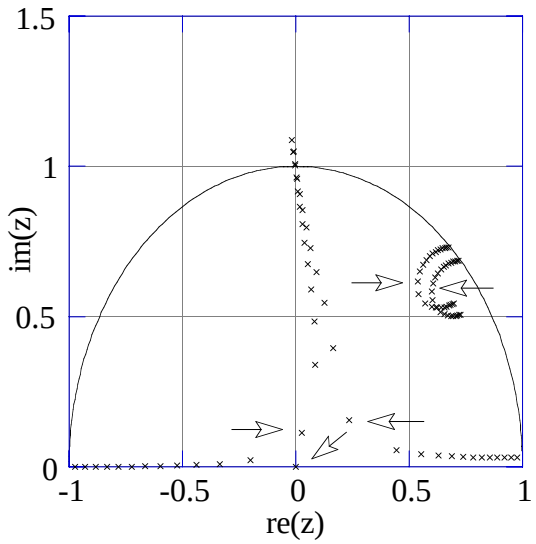

Fig. 5. Root loci at p= 100. k_p *goes from zero to* $2k_{pd}$.

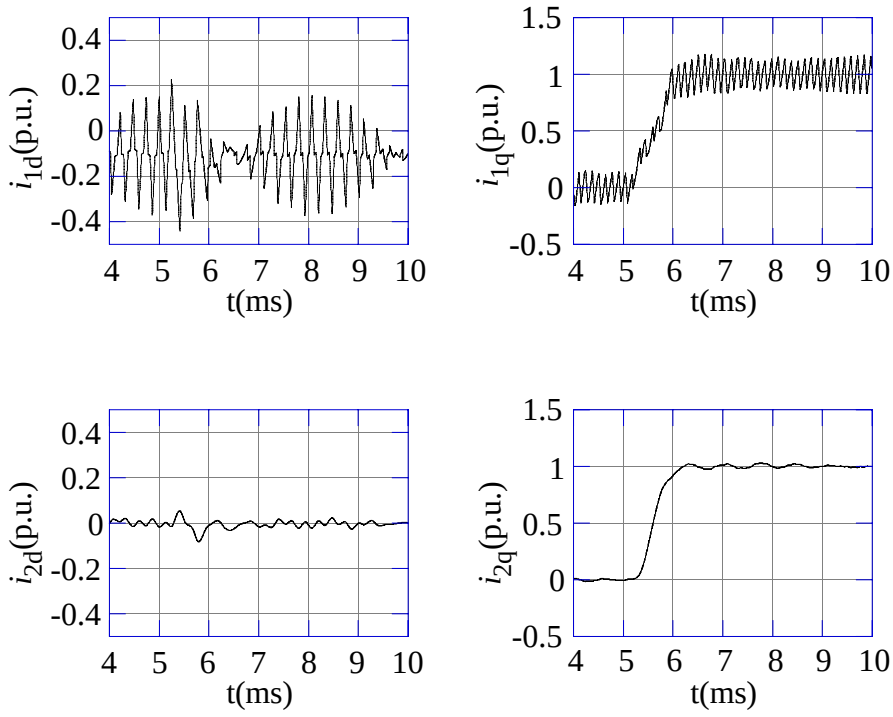

Fig. 6. Step response at p= 75. Converter current upper and line current lower. Direct current (left) and quadrature current (right).

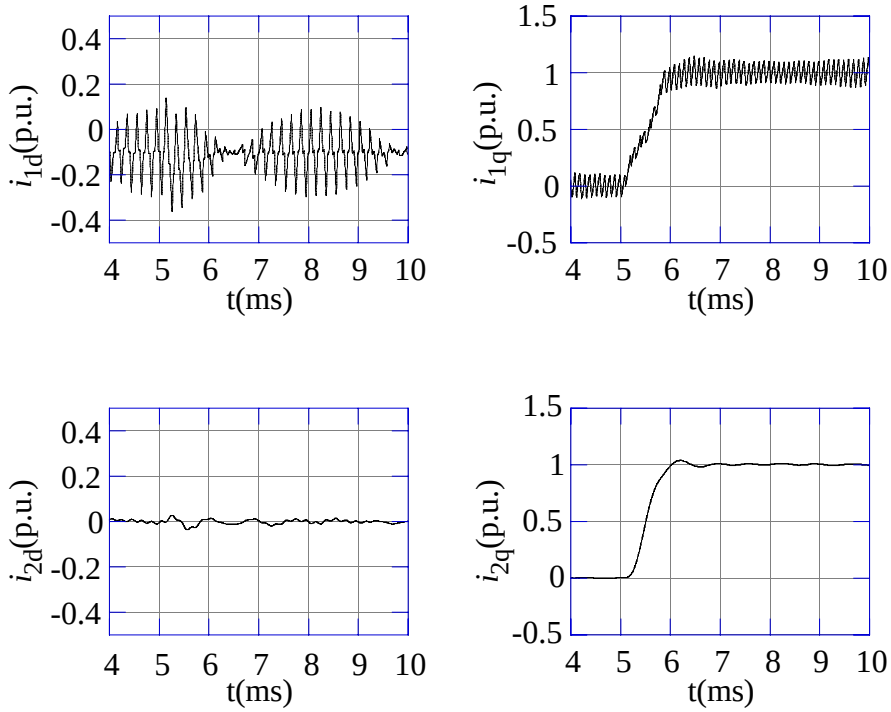

Fig. 7. Step response at p= 100. Converter current upper and line current lower. Direct current (left) and quadrature current (right).

B. Control using adaptive frequency ratio

As displayed in the previous section, the dynamic performance is dependent on the time delay. Consequently, to obtain high band width, the frequency ratio should be set high. However, in section II A, it was shown that a frequency ratio of p= 50 results in sufficiently low current harmonic distortion. If the frequency ratio is set low, the efficiency will be improved and the cost for cooling equipment reduced. This can be obtained by using different frequency ratios in steady state and transient state.

C. Influence of grid voltage distortion

If LCL-filters are used, line voltage distortion may cause energy oscillations between the inductive part of the grid and the filter capacitors. This occurs at line voltage harmonics close to the filter resonance frequency. If open loop control is performed, the resonance frequency of the filter has to be set to avoid voltage harmonics.Using the control principle proposed in this paper considerably reduces this problem. To analyse the influence analytically, the transfer function matrix of the closed loop system is used. The transfer functions from inputs to the direct component of the grid current are

$$i_{2d} = G_{31}u_{1d} + G_{32}u_{1q} + G_{33}u_{2d} + G_{34}u_{2q} \tag{21}$$

It is sufficient to consider the transfer functions G_{33} and G_{34}. The Bode plots of these transfer functions are displayed in Fig. 8. In Fig. 9, 0.05 p.u. voltage harmonic of 1250 Hz is applied. This is a positive order harmonic, thus the frequency is 1200 Hz in the dq-frame. From the Bode diagrams, the amplification of the direct grid voltage is 5.7 times and the phase shift -200 degrees. The quadrature voltage is amplified 0.8 times and the phase shift is -180 degrees. The amplitude of the total direct current is obtained by

$$|i_{2d}| = \sqrt{(5.7\cos(\frac{20}{180}\pi)^2 + (5.7\sin(\frac{20}{180}\pi) - 0.8)^2} \approx 5.75$$

According to the simulation i Fig. 9, the amplitude of the direct current is approximately 6 times the amplitude of the reference.

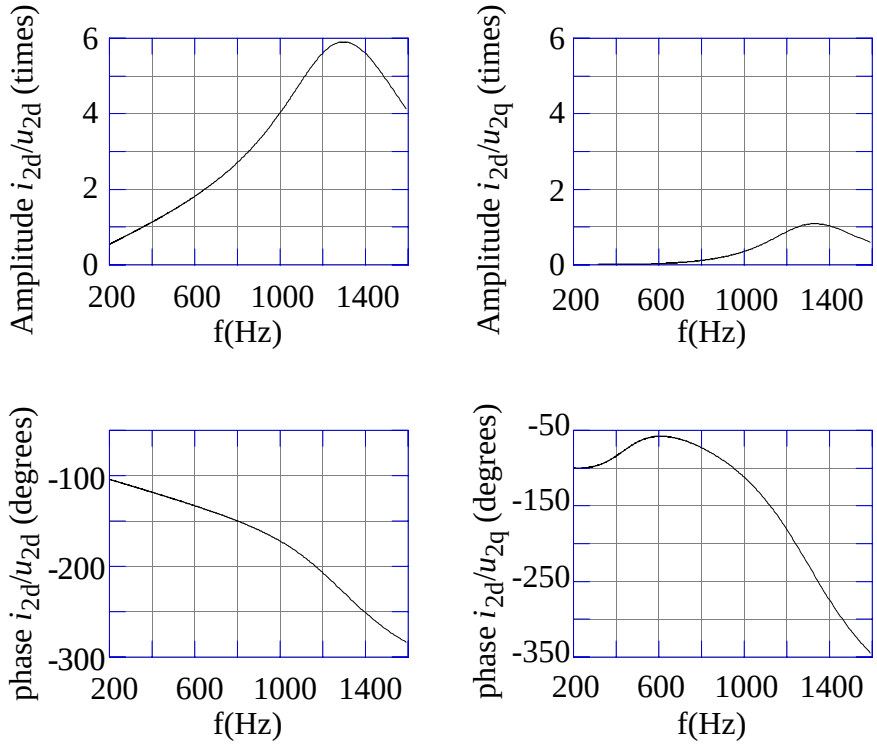

Fig. 8. Bode diagrams of G_{33} (left) and G_{34} (right).

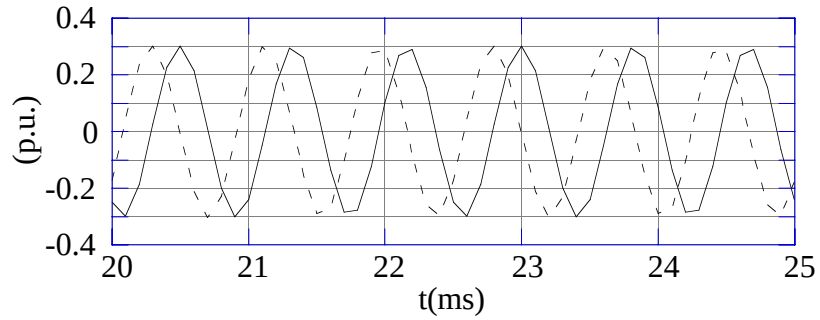

Fig. 9. Direct (dashed) and quadrature (solid) line current components at 0.05 pu voltage harmonic of frequency 1250 Hz.

V. Conclusions

A principle providing few measurements and time efficient controller equations is introduced. Thus it combines the advantages of control using observers and traditional low complexity controllers. The band width is dependent on the time delay in the feed back loop and the impedances selected. Band width sufficint for most utility applications can be obtained with the parameters proposed. A method to increase the dynamic performance without increasing the semiconductor losses conciderably is presented. Dynamic performance and influence of grid voltage harmonics is presented by using simulations and analytical analysis based on state space technique.

REFERENCES

[1] K.Yurugi, H.Yonemori and M.Nakaoga, "Next generation zero-voltage soft switched PWM three.phase Ac-Dc active power converter". Conference proceedings of the first international telecommunications energy special conference, Berlin 1994, p. 367-374.

[2] M. Lindgren and J. Svensson, "Connecting fast switching converters to the grid— harmonic distortion and its reduction". Accepted for presentation at Stockholm Power Tech conference- Stockholm, June 1995.

[3] Y. Ito, M. Iwata, S. Kawauchi, "Digital control of three phase PWM inverters for UPSs using dead beat observer". Conference record of the power conversion conference- Yokohama 1993. p. 79-84.

[4] J. Ollila. A PWM-rectifier without current measurement. EPE Journal. Vol. 4, No 2, p 14-19, June 1994.

Publication G

M. Lindgren, J. Svensson, "Control of a Voltage-source Converter Connected to the Grid through a LCL-filter — Application to Active Filtering," *IEEE Power Electronics Specialists Conference (PESC 98*), Fukuoka, Japan, May 17-22, 1998, Vol. 1, p. 229-235.

Edited version.

Control of a Voltage-source Converter Connected to the Grid through an LCL-filter—Application to Active Filtering

Michael Lindgren Jan Svensson

Chalmers University of Technology
Department of Electric Power Engineering
S- 412 96 Göteborg, Sweden
michael.lindgren@elkraft.chalmers.se, jan.svensson@elkraft.chalmers.se

Abstract- In this paper, a control principle for a voltage-source converter connected to the grid through an LCL-filter is presented. The dynamic performance is compared with the performance obtained with an L-filter and a dead-beat vector-control system. Measured frequency responses and an active filtering operation verify the control principle. By using an LCL-filter, high attenuation of harmonics caused by the PWM and high dynamic performance can be obtained simultaneously. Different methods for active filtering are compared. It is advantageous to use a Fourier-method since it allows for compensation for time delays occurring in the control system in the frequency domain. By using the LCL-filter along with compensation for time delays in the frequency domain, active filtering can be performed at moderate switching frequencies. This is a major advantage in systems, such as a rectifier with an active filtering option.

I. INTRODUCTION

In papers describing applications such as active filtering, the L-filter is usually proposed. With the L-filter, high switching frequencies must be used to obtain high dynamic performance and sufficient attenuation of harmonics caused by the PWM simultaneously. If a dead-beat vector control system is applied, operation at a high sampling frequency results in low phase-shifts at frequencies below 1 kHz. The phase shift caused by the sampled control system may also be reduced by using hysteresis control, which also results in high switching frequencies. By using a third-order LCL-filter, as presented in [1], a small line filter can be obtained at a low switching frequency, and EMC standards can be fulfilled also at moderate switching frequencies. It is also a major advantage in high-power systems in which the switching frequency is limited.

One drawback of the LCL-filter is that the control system becomes more expensive and complex. Not much attention has been given to control principles for the LCL-filter, so far. A control principle for a similar LC-filter has been described in [2]. By adding an inductor to the LC-filter, an LCL-filter is obtained. The line-side inductors of the LCL-filter prevent current harmonics injected by parallel loads from overloading the filter capacitors of the LCL-filter. However, it simultaneously determines the crossover frequency where resonance may be initiated by harmonics. As with a capacitor banks for static var compensation, frequencies with high distortion should be avoided. The control system for the VSC should also be designed to attenuate such oscillations due to resonances. Another drawback with the LCL-filter, is that it is difficult to obtain dead-beat response.

If an active filter with a low switching frequency is to be implemented, compensation for the time delays in the control system must be included. Usually, time delay compensation is performed in the time domain. If dead-beat response is not obtained, the compensation in the time domain becomes complex. However, compensation for the time delays in the control system can be incorporated by using a Fourier method for the active filtering. With such a method, compensation is performed in the frequency domain. This has also been reported in [3]. Control principles aiming at a low cost for the control system are reported in [4] and [5].

With the control principle described in this paper, the LCL-filter can be used in applications where high bandwidth is required. This is verified by measurements of frequency responses and by active filtering of the low-order harmonics caused by a line-commutated rectifier. In addition, the dynamic performance is compared with the measured dynamic performance obtained with an L-filter with a vector-control system operating at dead-beat gain. In the active filtering, compensation for the measured phase-shifts is realized. Small-signal analysis is used to evaluate phase-shifts from the measured frequency responses. To study if the phase-shifts can be predicted by an analytical model, measured frequency responses are compared with Bode diagrams from linear analytical models. Furthermore, the influence of filtering principles on the current control system and the choice of line filter is presented. Results from active filtering with three different methods are displayed in measurements for both filters. The first two methods are based on the instantaneous active and reactive currents [6]. The third method uses the discrete Fourier transformation.

II. System Description and Analytical Modeling

A. System Description

The system with the LCL-filter is displayed in Fig. 1. When active filtering is studied, a line-commutated rectifier is used to inject current harmonics. It is connected at the point of common connection (PCC). The parameters of the line filters are listed in Table 1. The inductance of the grid is assumed to be zero. The same inductance L_1 is used in both filters. The L-filter is, thus, obtained by deleting the capacitors and the inductor denoted by L_2 in Fig. 1. The crossover frequency of the LCL-filter is 2929 Hz. To compare the dynamic performance, the same switching frequency and sampling frequency are used with both filters. The switching frequency and the sampling frequency are 7200 Hz. At this sampling frequency, a sampling time, T_s=138.9 μs is obtained. Sub-oscillation optimized PWM is used. A DC-voltage of 650 V is used and the line-to-line voltage of the grid is 400 V. The line frequency is 50 Hz which gives an angular frequency ω_g=100π rad/s.

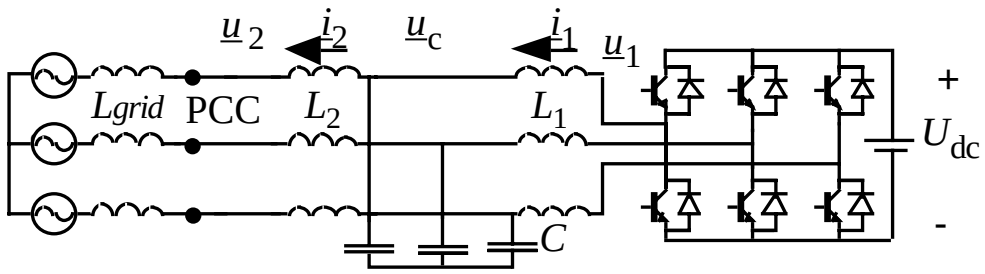

Fig. 1. A voltage-source converter connected to the grid through an LCL-filter.

TABLE 1.

LINE FILTER PARAMETERS

L-filter	LCL-filter
X_L = 0.05 p.u. (L_1 = 1	X_{L1} = 0.05 p.u. (L_1 = 1 mH)
	X_{L2} = 0.0025 p.u. (L_2 = 0.05 mH)
	X_C = 8.5 p.u. (C = 60 μF)

The experimental system consists of a VSC with IGBT valves (Toshiba MG400Q1US41 1200V, 400A) and a TMS320C30 control computer. In measuring the currents, LEM LA50-S/SP1 modules are used. In the inputs to the DSP-system, first order low-pass filters with a crossover frequency of 75 kHz are used. In the optical fibers between the control system and the control circuits for the valves, a time delay of 0.5 μs is introduced. Finally, a time-delay of 3 μs is introduced by the gate circuits for the valves.

B. Closed-loop Modeling and Analytical Line Filter Models

To obtain frequency responses of the closed-loop system, a discrete linear state-space equation of the closed-loop system is formed. The semiconductor valves are assumed to be ideal in the analytical model, and the space-vector average approximation is used to model the converter. Thus, the direct and quadrature components of the converter voltage are assumed to be equal to the reference voltage components requested by the controllers in the dq-frame. The modeling technique is described in detail in [7].

A state-space equation of the LCL-filter in the grid-flux oriented dq-system can be written as

$$\frac{d\mathbf{x}}{dt} = \mathbf{A}\mathbf{x} + \mathbf{B}\mathbf{u} \tag{1}$$

where

$\mathbf{x} = (i_{1d}, i_{1q}, i_{2d}, i_{2q}, u_{cd}, u_{cq})^T$ and $\mathbf{u} = (u_{1d}, u_{1q}, u_{2d}, u_{2q})^T$ are the state and input vectors, respectively. The matrices **A** and **B** are

$$\mathbf{A} = \begin{bmatrix} -\frac{R_1}{L_1} & \omega_g & 0 & 0 & -\frac{1}{L_1} & 0 \\ -\omega_g & -\frac{R_1}{L_1} & 0 & 0 & 0 & -\frac{1}{L_1} \\ 0 & 0 & -\frac{R_2}{L_2} & \omega_g & \frac{1}{L_2} & 0 \\ 0 & 0 & -\omega_g & -\frac{R_2}{L_2} & 0 & \frac{1}{L_2} \\ \frac{1}{C} & 0 & -\frac{1}{C} & 0 & 0 & \omega_g \\ 0 & \frac{1}{C} & 0 & -\frac{1}{C} & -\omega_g & 0 \end{bmatrix} \qquad \mathbf{B} = \begin{bmatrix} \frac{1}{L_1} & 0 & 0 & 0 \\ 0 & \frac{1}{L_1} & 0 & 0 \\ 0 & 0 & -\frac{1}{L_2} & 0 \\ 0 & 0 & 0 & -\frac{1}{L_2} \\ 0 & 0 & 0 & 0 \\ 0 & 0 & 0 & 0 \end{bmatrix}$$

The matrices for the L-filter are

$$\mathbf{A} = \begin{bmatrix} -\frac{R_1}{L_1} & \omega_g \\ -\omega_g & -\frac{R_1}{L_1} \end{bmatrix} \mathbf{B} = \begin{bmatrix} \frac{1}{L_1} & 0 & -\frac{1}{L_1} & 0 \\ 0 & \frac{1}{L_1} & 0 & -\frac{1}{L_1} \end{bmatrix}$$

The state vector and the input vector for the L-filter are $\mathbf{x} = (i_{1d}, i_{1q})^T$ and $\mathbf{u} = (u_{1d}, u_{1q}, u_{2d}, u_{2q})^T$.

The vector current controller operates in discrete time. To model the closed-loop systems, the state-space models of the line-filters are transformed into discrete time models as

$$\mathbf{x}(k+1) = \mathbf{F}\mathbf{x}(k) + \mathbf{G}\mathbf{u}(k) \tag{2}$$

where the matrices are obtained by

$$\mathbf{F} = e^{\mathbf{A}T_s} \text{ and } \mathbf{G} = \int_0^{T_s} e^{\mathbf{A}\tau} d\tau \mathbf{B} \tag{3}$$

The closed-loop state-space equations are obtained by modeling the controllers by using discrete states. Ten states are used to model the controller equations and, thus, sixteen states occur in the closed-loop model. Two states are used to model the time delay of one sample, two states for delay time compensation, and finally six states for the integral parts.

III. Control

A. Description of Controllers

In the control system, a compensation function is used to reduce the influence of the nonlinearities due to the blanking time and on-state voltage drops in the valves. As described in [8], the compensation function reduces the coupling between the d- and q-direction and improves the responses from the d- to d-direction and from the q- to q-direction. The same compensation function is used with both line filters. The compensation principle is based on the signs of the phase-currents at the commutations. The signs of the phase-currents are assumed to be constant during the sample interval. This is not the case close to zero, and the compensation function is not used when the phase currents are below 5 A. With the L-filter, discrete time PI-controllers with dead-beat gain are used according to

$$\underline{u}_1^*(k+1) = \underline{u}_2(k) + Z_1\,\underline{i}_1(k) + k_{p1}(\underline{i}_1^*(k) - \underline{i}_1(k)) + \underline{u}_{1I}(k) - \underline{\Delta u}_1(k) \tag{4}$$

where integration is performed by the term

$$\underline{u}_{1I}(k) = \sum_k k_i(\underline{i}_1^*(k-2) - \underline{i}_1(k)) \tag{5}$$

Compensation for the time delay of one sample is included as

$$\underline{\Delta u}_1(k) = k_{p1}(\underline{i}_1^*(k-1) - \underline{i}_1(k-1)) - \underline{\Delta u}_1(k-1) \tag{6}$$

The compensation principle is accurate only when dead-beat current response is obtained. Dead-beat gain is used according to

$$k_{p1} = \frac{L_1}{T_s} + \frac{R_1}{2} \tag{7}$$

The control principle used with the LCL-filter is illustrated in Fig. 2. As displayed in the figure, feedforward of the reference current vector of the line current is used. Impedances $Z_1 = (R_1 + j\omega_g L_1)$ and $Z_2 = (R_2 + j\omega_g L_2)$ are used. The reference current vector for the inner current loop is

$$\underline{i}_1^*(k) = \underline{i}_2^*(k) + j\omega_g C\,\underline{u}_c^*(k) + k_{p2}(\underline{u}_c^*(k) - \underline{u}_c(k)) \tag{8}$$

where the capacitor voltage vector is defined by

$$\underline{u}_c^*(k) = \underline{u}_2^*(k) + Z_2\,\underline{i}_2^*(k) + \sum_k k_i(\underline{i}_2^*(k-2) - \underline{i}_2(k)) \tag{9}$$

The inner current loop is defined by

$$\underline{u}_1^*(k+1) = \underline{u}_c(k) + Z_1\,\underline{i}_1(k) + k_{p1}(\underline{i}_1^*(k) - \underline{i}_1(k)) - \underline{\Delta u}_1(k) \tag{10}$$

As described above, the control principle uses the feedforward of the current references of the line current vector to the inner current loop to improve the dynamic performance. To obtain an accurate steady-state line current vector, an integral part is applied to the controllers of the capacitor voltage vector. Integrator wind-up is avoided by limiting the integral parts to±20 V.

To obtain optimal dynamic performance in the inner loop, deadbeat gain is used. The outer loop gain k_{p2} is set to obtain high dynamic performance and sufficient stability limits. A gain $k_{p2} = 0.2C'f_s$ is used. According to the root loci in Fig. 3, the system becomes non-stable if the gain is increased above $k_{p2} = 0.6C'f_s$. It is tuned by using the root-locus diagram displayed in Fig. 3. The eigenvalues at the gain selected are marked by arrows. As displayed, the eigenvalues of the closed-loop system occur close to the unit circle. Due to frequency dependent losses in the line filter and time-delays in the converter system, the dynamic performance at the crossover frequency is not easily predicted by a linear analytical model. To make sure that distortions at the crossover frequency do not give rise to a unstable system, a sufficient stability margin should be included in the analytical model. The stability margins in Fig. 3 should be increased. This can be done by changing the crossover frequency of the line filter. The system has, however, displayed the most stable operation during the measurements.

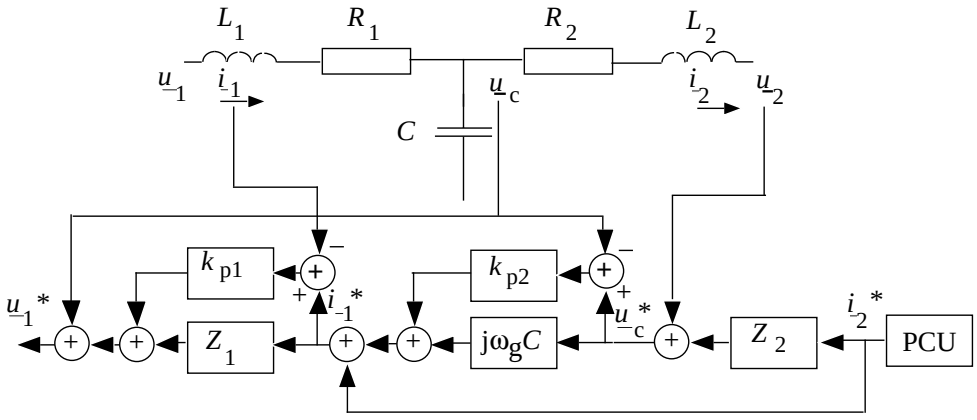

Fig. 2. Diagram of the control principle used with the LCL-filter.

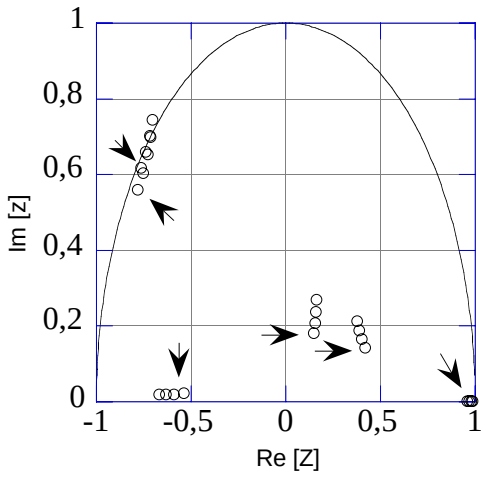

Fig. 3. Root loci of the closed loop system equation.

B. Analysis of Frequency Responses

To evaluate the dynamic performance of the converter systems, a small signal analysis is performed. In Figs. 4 and 5, responses for the L-filter are plotted. The gains are very close to 0 dB with a small attenuation close to 1 kHz. The deviation is higher with a reference in the d-direction. A deviation of 2 dB corresponds to an error of 26 %. As displayed in both Fig. 4 and Fig. 5, the coupling is changed at the same frequency as the errors occur in the gains. Thus, the errors at high frequencies seem to occur since the converter produces an erroneous voltage vector. This may be due to the minor time delays in the control system. The deviation can also be due to non-modeled losses in the line filter. The phase is predicted well by a linear analytical model. As presented in Figs. 4 and 5, the couplings are not accurately predicted at low frequencies; this deviation is due to very low signal-to-noise levels. However, the coupling is low at all frequencies below 1 kHz. The influence of nonlinearties are further described in [8].

In Figs. 6 and 7, frequency responses for the LCL-filter are plotted. As with the L-filter, a deviation between the analytical response and the measured response occurs at high frequencies. As with the L-filter, the coupling is low in both directions. In the d-direction, an attenuation of 2.5 dB is obtained at 1 kHz. In the q-direction, a gain of 1 dB is obtained at approximately 700 Hz. The main difference compared with the L-filter is that the phase shift is increased. At 600 Hz, the difference is approximately 5 degrees. At 600 Hz, an error of 7 degrees occurs in the d-direction.

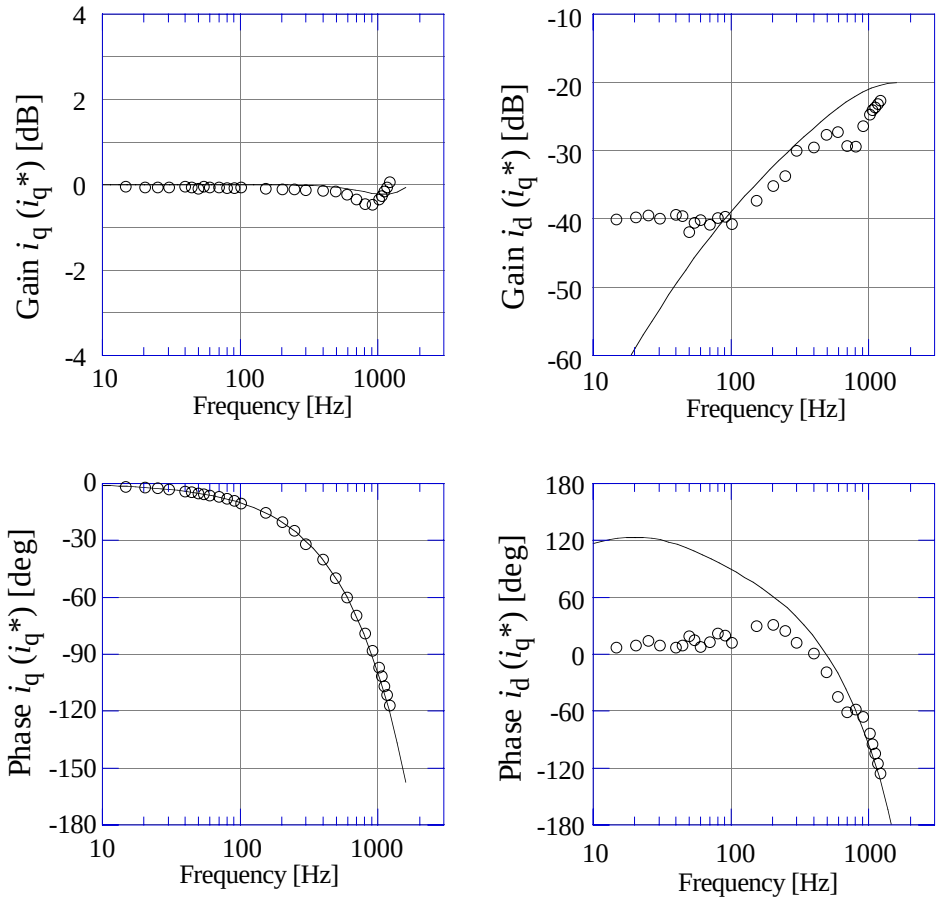

Fig. 4. Bode-diagrams of $i_q(i_q^*)$ and $i_d(i_q^*)$ with the L-filter. Analytical model (lines) and measured response (circles).

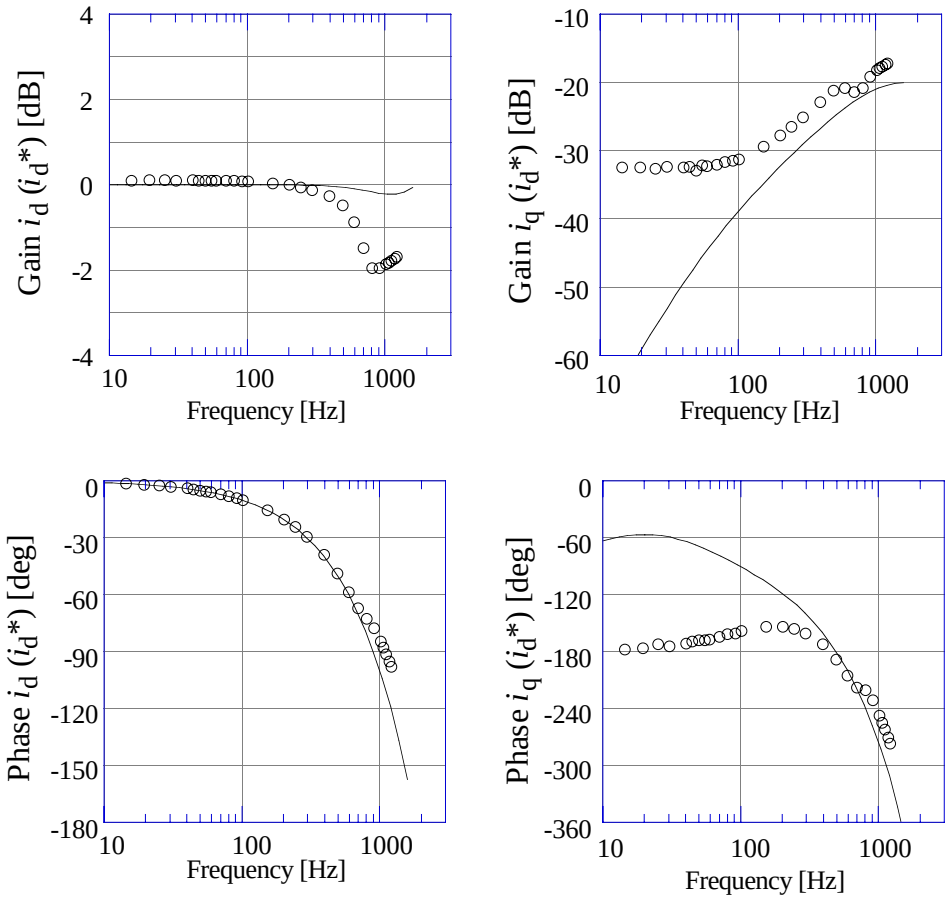

Fig. 5. Bode-diagrams of $i_d(i_d^*)$ and $i_q(i_d^*)$ with the L-filter. Analytical model (lines) and measured response (circles).

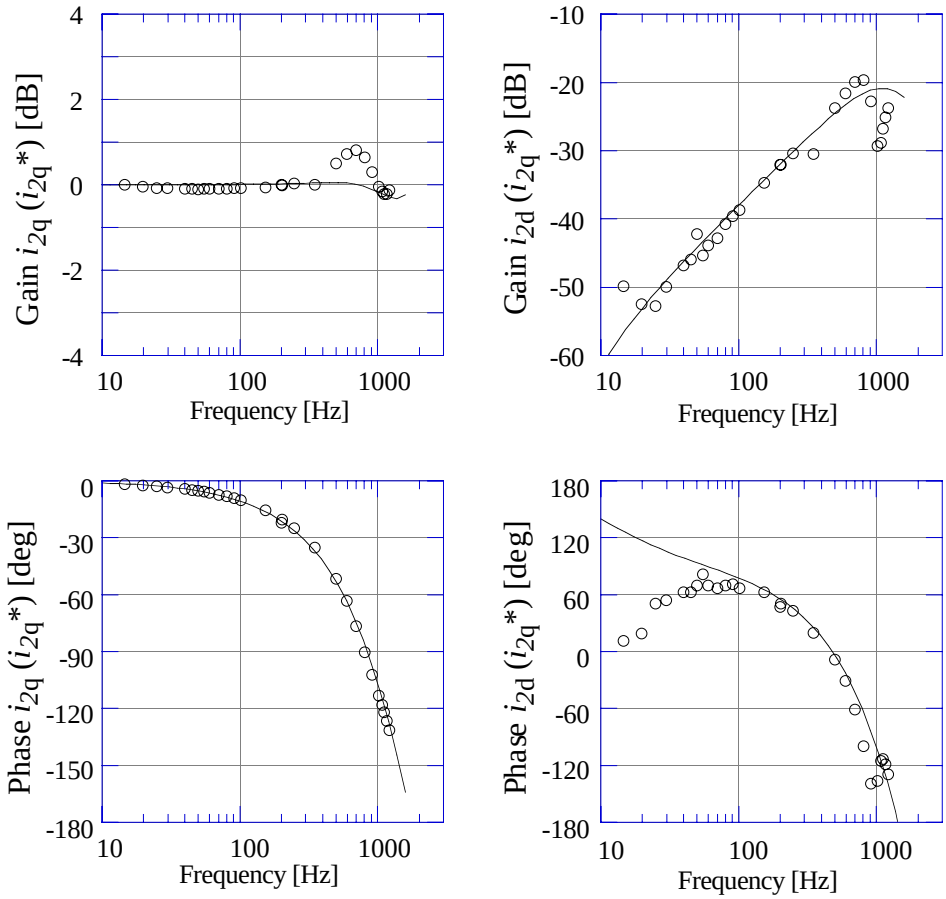

Fig. 6. Bode-diagrams of $i_{2q}(i_{2q}^*)$ and $i_{2d}(i_{2q}^*)$ with the LCL-filter. Analytical model (lines) and measured response (circles).

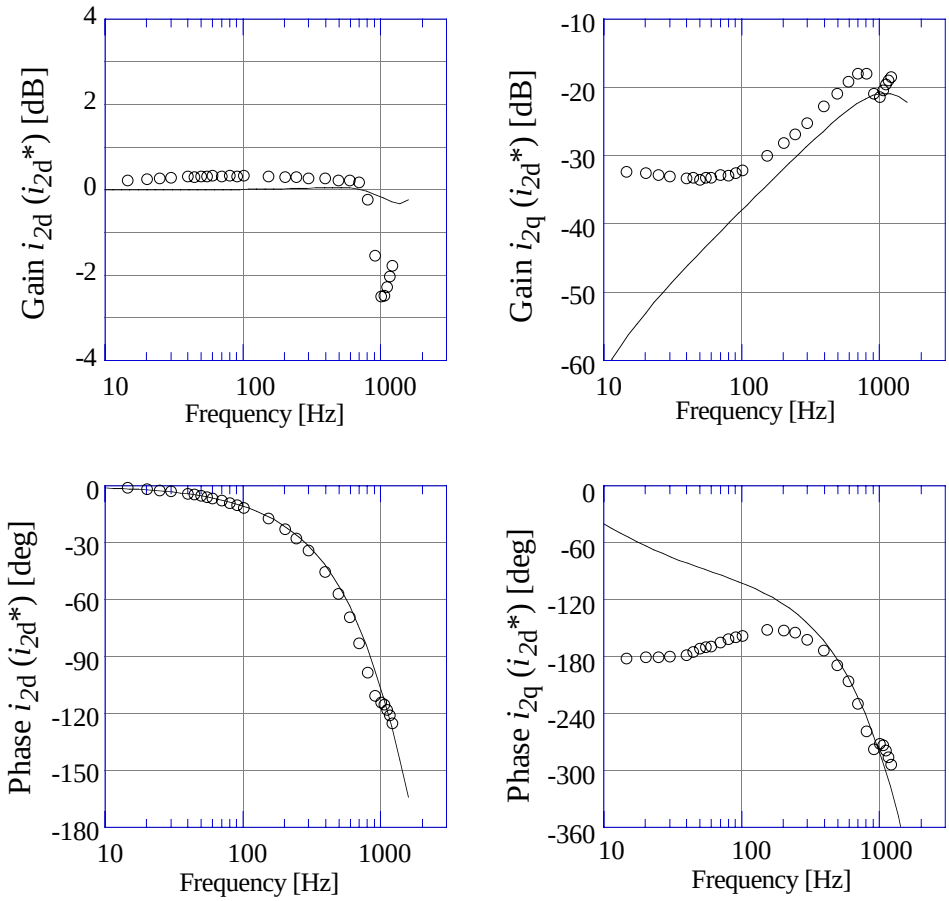

Fig. 7. Bode-diagrams of $i_{2d}(i_{2d}^*)$ and $i_{2q}(i_{2d}^*)$ with the LCL-filter. Analytical model (lines) and measured response (circles).

IV. Application to Active Filtering

A. Active Filtering Principles

Active filtering may be performed by using different strategies to obtain the reference currents for the current controllers. By using a Direct method based on the instantaneous active and reactive current, the reference current components of the active filter are set equal to the harmonic content of the d- and the q-components of the non-sinusoidal current to be filtered. With this principle, compensation is performed in the time-domain. As displayed in the next section, the same d- and q-components, respectively, are obtained six times during one cycle of the line voltage. To compensate for the time delay in the current control system, the reference-current components are set equal to the distortion current components at the sample, half a line-period plus two samples back. The two-sample shift is applied to compensate for the time delay of two samples in the current control system. Faster response to changes in the nonlinear load could be obtained by using a cycle time of 3.3 ms of the reference current components in the dq-frame.

Some advantages of this method of filtering are that all harmonics are obtained directly and that the calculations are not time consuming. A drawback is that high current derivatives occur in the reference current components since high-order harmonics are

included. The method is suitable for converter systems operating at high sampling frequencies, since a high sampling frequency reduces the current difference between two samples. Furthermore, if a vector control system operating at dead-beat gain is used, the line-filter inductors should be small to avoid saturating the controllers. The problem of saturation is avoided if a hysterisis controller is used.

Another method, the Fourier method, is based on individual compensation of different harmonics. The current components are obtained by an analytical evaluation of the harmonic components of the non-sinusoidal phase current of the nonlinear load. This is necessary to compensate for phase-shifts occurring in the current control system. As displayed in the Bode-diagrams in Section II, the phase-shift varies with the harmonic frequency. Furthermore, vectors of positive and negative order harmonics rotate in different directions in the dq-frame. This is taken into account in the compensation principle used in this paper. With this method, selective compensation may be applied. Another advantage of such a method is that the derivatives in the current references may be reduced by neglecting or reducing the compensation for high-order harmonics. This is advantageous since it is difficult to design the system with the L-filter to obtain a good transient response and sufficient attenuation of harmonics caused by the PWM simultaneously. Such a performance can, however, be obtained with the LCL-filter since a small inductance L_1 can be used. In this case, a high current harmonic distortion will occur in the inductor L_1, resulting in high losses. Furthermore, since compensation for time delays in the current control system is performed in the frequency domain, compensation can be incorporated also when dead-beat response is not obtained.

B. Reference Currents for Different Filtering Methods

When an active filter is designed, it is important to study the reference current components for the current control system. In Fig. 8, a phase current of a thyristor rectifier is plotted. As illustrated, high current derivatives occur at the commutation of the rectifier. In Figs. 9 and 10, reference d- and q-current components and d-and q-currents are shown for the Direct method and the Fourier method. Since the Direct method also includes high-order harmonics, high current derivatives occur. As shown in Fig. 9, oscillations are present in the current components. The oscillations are due to overmodulation and distortion caused by voltage harmonics in the line voltages. Overmodulation occurs mainly due to current errors in the q-direction since the line voltage is in the q-direction. When overmodulation occurs due to a current error in q-direction, control in d-direction is also distorted, due to erroneous voltage components in both directions. The time scales of the d-plot and q-plot are not synchronized; thus, it is not possible to see the influence of overmodulation in one direction on the current component in the other direction.

In Fig. 10, the current components obtained with the Fourier method are shown. In this paper, only harmonics five to thirteen are included in the Fourier method, and current reference components with low derivatives are obtained. It is clear that the distortion in the currents obtained is reduced significantly compared with the Direct method. Furthermore, in these figures, the fundamental component of the nonlinear load current is only 13 A, or 0.26 p.u. of the rated current of the PWM-converter system. Thus, overmodulation occurs at a very low level with the Direct method. By using the Fourier method, the fundamental component of the nonlinear load may be 1 p.u. without overmodulation.

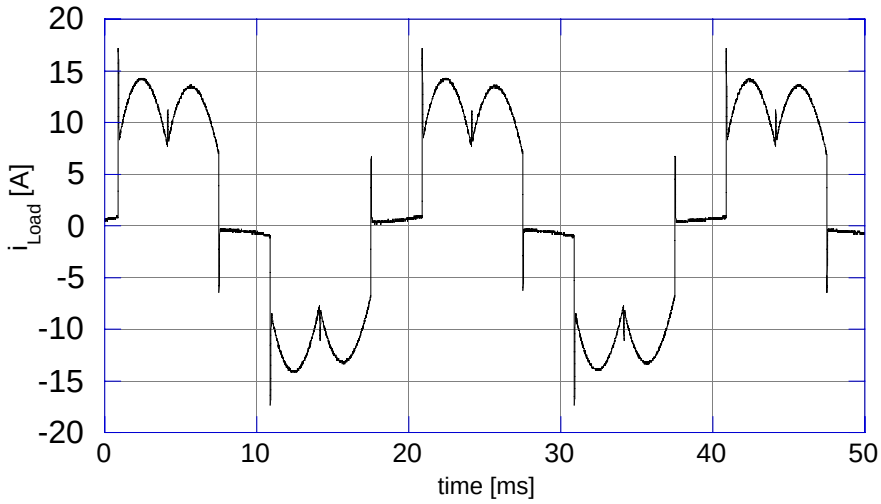

Fig. 8. Phase-current of the thyristor rectifier.

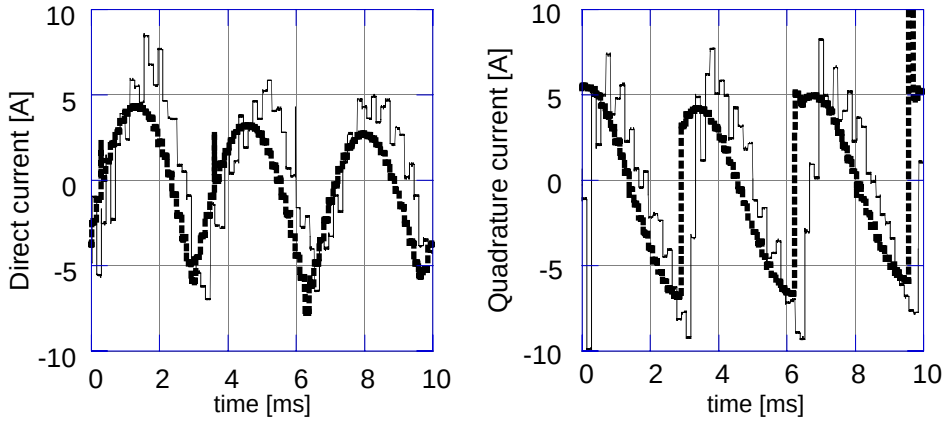

Fig. 9. Active filtering with the LCL-filter. Reference current components (fat dotted lines) and current components obtained (solid lines) with the Direct method with compensation for time delay in the control system. Direct components left and quadrature components right.

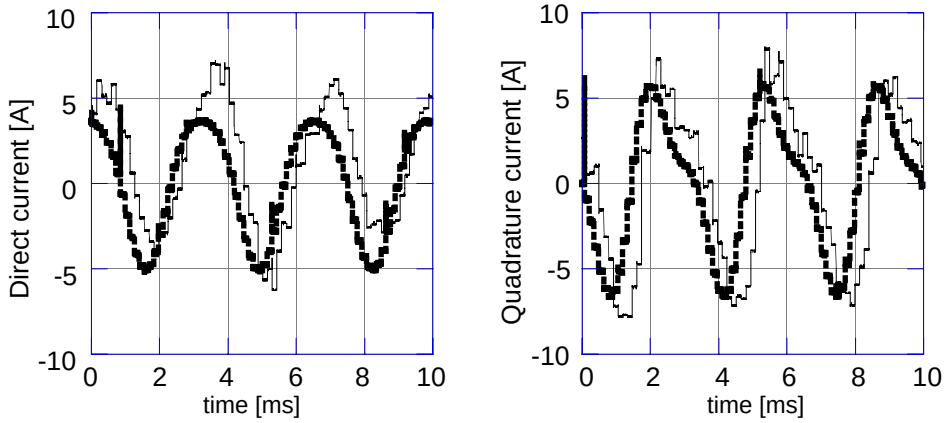

Fig. 10. Active filtering with the LCL-filter. Reference current components (fat dotted lines) and current components obtained (solid lines) with the Fourier-method with compensation for phase shifts in the control system. Direct components left and quadrature components right.

C. Resulting Line Currents with Different Line Filters

In Figs. 11 and 12, the line-currents obtained with the Direct method and the Fourier method are plotted for the L-filter and the LCL-filter. In Fig. 11, it is clear that the LCL-filter has a higher attenuation of the harmonics caused by the PWM. The difference is, however, much more significant in Fig. 12. In Fig. 11, the direct method of filtering results in overmodulation, which yields a frequency spectrum with harmonics of a lower order when compared with the spectrum without overmodulation. As shown in these figures, overmodulation should be avoided to obtain the distortion predicted. In Fig. 13, the result of active filtering at a higher power level is shown. The harmonics caused by the PWM are much more effectively attenuated with the LCL-filter than with the L-filter.

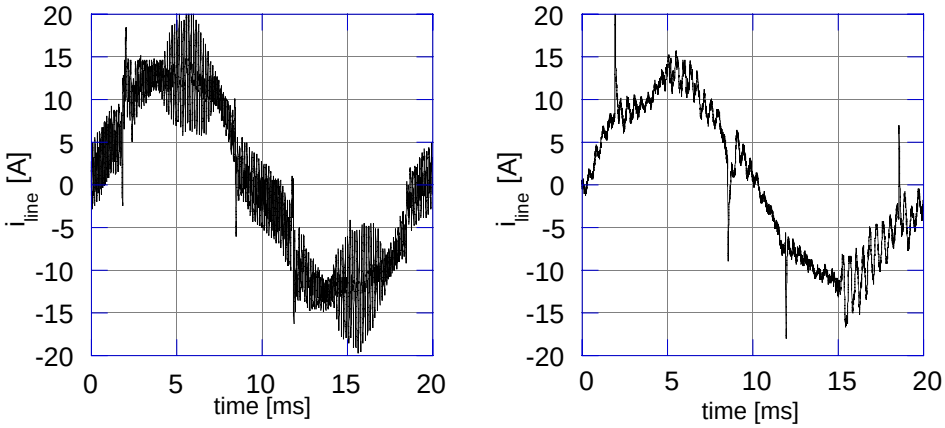

Fig. 11. Resulting line current using the Direct method with compensation for time delay in the control system. L-filter (left) and LCL-filter (right).

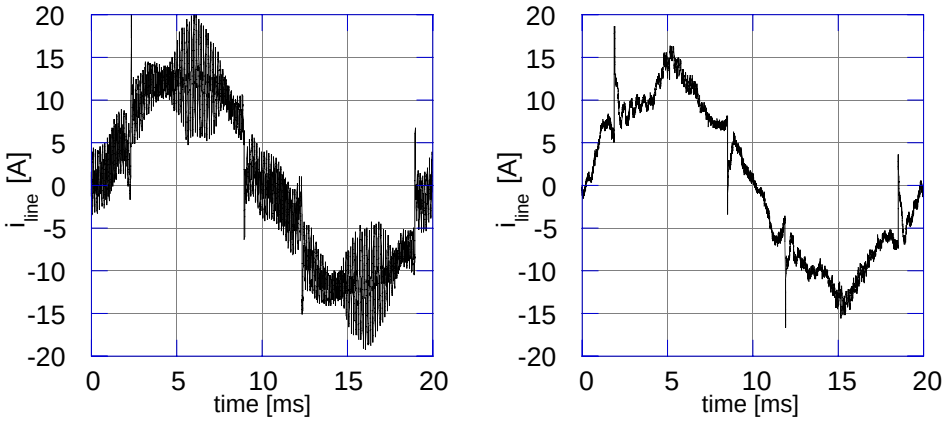

Fig. 12. Resulting line current using the Fourier-method and compensation for phase shifts in the control system. L-filter (left) and LCL-filter (right).

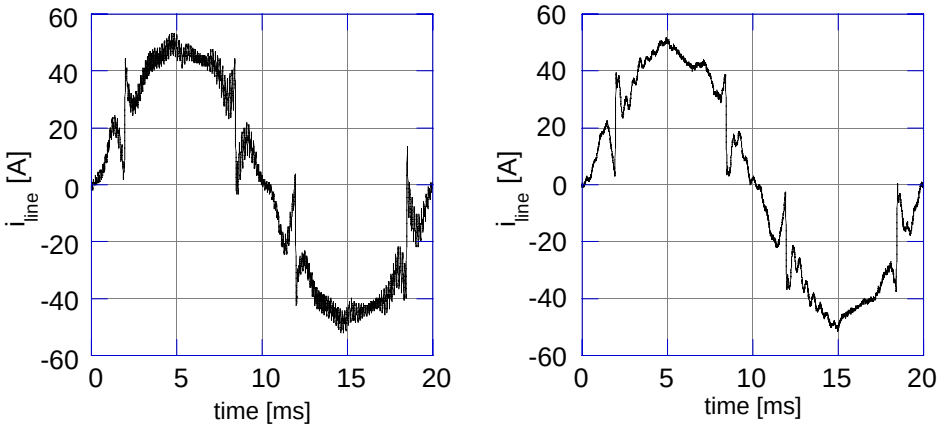

Fig. 13. Resulting line current using the Fourier-method and compensation for phase shifts in the control system. L-filter (left) and LCL-filter (right).

In Figs. 14 to 16, the results are presented in the frequency domain. Figs. 14 and 15 correspond to Figs. 11 and 12. In Figs. 14 and 14, the distortion caused by voltage harmonics in the line voltage and nonlinearities due to the PWM reduces the performance of the current control system and distorts the results. As shown, the Direct method without any compensation for the time delay in the control system yields poor compensation. The time delay corresponds to a phase shift, which increases with the frequency. Consequently, at harmonics 11 and 13, the active filter adds distortion to the line current. The LCL-filter results in higher phase shifts, and the best compensation is obtained with the L-filter. This also applies to active flitering with the compensation for the time delay. This is due to the fact that the compensation in the time domain is based on deadbeat response. With the Fourier method, similar compensation is obtained with both filters. In Fig. 16, results of the Fourier method with the currents in Fig. 13 are plotted. A similar performance is obtained at the 5th and 7th harmonics. At harmonic 11, the L-filter yields the best compensation. This is partly due to different phase shifts in the d- and q-direction at 300 Hz in the frequency responses of the LCL-filter. In the compensation function, the average value is used, which results in a non-ideal compensation.

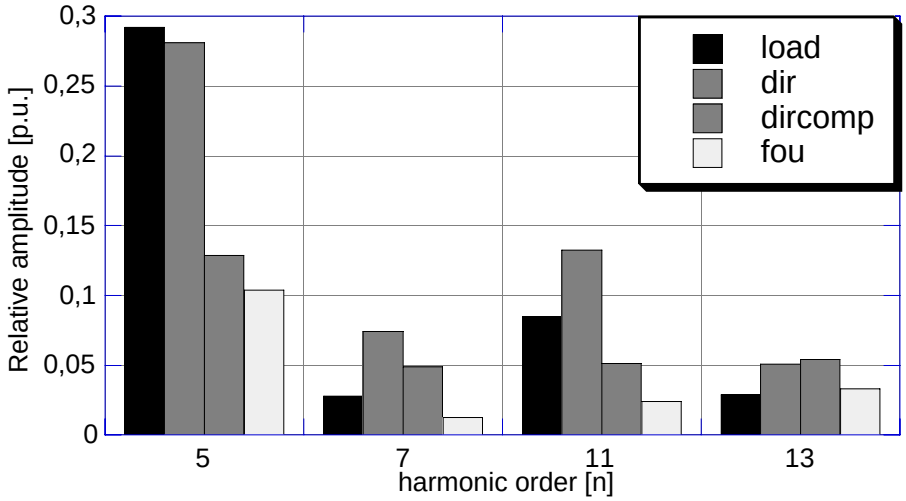

Fig. 14. Active filtering with the LCL-filter at a low power level. Resulting relative harmonic distortion at selected harmonics. Direct method without compensation for time delay in the control-system (dir), Direct method with compensation for time delay in the control-system (dircomp), Fourier method with compensation for phase-shifts in the control-system (fou).

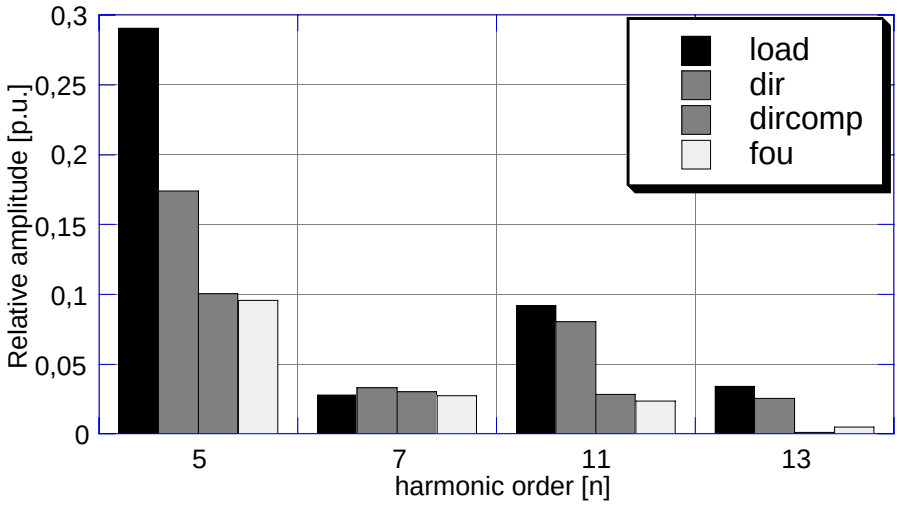

Fig. 15. Active filtering with the L-filter at a low power level. Resulting relative harmonic distortion at selected harmonics. Direct method without compensation for time delay in the control-system (dir), Direct method with compensation for time delay in the control-system (dircomp), Fourier-method with compensation for phase-shifts in the control-system (fou).

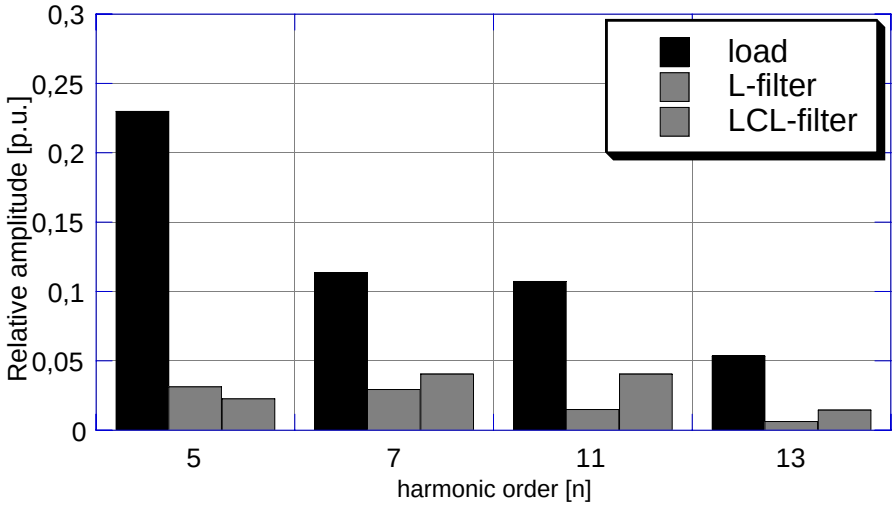

Fig. 16. Resulting relative harmonic distortion at selected harmonics with the L-filter and the LCL-filter. Fourier-method with compensation for phase-shifts in the control-system.

V. Conclusion

A vector-control principle for a voltage-source converter connected to a grid by a third-order LCL-filter is introduced. The dynamic performance is compared with the performance of a first-order L-filter with a vector-control system set at deadbeat gain. As presented by means of frequency responses and measurements of active filtering, the dynamic performance obtained with the LCL-filter is sufficient for high-performance rectifiers and active filters. The control principle is based on feedforward and results in dynamic performance are very close to the dynamic performance measured for the L-filter. A comparison of measured responses and Bode-diagrams from linear analytical models are included. At high frequencies, a small deviation occurs between the measured frequency responses and the Bode-diagrams obtained for the analytical linear system model. Similar deviations occur in the responses for the L-filter and the LCL-filter.

As shown, the filtering method used affects the performance of the active filter and the system design. If a Direct method based on the instantaneous current is used, the L-filter performs better since the time-domain compensation is based on a dead-beat response. A Direct method yields current components with high derivatives in the control system. To follow the reference currents, a line filter with a low inductance should be used. This, however, gives rise to a high current harmonic distortion caused by the PWM, and thus, a switching frequency higher than the switching frequency used in this paper should be used. A more efficient system is obtained by using the Fourier method, since lower derivatives in the reference current components are then, obtained. Phase-shift compensation can be implemented, and dead-beat response is, consequently, not requested. Consequently, the switching frequency may be reduced. Measurements show that similar filtering performance is obtained with the L-filter and the LCL-filter. One major advantage of the LCL-filter compared with the L-filter is that the harmonics due to the PWM are much more efficiently attenuated. Using LCL-filters also makes it possible to fulfill EMC standards at moderate switching frequencies. This is most advantageous, especially when considering applications with high power ratings and reduced switching frequencies.

VI. References

[1] M. Lindgren and J. Svensson, "Connecting Fast Switching Voltage Source Converters to the Grid—Harmonic Distortion and its Reduction". *IEEE Stockholm Power Tech Conference*, Stockholm, June 18-22, 1995, Proceedings of Power Electronics, p. 191-195.

[2] T. Kawabata, T. Miyashita, Y. Yamamoto, "Dead Beat Control of Three Phase PWM Inverter". *IEEE Transactions on Power Electronics*, vol. 5, no. 1, January 1990, p. 21-28.

[3] F. Abrahamsen, A. David, "Adjustable Speed Drive with Active Filtering Capability for Harmonic Current Compensation". *IEEE Power Electronics Specialists Conference (PESC'95)*, Atlanta, USA, 18-22 June, 1995, Proceedings, vol. 2, p. 1137-1143.

[4] J. Ollila, "A PWM-Rectifier without Current Measurement". *EPE Journal*, vol. 4, no. 2, June 1994, p. 14-19.

[5] M. Lindgren, "Feed forward- Time Efficient Control of a Voltage Source Converter Connected to the Grid by Lowpass Filters". *IEEE Power Electronics Specialists Conference (PESC'95)*, Atlanta, USA, 18-22 June, 1995, Proceedings, vol. 2, p. 1028-1032.

[6] H. Akagi, Y. Kanazawa, and A. Nabae "Instantaneous Reactive Power Compensators Comprising Switching Devices without Energy Storage Components ". IEEE Transactions on Industry Applications, Vol. IA- 20, No. 3, May/ June 1984.

[7] M. Lindgren. "Analysis and Simulation of Digitally Controlled Grid-connected PWM-converters using the Space-vector Average Approximation". *IEEE5th Workshop on Computers in Power Electronics*, 11- 14 August 1996, p. 157-162.

[8] J. Svensson, M. Lindgren. "Vector Current Controlled Grid Connected Voltage-source Converter. Influence of Non-Linearities on the Performance". *IEEE, Power Electronics Specialists Conference, (PESC-98*), Fukuoka, Japan, May 17-22, 1998. In press.